Non-canonical members of circuits:

A role for the locus coeruleus in reward related place field plasticity, and investigating differences in astrocyte calcium signaling between hippocampal layers

Alexandra Mansell Kaufman

Submitted in partial fulfillment of the
requirements for the degree of
Doctor of Philosophy
under the Executive Committee
of the Graduate School of Arts and Sciences

COLUMBIA UNIVERSITY

2020

Abstract

Non-canonical members of circuits:

A role for the locus coeruleus in reward related place field plasticity, and investigating differences in astrocyte calcium signaling between hippocampal layers

Alexandra Mansell Kaufman

The hippocampus (HPC) is a brain area in the medial temporal lobe involved in spatial navigation, as well as the formation of episodic memories. A subset of the principal cells of the HPC, known as place cells, are active in specific locations of an environment, called the place fields. Dorsal hippocampal area CA1 contains place fields that are known to change their firing during spatial tasks where animals learn the location of a reward, known as goal-oriented learning (GOL) – CA1 place fields shift toward rewarded locations. Previous studies suggest that this preferentially occurs at novel rewarded locations in a familiar environment, but the mechanism is unknown. The locus coeruleus (LC) is a neuromodulatory nucleus in the brainstem that projects throughout the brain and releases norepinephrine and a small amount of dopamine. Stimulating locus coeruleus-hippocampal area CA1 projections (LC-CA1) was recently shown to improve performance on spatial memory tasks. Since performance on the GOL task is correlated with the degree of overrepresentation of rewarded locations, we hypothesized that the LC-CA1 projection was involved in reward-related place field reorganization.

Using *in vivo* two photon calcium imaging, we recorded the activity of the LC-CA1 projection during a head fixed GOL task with two phases – during the first phase, a water reward was presented in one location (RZ1), and in the second phase, it was moved to a novel location (RZ2). In the first phase of the task, the LC-CA1 axons were correlated with running, but in the second phase they showed an increase in activity preceding RZ2. To determine whether the LC-CA1 is involved in place field reorganization that normally occurs in RZ2, we optogenetically activated the projection just before RZ1, and saw a pronounced place field reorganization right before the reward. Conversely, inhibition of LC-CA1 at RZ2 attenuated place field reorganization at this site. Finally, LC-CA1 stimulation away from the reward did not lead to place field reorganization, indicating that the LC influences place field shifts in conjunction with other signals that are differentially active around rewards.

A full account of the effects of neuromodulation should also include astrocytes, since they respond to neuromodulators with large calcium signals that may be able to affect the function of neurons. We also recorded HPC astrocyte calcium activity during different behavioral tasks. Astrocytes showed occasional large calcium signals, with some differences in synchronicity and activity levels between hippocampal layers and behavioral paradigms. Future studies should determine whether the LC-CA1 projection affects place fields directly by affecting neural activity, indirectly via astrocytes, or both.

Table of Contents

List of Tables

List of Figures

Acknowledgments

I would like to acknowledge my advisor and my lab, for being a rigorous and competitive environment in which to do science. The tools and brain power I have had access to here is unmatched. I would like to thank Dr. Tristan Geiller, for helping push me over the finish line and being a good teammate on the LC project.

I would like to thank my family, for their love, support and patience with me, and their willingness to listen to me talk about science. I would also like to thank my friends, especially Dena Tasse-Winter, Joelle Rotman, and Deborah Kanter, for being incredibly helpful and supportive during a mentally difficult time. I would especially like to thank my roommate, Deb, for putting up with me while I write my thesis while being quarantined in the middle of a pandemic, particularly my obsessive baking, fermenting, and consumption of beans. I would like to thank all the people who have loved me, and shown me their love, throughout this PhD and throughout my life.

Table of Abbreviations

Anatomy and cell types		
Abbreviation	Meaning	Definition
PC	Pyramidal cell	Excitatory neurons, here referring to those located in the hippocampus
HPC	Hippocampus	A part of the medial temporal lobe involved in navigation and memory
CA1	Cornu ammonis 1	Part of the hippocampus, the major output structure, contains place cells
CA1PC	CA1 pyramidal cell	Pyramidal cell located in area CA1
CA2	Cornu ammonis 2	Part of the hippocampus, involved in recognition of social stimuli
CA3	Cornu ammonis 3	Part of the hippocampus, major input structure for CA1
DG	Dentate gyrus	Major input to CA3, site of neurogenesis throughout adulthood
SO	Stratum oriens	Layer located just ventral to the hippocampal surface, contains PC dendrites and interneurons
SP	Stratum pyramidale	Layer of the hippocampus where cell bodies of PCs are located
SR	Stratum radiatum	Layer of the hippocampus where PC dendrites are located, location of synapse from CA3-CA1
SLM	Stratum lacunosum moleculare	Layer of the hippocampus where the distal tuft of the PC dendrites are located, also the site of direct projections from entorhinal cortex
EC	Entorhinal cortex	Major input to hippocampus
VTA	Ventral tegmental area	A brain area that sends dopamine to other brain areas
MS	Medial septum	A brain area that sends acetylcholine to the hippocampus, as well as inhibitory projections
LC	Locus coeruleus	A neuromodulatory nucleus located in the brainstem that releases norepinephrine and dopamine
LC-HPC	Locus coeruleus-hippocampal projections	Axons projecting from the locus coeruleus to the hippocampus
NE	Norepinephrine	A catecholamine that acts as a neuromodulator
DA	dopamine	A catecholamine, similar in structure to NE, also acts as a neuromodulator
Subcellular compartments and receptors		
Abbreviation	Meaning	Definition
GPCR	G-protein coupled receptor	A metabotropic receptor type that, after a ligand binds to it, stimulates a cascade of signaling through G proteins

ER	Endoplasmic reticulum	Cellular organelle that is involved in synthesizing protein, also acts as a calcium storage location
IP3R	Inositol triphosphate receptor	A receptor located on the ER membrane, activated downstream of GPCRs – IP3R2 is the subtype expressed in astrocytes
GFAP	Glial fibrillary acidic protein	A protein selectively expressed in astrocytes in adulthood (and radial glia). Increases expression levels after injury.
Th	Tyrosine hydroxylase	Enzyme involved in the synthesis of catecholamines
Tools		
Abbreviation	Meaning	Definition
rAAV	Recombinant adeno-associated virus	A replication-incompetent virus that can be used to deliver DNA into cells to produce a desired protein
Cre	Cre recombinase	An enzyme that can cleave specific sites of DNA, can be used for inducible gene expression
ChR	Channel rhodopsin	A light-activated nonselective cation channel that causes membrane depolarization, activating neurons
bReaChes	--	Red shifted channel rhodopsin, activated by red light
Arch	Archaerhodopsin	A light-activated chloride channel that
GCaMP	circularly permuted green fluorescent protein (cpGFP), calmodulin (CaM), and the Ca^{2+}/CaM-binding "M13" peptide (M13pep).	A green fluorescent protein that becomes brighter when bound to calcium, used as a readout of activity
$\Delta F/F$	Change in fluorescence/baseline fluorescence	A method to normalize the calcium signal recorded from GCaMP or other fluorescent indicators
2p	Two photon	Two-photon microscope, a tool that can be used to chronically image small structures *in vivo*
LFP	Local field potential	A method to record from multiple neurons in a certain brain area
Concepts in neural plasticity		
Abbreviation	Meaning	Definition
LTP	Long term potentiation	A mechanism by which synapses increase in strength
LTD	Long term depression	A mechanism by which synapses decrease in strength
STDP	Spike-timing dependent plasticity	A phenomenon whereby synapses change strength, but a specific time sequence of inputs is required

BTSP	Behavioral time scale plasticity	A phenomenon whereby synapses change strength, involving a slow membrane ramp, that occurs on the order of seconds
Behavioral paradigms and stimuli		
Abbreviation	Meaning	Definition
RZ	Reward zone	Location on the cued belt where a water reward is delivered
GOL	Goal-oriented learning	A spatial learning task where the animal needs to learn and remember the location of a reward
RF	Random foraging	A non-spatial task where animals run in a context and are delivered rewards in randomized locations
Analysis methods		
Abbreviation	Meaning	Definition
GLM	Generalized linear model	A method to estimate the predictive contribution of variables to an output signal
PCA	Principal component analysis	A method to cluster results into a space that maximizes the distance between groups

Tables of Reagents and Resources

Antibodies

Antigen	Animal generated in, concentration	Source and catalog number
Anti-GFP	Chicken, 1:500- 1:1000	Abcam, ab13970
Anti-dsRed	Rabbit, 1:1000	Takara, 632496
Anti-Th	Chicken, 1:500	Abcam, Ab76442
Anti-Th	Rabbit, 1:100	Millipore, AB152
Anti-GFAP	Rabbit, 1:500 – 1:1000	Life technologies, OPA1-06100
Anti-Iba1	Rabbit, 1:500	Wako, 019-19741
Anti-NeuN	Mouse, 1:500	Millipore, MAB377
Anti-IP3R2	Goat, 1:500	Novus Bio, NB100-2466
Anti-chicken Alexa 488	Donkey, 1:300	Jackson, 703-545-155
Anti-chicken Alexa 647	Donkey, 1:300	Jackson, 703-605-155
Anti-rabbit Alexa 568	Goat, 1:300	Abcam, ab175692
Anti-rabbit Alexa 647	Donkey, 1:300	Jackson, 711-605-152
Anti-mouse Dylight 649	Donkey, 1:300	Jackson, 205-492-176
Anti-goat Alexa 647	Donkey, 1:300	Jackson, 705-605-147

Viruses

Name	Source	Catalog number
rAAV2/1: Ef1α-(GCAMP6s)$_{Cre}$	Boris Zemelman	N/A
rAAV2/1: Ef1α -(GCAMP6s)$_{Cre}$	Boris Zemelman	N/A
rAAV2/1: Ef1α -(Arch-tdTomato)$_{Cre}$	Boris Zemelman	N/A
rAAV2/1: Ef1α -(bReaChES-tdTomato)$_{Cre}$	Boris Zemelman	N/A
rAAV2/1:Syn-GCaMP6f	UPenn Virus core, Addgene	Addgene 100837-AAV1
rAAV2/1:CaMKII-GCaMP6f	UPenn Virus core, Addgene	Addgene 100834-AAV1
rAAV2/5:gfaABC1D-cyto-GCaMP6f (aka GFAP-GCaMP6f)	Generated by Baljit Khakh's lab, purchased from UPenn Virus Core, Addgene	Addgene 52925-AAV5

Chemicals

Name	Source	Catalog Number
PBS	Thermo Fisher	7732-18-5
PFA	Electron Microscopy Sciences	15714-S
Triton X-100	Sigma-Aldrich	T8787-100ML
Normal Donkey Serum	Jackson Immuno	017-000-121
Aquamount	Fisher Scientific	14-390-5

Mice

Th-IRES-Cre	Lindeberg et al. 2004, from Dr. Eric Kandel	
Th-IRES-Cre x Ai9 (ROSA-lsl-tdTomato)	Th-IRES-Cre mice crossed with Ai9 mice from The Jackson Laboratory	Ai9: 007909
VIP-IRES-Cre	The Jackson Laboratory	010908
Th-IRES-Cre x VIP-IRES-Cre	This lab	N/A
Aldh1L1-CreER x	The Jackson Laboratory, generated by Baljit Khakh's lab	031008
IP3R2$^{fl/fl}$	Obtained from Dr. Martin Paukert	Itpr2 $^{Tm1\ Chen}$

Aldh1L1-CreER x IP3R2$^{fl/fl}$	Bred in this lab for this project	
C57Bl6J (Wild Type)	Jackson Labs	

Software

Python 2.7.15	https://www.python.org	
SIMA	Kaifosh et al., 2014	https://github.com/losonczylab/sima
BehaviorMate	Created by Jack Bowler	

Introduction

One of the questions that has been a major focus of neuroscience since its inception is the formation and storage of memory. Episodic memory is a form of memory that includes experiences that can be described, memories of events that occurred. The hippocampus was first discovered to be involved in episodic memory due to a patient known as H.M. He presented with severe epilepsy originating in the medial temporal lobe. Since no one knew the function of this brain area, his surgeon, Dr. Scoville, removed it bilaterally. H.M.'s epilepsy was cured, but the removal of this brain area caused him to have severe anterograde amnesia, meaning that he could not form new declarative, or episodic, memories. While he could incorporate some form of memories, such as procedural memories that involved tracing shapes in a mirror, he had no accessible conscious memory of the experience of learning to trace these shapes. The extent of H.M.'s lesion is debated, but studies by Dr. Brenda Milner, describing and cataloguing H.M.'s symptoms, provided a basis for scientists' understanding of the function of the human hippocampus (HPC), a structure in the medial temporal lobe (Milner, 2005; Scoville and Milner, 1957).

Naturally, once scientists became interested in the hippocampus, they wanted to study its function in animal models such as rodents. However, when electrophysiological recordings of the rat hippocampus were first performed, O'Keefe and Dostrovsky observed cells that responded to certain locations in an environment (O'Keefe and Dostrovky, 1971). These spatially-tuned cells were called place cells, with their receptive fields being called place fields. More recent work has uncovered other types of spatially tuned cells, such as grid cells in the medial entorhinal cortex (mEC), border cells, head direction cells, and others (Sasaki et al., 2015). A few studies that may begin to reconcile the apparent navigational function of the hippocampus have described "place

cells" that respond to other types of stimuli, when they are presented in a pattern – these include time cells (Howard and Eichenbaum, 2015) as well as cells that respond to specific auditory tones when the tones are given a behaviorally relevant meaning (Aronov et al., 2017). In fact, navigation involves a significant memory component: to understand where one is in space, one needs to recognize that space from previous experience. It is certainly possible to reconcile the mnemonic and spatial functions of the hippocampus (Lisman et al., 2017; Moser et al., 2015).

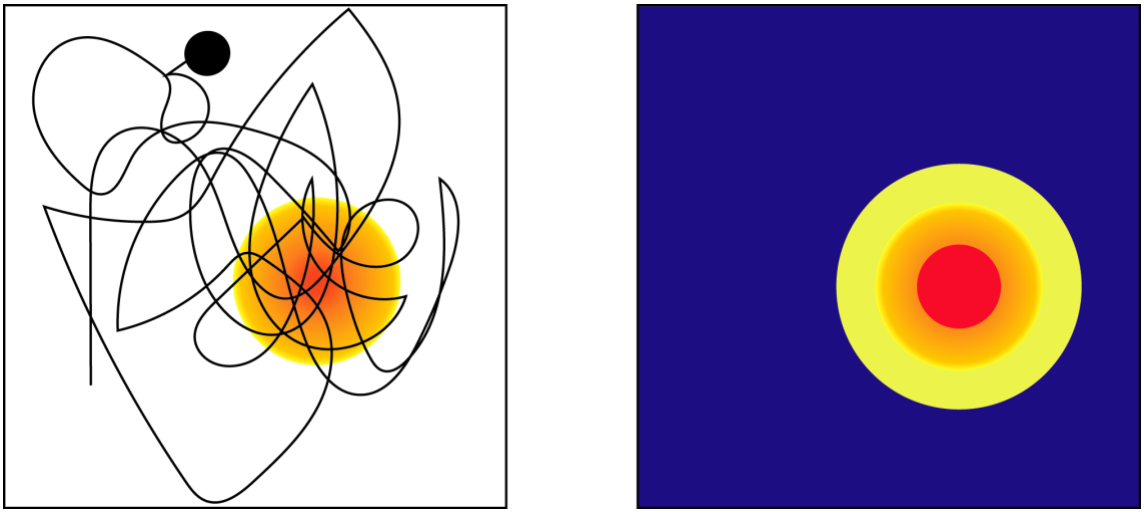

Figure 1. Place cells. A cartoon of the location of a rodent over time in a box is presented on the left. The rodent is the black dot, its path is the thin black line, and the location where one place cell in CA1 is active is demarcated by the yellow and orange circle. On the right, a cartoon of a heatmap of the firing of the place cell is overlaid on the box. The cell is active when the animal is in a specific location, and therefore the cell is a place cell (adapted from Moser et al., 2015).

The hippocampus can thus be thought of as the neural substrate of the cognitive map, an internal representation of the world (O'Keefe and Nadel, 1978; Tolman, 1948). Place cells (**Figure 1**), are one example of this cognitive map (O'Keefe and Dostrovky, 1971). To maintain a behaviorally relevant schema, hippocampal neurons, including place cells, must be able to flexibly reconfigure how they respond to external stimuli, particularly when those stimuli are important, or

when contingencies for reinforcement change (Colgin et al., 2008). This is evident during a spatial learning paradigm known as goal oriented learning (GOL), where place cells shift their place fields toward rewarded locations (Danielson et al., 2016b; Dupret et al., 2013; Hollup et al., 2001; Kaufman et al., 2020; Turi et al., 2019; Xu et al., 2019; Zaremba et al., 2017). However, the mechanism for this shift is unknown.

Neuromodulation is a good candidate mechanism for place field shifts toward rewards for several reasons – neuromodulators influence how neurons respond to the excitatory or inhibitory inputs they already receive, they tend to be released during different kinds of behavioral states that involve uncertainty (Yu and Dayan, 2005), and dopaminergic input (one form of neuromodulation) from the ventral tegmental area (VTA) has been shown to improve place cell representations of reward (McNamara et al., 2014). The hippocampus is under neuromodulatory control from a variety of sources (Palacios-filardo and Mellor, 2019). We chose to focus on the locus coeruleus (LC), a brainstem nucleus that projects throughout the brain and releases norepinephrine and a small amount of dopamine, because two recent publications stimulated the projections from the locus coeruleus to area CA1 of the hippocampus (LC-CA1), and found that this stimulation improved performance on spatial memory tasks (Duszkiewicz et al., 2019; Kempadoo et al., 2016; Takeuchi et al., 2016).

The degree of place field shifts toward rewards also predicts performance on spatial memory tasks (Danielson et al., 2016b; Dupret et al., 2013; Hok et al., 2007; Hollup et al., 2001; Kobayashi et al., 2003; Zaremba et al., 2017). Our lab has consistently demonstrated that place fields tend to shift toward rewards when a reward is presented in a novel location in a familiar environment (Danielson et al., 2016b; Kaufman et al., 2020; Turi et al., 2019; Zaremba et al., 2017). Therefore, we hypothesized that the LC-CA1 projection might be involved in these place

field shifts toward rewarded locations. We performed a series of experiments that examined the activity of the LC-CA1 during a GOL task.

We used several state-of the art tools in these *in vivo* studies. Calcium imaging uses fluorescent indicators of cellular calcium concentrations, which are interpreted as a proxy for neural activity. The development of genetically encoded calcium indicators, such as GCaMP, which is constructed from a circularly permuted green fluorescent protein (cpGFP), calmodulin (CaM), and the Ca^{2+}/CaM-binding "M13" peptide (Akerboom et al., 2012), has allowed for visualization of the activity of specific types of cells. While calcium activity can be examined with many types of microscopy, we used two-photon microscopy. Two-photon microscopes are particularly useful in our studies for several reasons – they use a wavelength of light where each photon contains half the necessary energy to excite fluorescent molecules, thus requiring two photons to excite each molecule to fluoresce. Because this event is rare, a small number of fluorescent molecules will be excited at once. When light is emitted from a single point, it spreads out as distance increases from that point, in a pattern called the point spread function. If multiple fluorescent molecules are excited simultaneously, their point spread functions will overlap, making resolution of small structures difficult. Two-photon microscopy is therefore excellently suited for the study of small compartments, such as axons (Denk et al., 1990; Lichtman and Denk, 2011). Additionally, since two-photon microscopy uses wavelengths with lower energy than one-photon microscopy, is less damaging to tissues than one-photon microscopy, and these longer wavelengths penetrate deeper and scatter less in tissue; these two properties make it an ideal tool for imaging deep structures and for chronic imaging that is necessary to study processes such as learning. Finally, two-photon microscopy allows the recording of large populations of cells compared with electrical recordings, allowing for the effective study of learning-related population dynamics of

neural representations. We also used optogenetics, which allows for activation and inactivation of neurons with light-activated ion channels (Deisseroth, 2015).

We used a genetically encoded calcium indicator expressed in the LC, along with two-photon imaging of the LC-CA1 projection, and found that this projection was differentially active at a novel rewarded location compared with a familiar one. Optogenetic stimulation of the LC-CA1 projection near a familiar rewarded location led to place field shifts toward that location. Inhibition of the LC-CA1 projection near a novel reward prevented place field shifts in experimental, but not control mice. Stimulating the LC-CA1 projection far from a reward did not lead to place field shifts toward the stimulated location. Finally, stimulating the LC-CA1 projection during a non-spatial task in which rewards were randomly delivered did not cause place field shifts toward the stimulated location, either alone, in conjunction with the addition of a cue, or in combination with stimulation of disinhibitory circuits to depolarize the pyramidal neurons. We conclude that the LC-CA1 projection acts in combination with other as yet unknown factors that are active near rewards to influence place field shifts. This work was performed in close collaboration with a postdoctoral fellow in the lab, Dr. Tristan Geiller, and was recently published in Neuron (Kaufman et al., 2020).

A possible candidate mechanism for the effects of the LC-CA1 projection on place fields is the effect of neuromodulators on astrocytes. Astrocytes respond to neuromodulators with large calcium signals, which may lead to changes in the function of neurons. We investigated the calcium activity of HPC astrocytes during behavior, and determined that astrocytes in the hippocampus show large calcium signals during behavior, similar to their activity in other brain areas (Bekar et al., 2008; Paukert et al., 2014; Takata et al., 2011). However, consistent with published data, astrocytes are not active every time a particular stimulus occurs (Paukert et al.,

2014). It has been shown that astrocytes respond with large calcium increases only after a large, consistent signal from the LC (Oe et al., 2020).

In recently published study, astrocytes were shown to integrate information over long timescales, then influencing behavior (Mu et al., 2019). It is possible that astrocytes need a certain threshold of norepinephrine (or dopamine) to be received from the LC in order to initiate downstream signaling consequences of responses to neuromodulators; it is also possible that astrocytes, perhaps depending on the circuit in which they are located, either require simultaneous input from different neuromodulatory systems, or there may be a threshold that can be passed either by one neuromodulator, or a combination of neuromodulators (Hirase et al., 2014).

Within the hippocampus, neuromodulatory projections, while relatively ubiquitous, are not homogeneous in the degree of innervation across hippocampal layers and subregions (Palacios-filardo and Mellor, 2019). We observed differences in the activity levels of astrocytes in different layers of the hippocampus, with astrocytes in the stratum radiatum being more active and perhaps slightly more synchronous than astrocytes in the stratum pyramidale and stratum oriens. It is unknown whether this is due to differences in the astrocytes themselves, as has been observed across brain areas (Lin et al., 2017; Morel et al., 2019) or even within brain areas (Martin et al., 2015), differences in neuromodulatory input to the astrocytes either in type or amount, or differences in the surrounding neural milieu that could potentially affect astrocyte responses.

The differences we observed across hippocampal layers were relatively consistent across the behavioral paradigms we tested, including simple rewarded running on a treadmill, running for non-spatially delivered rewards in a cued context, and running for spatially delivered rewards. In another behavioral paradigm, several stimuli of neutral, rewarding or aversive valences were

delivered in a randomized order and at randomized times. This paradigm evoked more responses, and more consistent responses, across hippocampal astrocytes in all measured layers.

Furthermore, while the calcium activity of astrocytes within a field of view was highly correlated, there were occasional large calcium signals that occurred in individual or a few astrocytes, as well as astrocytes that did not participate in all large calcium events. The degree of astrocyte participation in calcium responses during certain types of behavioral events should be quantified. Additionally, it is unknown whether astrocytes are spatially tuned, although we believe this is unlikely to be the case, given that in awake animals, astrocytes are more likely to respond to events such as startle than the types of stimuli that the surrounding brain areas normally respond to, such as visual stimuli, whisker stimulation, or movement (Bekar et al., 2008; Paukert et al., 2014).

We have obtained and modified a tool in the lab to manipulate astrocyte function, an inducible mouse line to knock out the IP3R2 (Srinivasan et al., 2015), which is downstream of Gq-coupled receptor signaling, selectively in astrocytes using a mouse line that expresses inducible Cre in astrocytes on the Aldh1L1 promoter (Srinivasan et al., 2016). We confirmed that the IP3R2 is selectively knocked out in astrocytes via immunohistochemistry. While we have not yet had the opportunity to use this tool, it could help to clarify the role of astrocytes as an active player in neural plasticity.

Overall, this thesis implicates neuromodulatory input from the LC-CA1 projection to the HPC as a player in reward-related place field reorganization. It presents an interesting hypothesis that part of the mechanism of action of this input could be achieved though astrocytes, perhaps representing a brain-wide mechanism whereby neuromodulators use astrocytes to amplify and

broadcast their effects to many synapses in a particular brain region. Whether this is true remains unresolved.

In addition to providing ample opportunities for future research, this study significantly contributes to the body of literature on place field shifts around rewards, and perhaps provides a possible mechanism for place field shifts in general, as well as gain-related effects of LC signaling.

Hippocampal formation

Cognitive maps and memory

The concept of a cognitive map, an internal representation of the world, has been a part of neuroscience for over half a century (Tolman, 1948). Another foundational concept in neuroscience is that the brain devotes more resources, and therefore, more neurons, to representing important stimuli. Additionally, studying how, when and why internal representations of the external world change with learning and over time can help us understand what happens when this process goes awry, as it can in psychiatric diseases or dementia.

The hippocampus is implicated as a likely substrate of cognitive maps. It is involved in episodic memory, the type of memory that allows us to describe experiences such as what we had for breakfast (Eichenbaum, 2017). This is perhaps a form of cognitive map that represents our experiences. The hippocampus was discovered to be involved in memory in a tragic surgery that was intended to cure the epilepsy of Henry Molaison, a patient known as H.M. until his death. The epilepsy originated in the medial temporal lobe, where the hippocampus is located, and since no one knew the function of this brain area, his surgeon, Dr. Scoville decided to bilaterally remove parts of the medial temporal lobe that included the hippocampus and parts of the entorhinal and perirhinal cortices (Andersen et al., 2007). After the surgery, H.M. had severe, nearly total

anterograde amnesia, and could not form new episodic memories, as detailed in many years of research conducted by Dr. Brenda Milner (Milner, 2005). However, his older memories remained intact, indicating that the hippocampus is involved in transferring memory from short term to long term, whereby it must be represented in another location.

Cellular substrates of hippocampal navigational and memory functions: 'place cells'

Since vital function of the hippocampus had recently been discovered, researchers wanted to learn more about its function in animal models. Using electrophysiology, a method by which the activity of neurons can be recorded using wires lowered into the brain, researchers began studying the hippocampus of rats. Surprisingly, scientists discovered a more literal form of cognitive map, known as place cells (O'Keefe and Dostrovky, 1971; O'Keefe and Nadel, 1978). Place cells are neurons which are active at specific locations in an environment, known as the place field of the cell (**Figure 1**). Subsequent studies have added many details to our understanding of when place cells are active (Dupret et al., 2010; Harris et al., 2003; Leutgeb et al., 2008, 2004; Xu et al., 2018), how they may form (Bittner et al., 2017, 2015), how they change their representations over time (Ziv et al., 2013), and what types of factors influence how stable their representations of space remain over time (Kentros et al., 2004). Place cells have also been described in other animals, including bats (Ulanovsky and Moss, 2007), non-human primates (Rueckemann and Buffalo, 2017), and humans (Tsitsiklis et al., 2020).

Several other types of spatially responsive cells have also been discovered, including grid cells in the entorhinal cortex, the major input to the hippocampus (Hafting et al., 2005). These cells are active in specific locations, like place cells, but their firing fields are repeated in a hexagonal pattern that tiles the entire environment. Other types of spatial cells include head direction cells,

which fire at a preferred direction of the head, border cells, which fire as animals approach borders, and conjunctive cells that respond to multiple types of spatial stimuli, such as combined border/head direction cells (Moser et al., 2015).

Rather than representing a simple neural GPS, recent studies have begun to describe place-like cells that represent conceptual patterns. For example, an elegant study from the Tank lab at Princeton found that when rats need to navigate within a "tone space," using a joystick to make a constant tone increase or decrease in pitch, and remember the tone at which a reward is delivered, they develop "tone space cells" that selectively fire in response to different tones. These tone cells do not fire when the tones are played separately from the context in which the rewards are delivered (Aronov et al., 2017). Similar cells have been found to represent a "smell space," and other cells such as time cells have been described as well (Fischler et al., 2019; Kraus et al., 2013). These studies may help resolve the dual functions of the hippocampus as a memory apparatus and navigational structure, since they indicate a more general function, returning to the concept of a cognitive map of conceptual spaces and patterns, much like memory.

The 'Engram' concept

Another concept that has helped to tie together the memory and navigational functions of the hippocampus is the engram. Several years ago, in a seminal study from the Tonegawa lab, a mouse was developed that allowed researchers to mark which cells were active in a particular context. They determined that the same set of cells was active over repeated exposures to the same context, and that optogenetic reactivation of those cells caused mice to behave in the manner they had behaved in the original context, freezing after contextual fear conditioning (Liu et al., 2012). This has been replicated in multiple studies, showing that reactivation of engrams can influence

learning and behavior (Poo et al., 2016; Tonegawa et al., 2015), describing how engrams are affected by time of exposure to environments, and that they are less consistent in aged mice (Cai et al., 2016). Other studies have shown that over time, engrams shift from the hippocampus into the prefrontal cortex (Tonegawa et al., 2018), perhaps explaining the specific anterograde memory deficit exhibited by H.M. after bilateral removal of the hippocampus.

The phenomenon that is used to study engrams is known as immediate early genes (IEGs). These are a set of genes that quickly increase their expression in response to novel stimuli. Engrams take advantage of this concept, with researchers either staining for the presence of IEGs or expressing indicators or optogenetic effectors on the promoters of IEGs. However, they are an imperfect tool, partially because the function of IEGs, the circumstances in which they are expressed, and the relationship between IEG expression and neural activity, specifically place cells, is not fully understood (Tanaka et al., 2018).

The hippocampal circuit and place cell formation

In studying how the hippocampus acts as a substrate for the cognitive map, it is important to describe the inputs, outputs and circuit within the hippocampus. The structure of the hippocampus is evolutionarily conserved, and although this circuit is slightly different in humans, and I will focus on the rodent circuit, since that is our model of choice. The hippocampus is a bilateral structure that extends quite far in the anterior-posterior direction. The more anterior and superior part of the hippocampus in rodents is known as the dorsal hippocampus, while the more posterior and ventral part is the ventral hippocampus. The dorsal hippocampus contains place cells and other tuned cells, while the ventral hippocampus, while it also contains place cells, represents some emotion-related stimuli such as those that are associated with anxiety (Jimenez et al., 2018).

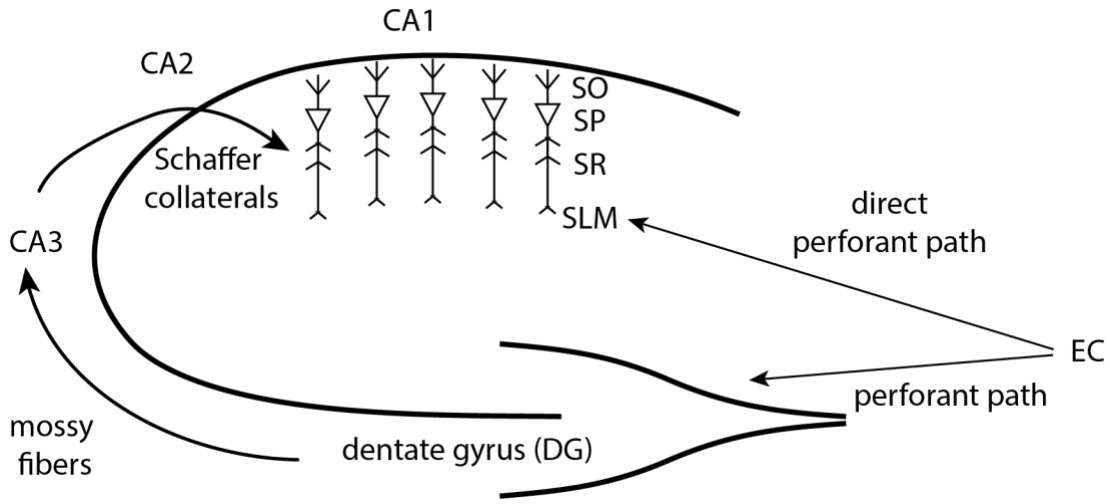

Figure 2. Hippocampal layers and circuit. A diagram of the dorsal hippocampus. Major areas of the hippocampus are the dentate gyrus (DG), cornu ammonis 3 (CA3), cornu ammonis 2 (CA2) and cornu ammonis 1 (CA1). Inputs to the hippocampus come from the entorhinal cortex (EC) via the perforant path. These inputs either synapse directly onto distal dendrites of pyramidal cells in CA1 (CA1PCs), or travel to CA1 via the trisynaptic pathway, from the DG to CA3 via mossy fibers, then CA1 via Schaffer collaterals. Different cellular compartments of CA1PCs are located in different layers in CA1 – the stratum oriens (SO) is the most dorsal, followed by the stratum pyramidale (SP), where cell bodies of PCs are located, then the stratum radiatum (SR), which contains PC dendrites and the synapses coming from CA3, then the stratum lacunosum moleculare (SLM), which is innervated directly by the EC. The orientation of CA1PCs is demonstrated. Adapted from Basu and Siegelbaum, 2015.

Cortical inputs to the hippocampus mostly come from layers two and three of the entorhinal cortex (**Figure 2)**. The major output of the hippocampus is the subiculum and deep layer of the entorhinal cortex (EC), which then projects to cortical and subcortical regions (Andersen et al., 2007). Within the hippocampus, the first element in the trisynaptic circuit is the dentate gyrus (DG), which is thought to be involved in pattern separation. Small, densely packed granule cells provide a sparse representation of different contexts, and the DG is one of the few areas in the adult brain where neurogenesis occurs and new granule cells are integrated into the network (Tuncdemir et al., 2019). The DG then projects to area CA3 via mossy fibers. CA3 contains pyramidal cells with highly recurrent connections, hypothesized to allow for pattern completion

(Leutgeb and Leutgeb, 2007). CA3 is somewhat similar to the major output structure of the hippocampus, with a row of pyramidal neurons in the pyramidal layer. In the canonical trisynaptic circuit, CA3 then projects to CA1, the principal output structure of the hippocampus (Basu and Siegelbaum, 2015). Place cells have been observed in all three of these locations, the dentate, CA3, and CA1, and are extensively studied in CA1. CA2, a small and rarely studied area between CA3 and CA1, is thought to represent social stimuli, and contains receptors for molecules such as oxytocin and vasopressin that are thought to be involved in social interactions (Donegan et al., 2019; Hitti and Siegelbaum, 2014).

Because the HPC is an older part of the cortex known as archicortex, it has a simpler three-layered structure compared with the six layers of the evolutionarily more recent neocortex (Andersen et al., 2007). In area CA1 of the hippocampus, the principal neurons, pyramidal cells (CA1PCs) that are thought to carry information, are positioned in the tightly packed pyramidal layer, or stratum pyramidale (SP). A subset of these neurons will become place cells in a given environment. Dendrites extend in both directions, up into the stratum oriens (SO), and down into the stratum radiatum (SR), where they receive input from CA3, and further down into the stratum lacunosum moleculare (SLM), where they form an apical tuft. SLM receives input from another pathway, known as the temporo-ammonic pathway or direct perforant path, which projects directly from the entorhinal cortex (Andersen et al., 2007). A precise relationship between the timing of inputs onto pyramidal neurons from the perforant path and the trisynaptic pathway has been shown to cause a form of plasticity known as STDP, or spike timing dependent plasticity (Basu and Siegelbaum, 2015).

The mechanism of place cell formation is still unknown

Place cells provide a remarkable neural readout of experience, but the way they form is still unknown. When grid cells were discovered in one of the primary input structures to the HPC, the medial entorhinal cortex (mEC), it was hypothesized that place cells were generated from the integration of grid cell information (Bush et al., 2014). However, studies inactivating grid cells in the mEC did not prevent place cell activity or formation, casting doubt on this model (Brandon et al., 2015; Sasaki et al., 2015). Researchers have also examined plasticity within the hippocampus itself to gain insight into mechanisms of place cell formation.

A form of plasticity that involves NMDA receptors at the apical tuft of CA1PCs, in SLM, is known as a plateau potential. These plateau potentials occur spontaneously before place field formation, and their induction at the apical tuft of pyramidal neurons has been shown to lead to the subsequent experimentally induced formation of a place field (Bittner et al., 2015). Additionally, before the plateau potential occurs, there is a small rise in membrane potential, known as a ramp, that begins several seconds before the eventual formation of a place field. This form of plasticity is called behavioral time scale plasticity, or BTSP, because unlike traditional forms of plasticity, it occurs over a seconds-long timescale, the timescale of behavioral events (Bittner et al., 2017). While it is not fully understood how place fields form, this promising set of publications from the Magee lab has improved our understanding of the ingredients that may be required to form place cells. Other labs have shown that place fields can form with injection of current directly into neurons (Diamantaki et al., 2018), but this does not agree with results from the Magee lab, which showed that plateau potentials were required (Bittner et al., 2015). Dendritic excitability, synapses, and NMDA receptors are also all affected by neuromodulators, making their contributions a necessary extension of the place cell formation model (Magee and Grienberger, 2020).

Interneurons

There are a wide variety of inhibitory interneuron subtypes across the brain, and within the hippocampus they have been relatively well characterized, although more work is needed to understand their precise functions (Klausberger and Somogyi, 2008). These subtypes differ with respect to cellular markers, their location across the layers of the hippocampus, and their subcellular targets such as somata, the axon initial segment or specific parts of the dendrites. Some, the interneuron specific interneurons, selectively target other interneurons such that their activity will disinhibit pyramidal neurons (Francavilla et al., 2018). Different interneurons are also known to be selectively active at different phases during behavioral state-dependent network oscillations such as theta (Klausberger and Somogyi, 2008) and sharp wave ripples (Buzsáki, 2015). Other, more long ranging interneurons, project to the hippocampus from different brain areas such as the medial septum and the entorhinal cortex.

Oscillations

Oscillations are a brain phenomenon that can be measured using local field potential (LFP) recordings. The activity of individual neurons creates an electrical signal that can be broken down into components that oscillate at different frequencies using a Fourier transform. While the exact mechanism by which oscillations occur, and their function, is still incompletely understood (Buzsáki et al., 2016), they correlate well with different behavioral states, such as locomotion or resting (Buzsáki and Tingley, 2019). When different brain areas oscillate at the same frequency, they are thought to be acting together (Buzsáki and Schomburg, 2016).

Theta, an oscillation that occurs at a frequency of 6-10 Hz, can be measured in with an electrode or silicon probe placed within the pyramidal layer of the hippocampus (Colgin, 2016). It is known to occur during running in rodents. Theta also occurs during visual exploration of environments in humans and primates (Hoffman et al., 2013; Jutras et al., 2013). Taken together, this suggests that theta occurs during attentive states. One putative source of synchronized firing that is read out as the hippocampal theta rhythm are parvalbumin-expressing interneurons (PV neurons) that are located in the medial septum and project to the hippocampus (Amilhon et al., 2015).

As animals traverse a place field multiple times, its place cells gradually begin to fire earlier than the normal phase of extracellular theta, a phenomenon known as phase precession (Colgin, 2016; Skaggs et al., 1996). While theta generally occurs during locomotion or other attentive states, a phenomenon that occurs during resting is known as sharp wave ripples. During REM sleep and other resting states, sudden fast bursts of synchronized pyramidal cell activity occur (Buzsáki, 2015). These are known as sharp wave ripples (SWRs); the sequence of neuronal firing during SWRs often occurs in the same order as recent place cell activity, in which case it is called replay (Louie and Wilson, 2001; Wilson and Mcnaughton, 1994) while if it occurs in the reverse order it is known as reverse replay. These SWRs are thought to be involved in strengthening the co-activity of neurons that occur during important or salient events, and the frequency with which they occur is associated with better performance on spatial memory tasks (Dupret et al., 2010). Another phenomenon, known as preplay, describes sequential activity of neurons that occurs before animals are even exposed to a particular environment, and is hypothesized to reflect an innate state of the hippocampal network (Dragoi and Tonegawa, 2011; Grosmark and Buzsáki, 2016).

Subcortical inputs to the hippocampus

The hippocampus receives input from different subcortical structures. These provide neuromodulatory input – broadly defined, neuromodulators affect the way neurons respond to excitatory or inhibitory inputs that they receive. The medial septum (MS), whose PV interneurons are a putative source of the theta rhythm, also provides acetylcholine via cholinergic inputs. The diagonal band of Broca also provides cholinergic input to the hippocampus (Palacios-filardo and Mellor, 2019).

The ventral tegmental area (VTA) provides dopaminergic input to the hippocampus. It is thought to be involved in reward-related signaling during spatial learning (Dupret et al., 2013, 2010; McNamara et al., 2014). However, its input is much more sparse than would be expected given the strong effect of dopamine on lasting changes to synaptic strength (Kempadoo et al., 2016; Takeuchi et al., 2016).

Another subcortical input to the hippocampus, the locus coeruleus (LC), canonically releases norepinephrine, but has been shown to release a small amount of dopamine as well, perhaps helping resolve the mystery of the sparse VTA projection to the hippocampus (Beas et al., 2018; Kempadoo et al., 2016; Smith and Greene, 2012; Takeuchi et al., 2016). The LC is a brainstem nucleus that projects throughout the brain, including the hippocampus. Stimulating projections from the LC to are CA1 of the hippocampus improves performance on spatial memory tasks (Kempadoo et al., 2016; Takeuchi et al., 2016), while inhibiting LC projections to CA3 during exposure to a context during fear conditioning prevents a fear response upon re-exposure to the context (Wagatsuma et al., 2018). This suggests that the LC may be involved in affecting hippocampal responses to important or salient stimuli or situations.

Long term synaptic plasticity

Long term potentiation (LTP) was discovered by Bliss and Lomo while recording from the dentate gyrus of rabbits after stimulation of the perforant path. They observed an increase in excitability of granule cells after perforant path stimulation (Bliss and Lomo, 1973). LTP has subsequently been studied throughout the brain, and much of this research is performed in the hippocampus. LTP is thought to be the one of the primary mechanisms by which synapses increase in strength. LTP is commonly read out using electrophysiology, through an increase in neural responses to synaptic stimulation. The initial discovery that neurons, through repeated co-activity, physically increase the size of their connections, resulted in Eric Kandel's Nobel prize (Asok et al., 2019). It provided evidence for Donald Hebb's famous concept that neurons that fire together wire together (Hebb, 1949). One of the major mechanisms of LTP is coincidence detection via the NMDA receptor, which allows for the flux of ions only during concomitant postsynaptic depolarization and presynaptic glutamate release, initiating downstream signaling cascades via the use of calcium as a second messenger (Asok et al., 2019). Synapses must be able not only to strengthen, but also decrease their strength when they are no longer needed. This is known as long term depression (LTD) (Lisman, 2017).

The mechanisms of both LTP and LTD involve changes in receptor expression, including AMPA receptors and NMDA receptors. LTP also has different time courses – the induction of LTP may not always last, and when it does it is known as late LTP – these processes each require different mechanisms (Lisman, 2017). STDP occurs via LTP or LTD (Basu and Siegelbaum, 2015), while the mechanism for BTSP is still unclear (Bittner et al., 2017).

Neuromodulation plays a role in synaptic plasticity as well, both LTP and LTD. It is thought that dopamine may be involved in marking specific synapses for strengthening, known as

the synaptic tagging and capture hypothesis (Redondo and Morris, 2011). This is supported by the finding that blocking dopamine receptors prevents both LTP and spatial learning (Lisman et al., 2017; Takeuchi et al., 2013; Wang et al., 2010). Acetylcholine is thought to be involved in LTP and LTD (Hasselmo, 2006; Palacios-filardo and Mellor, 2019), while norepinephrine can also facilitate LTP in CA1, and LTP and LTD in the DG-CA3 circuits. Serotonin can enhance LTP expression in CA1 also (Palacios-filardo and Mellor, 2019).

The hippocampus and goal oriented spatial learning

Given the fact that the hippocampus contains place cells, it is unsurprising that it is involved in learning to navigate spaces. One type of spatial learning paradigm, known as goal-oriented learning (GOL), encompasses a broad range of tasks during which animals must learn and remember the location of a goal, either a reward or the removal or an aversive stimulus. One of the first studies to show that this type of task required the hippocampus was performed by Richard Morris. He designed the now commonly used Morris water maze, in which animals are placed in a pool of water and need to learn and remember the location of a hidden platform in relation to cues. After a hippocampal lesion, animals were unable to find the platform (Morris et al., 1982). A similar GOL task is called a Barnes maze, in which animals are in a box with a bright light and a loud sound which are turned off when the animal goes to a specific location within the box (Barnes, 1979). Another version is a cheeseboard maze, in which rewards are located in a few of many holes, and animals learn where the rewards are located (Lopez et al., 2010). This is also similar to a sandwell digging task that is used by the Morris lab (Takeuchi et al., 2016).

All of the above GOL paradigms are performed with freely moving animals. Two-photon calcium imaging requires head fixation. To adapt these tasks to a head-fixed paradigm, the

Losonczy lab designed a tactile environment using a treadmill belt containing different types of fabrics and textural cues, similar to a paradigm used by Attila at Janelia (Royer et al., 2012). Animals are water deprived, and given a water reward if they lick a spot in a certain location on the belt relative to cues. The first studies in the lab using this paradigm showed that mice learn the task and the hippocampus forms place cells (Danielson et al., 2016b, 2016a; Zaremba et al., 2017), and it has since been used by other labs (Bittner et al., 2017, 2015), and adapted to visual stimuli in a virtual reality setup by multiple labs (Dombeck et al., 2007; Gauthier and Tank, 2018a; Sheffield and Dombeck, 2014).

Rewards are a particularly salient stimulus. If an animal obtains a reward, it would be useful to remember the sequence of actions leading to the reward. In fact, in a study with human participants where people navigated around a virtual environment, objects that were randomly presented just before a reward were remembered better than objects that were presented at other times during the task (Braun et al., 2018). A general principal of neuroscience is that more neurons are devoted to representing more important stimuli in the world. Accordingly, place cells have repeatedly been shown to overrepresent rewarded locations in GOL tasks (Danielson et al., 2016b; Hok et al., 2007; Hollup et al., 2001; Kobayashi et al., 1997; Turi et al., 2019; Zaremba et al., 2017).

Using the head fixed tactile GOL task, our lab showed that place fields shift toward an unfamiliar rewarded location in a familiar environment. Along the dorsal-ventral axis of the pyramidal layer, deep cells, which are closer to the stratum oriens, shifted more easily toward rewards and in response to environmental changes, while superficial cells, which are closer to the stratum radiatum, were more stable (Danielson et al., 2016b). In addition, in a mouse model of schizophrenia, animals did not learn the task as well as control mice, and their place cells also did

not shift toward rewarded locations (Zaremba et al., 2017). In fact, the degree of place field shifts toward reward is correlated with behavioral performance on GOL tasks (Dupret et al., 2013). Even grid cells, which were thought to be relatively invariant even across environments, show some remapping toward rewards, but only in spatial tasks (Butler et al., 2019; Xu et al., 2012). One study found a dedicated population of reward cells that followed a shifting reward location (Gauthier and Tank, 2018), but these results are not consistent with results from our lab, perhaps due to differing task structure.

Not only do place fields shift toward rewards, but they also more stably represent the same location in an environment when animals perform spatial tasks, rather than randomly foraging for rewards. This was found to be disrupted by dopamine antagonists, leading to the hypothesis that greater attention leads to a more stable representation (Kentros et al., 2004).

Taken together, these results suggest that place fields are influenced by attention and learning, either making global representations more stable, or shifting place fields toward rewarded locations. The role of dopamine in place field stability, and LTP, combined with a suggested role of the LC in attention, points to neuromodulation from the LC as a possible player in reward-related place field reorganization.

Neuromodulation

The line between a neuromodulator and a neurotransmitter can be somewhat blurry, but broadly defined, excitatory neurotransmitters (such as glutamate) and inhibitory neurotransmitters (such as GABA and glycine), make neurons more or less likely to fire, respectively. One definition of a neuromodulator is a substance that affects a neuron's response to neurotransmitters, or its intrinsic firing properties (Marder, 2012). They are often released at sites that are not conventional

synapses, a phenomenon known as bulk release or volume transmission, and can affect receptors that are located extrasynaptically (Hirase et al., 2014). In this way, they can affect the activity of many neurons simultaneously. The neuromodulators I will focus on are serotonin, acetylcholine, dopamine, and norepinephrine.

Neuromodulation is conserved

Neuromodulation is conserved across species. One of the pioneers in the field of neuromodulation, Eve Marder, performed her research on the crab stomatogastric ganglion. She found that the application of neuromodulators profoundly changed the firing patterns of stomatogastric ganglion neurons, and in more natural scenarios, are released during different behavioral states and profoundly affect circuit function (Marder, 2012). Cori Bargmann studies neuromodulation in c. elegans, where serotonin can change their entire behavioral program, switching them from a resting state into a wandering state (Flavell et al., 2013). In drosophila melanogaster, dopaminergic signaling is well-studied, and has a profound effect on neural activity via different receptor types (Handler et al., 2019), while serotonin can influence motor responses (Howard et al., 2019), and octopamine, the drosophila analog of norepinephrine, indirectly affects the responses of dopaminergic cells in drosophila larvae via signaling through astrocytes (Ma et al., 2016).

Experimental approaches to measure neuromodulator release

The activity of neuromodulators can be studied in a variety of ways. One can study anatomy, and determine the location of receptors for neuromodulators, as well as the location of vesicles. There is also voltammetry, which measures the presence of certain chemicals due to their

electrical charges and can be performed in vivo (Donita et al., 2003). Additionally, microdialysis can be performed, followed by techniques such as high performance liquid chromatography (HPLC) to determine which substances are present in brain slices or in cerebrospinal fluid (CSF) taken from the brain (Kempadoo et al., 2016). Electrophysiology can be performed on the cell bodies of within neuromodulatory brain areas. One can also image the activity of projecting neuromodulatory fibers using fiber photometry (Li et al., 2019).

Fluorescent false neurotransmitters, which are similar in structure to the neurotransmitter in question, can also be used to visualize the release of transmitters (Rodriguez et al., 2013). Recently, more fluorescent tools have been developed to visualize various neuromodulators, such as dLight (Patriarchi et al., 2018).

One can also image calcium concentrations in axons. This does not provide a direct measure of neurotransmitter or neuromodulator release, but it is a proxy for axonal activity, and is commonly used as such (Basu et al., 2016; Howe and Dombeck, 2016; Kaifosh et al., 2013). Two-photon imaging provides single axon, and in some cases, single synapse resolution. This is the method that we have chosen to study the activity of the LC-HPC projection (Kaufman et al., 2020).

Serotonin

The serotonergic system is implicated in depression. Selective serotonin reuptake inhibitors are one of the most commonly prescribed antidepressants. The median raphe (MR) projects thoughout the brain and provides serotoninergic input. Serotonin may also be involved in learning. There are seven families of seroninin recpetors, 5-HT1 through 5-HT7, and all of them are G protein coupled except the 5HT3, which are ionotropic. Serotonin can increase excitability and facilitate LTP in CA1. However, it is mostly inhibitory in CA3, and prevents LTP and LTP at

mossy fiber-CA3 synapses. Thus, serotonin signaling can have quite diverse effects (Palacios-filardo and Mellor, 2019).

Acetylcholine

Acetylcholine is released in response to both rewarding and aversive stimuli (Hangya et al., 2015). Acetylcholine is also thought to help process novelty, in situations of "expected uncertainty," such as foraging in a new environment, while norepinephrine is posited to be active in situations of "unexpected uncertainty," such as an initial trial of a reversal learning task, where reward contingencies are changed (Hasselmo, 2006; Yu and Dayan, 2005).

The sources of acetylcholine in the brain are the medial septum (MS) and diagonal band of broca (DBB), and the nucleus basalis of Meynert (NB). The hippocampus primarily receives cholinergic input from the MS and DBB (Palacios-filardo and Mellor, 2019).

There are two major types of receptors for acetylcholine, the ionotropic and metabotropic receptors. Ionotropic receptors are ion channels, while metabotropic affect downstream signaling via second messengers. The nicotinic acetylcholine receptors are ionotropic receptors that flux cations, including sodium, potassium and, depending on the subtype, calcium (Palacios-filardo and Mellor, 2019). One subtype of nicotinic acetylcholine receptors, the α7nAChR, is located on astrocytes, and may be involved in the regulation of sleep (Papouin et al., 2017).

Metabotropic receptors exist in two major groups, the M1/M3/M5, and M2/M4. The M1/3/5 subtypes are Gq coupled receptors, resulting in an increase in intracellular calcium and thus have a primarily excitatory effect, while the M2/M4 signal through Gi/o, usually resulting in an inhibitory effect (Palacios-filardo and Mellor, 2019). Given that these two subtypes have

opposite effects on their downstream targets, it can be difficult to predict the effects of acetylcholine release.

Catecholamine synthesis

Catecholamines are a group of molecules that include dopamine, epinephrine and norepinephrine. They are molecularly similar, and share a synthesis pathway. Briefly, tyrosine is converted into 3, 4-dihydroxyphenylalanine (L-DOPA) by tyrosine hydroxylase (Th). Then, aromatic L-amino acid decarboxylase (AADC), converts L-DOPA to dopamine. In neurons that use norepinephrine or epinephrine, dopamine is then converted to norepinephrine by dopamine beta hydroxylate (DBH), and phenylethanolamine N-methyltransferase (PNMT) converts norepinephrine into epinephrine (Kandel et al., 2013).

Dopamine

Dopamine has two major functions in the brain. The first is the control of movement, while the second major function is to signal the presence of salient stimuli, either appetitive or aversive. The major sources of dopamine within the brain are the substantia nigra (SN) and ventral tegmental area (VTA) (Kandel et al., 2013). The role of dopamine in signaling appetitive and aversive stimuli was first described in the context of reward signaling. One of the major figure in this field is Wolfram Schultz, who published a series of studies on the relationship between dopamine and reward in primates. During associative conditioning, in which a cue is presented, followed by a reward, dopamine is initially released when the reward is delivered. After multiple trials, however, the dopaminergic signal is transferred to the cue, rather than the reward. If the reward is not delivered as expected, there is a decrease in dopamine release, known as the reward prediction

error (RPE). This indicates that dopamine plays a significant role in learning (Schultz, 2016). A relatively recent study imaging dopaminergic axons within the striatum found the activity of some to be correlated with movement, while the activity of others was correlated with reward (Howe and Dombeck, 2016).

Similarly to the metabotropic acetylcholine receptors, there are two major classes of dopamine receptors, both of which are metabotropic. The D1/D3/D5 class of receptors are Gq coupled, and cause an increase in intracellular calcium, thus having a mostly excitatory effect. The D2/D4 class of receptors signals are Gi coupled, and their activation has an inhibitory effect (Kandel et al., 2013).

Norepinephrine

The LC is a small nucleus located in the pons within the brainstem that projects throughout the brain. LC neurons project 90% ipsilaterally, and their axons are mostly unmyelinated, releasing transmitter via bulk release rather than active zones (Foote et al., 1983). However, even with a small number of cells, the anatomy is specialized – more anterior portions of the nucleus project more anteriorly within the brain, while more posterior regions tend to project more posteriorly. However, LC neurons seem to receive similar inputs (Schwarz et al., 2015).

Norepinephrine is involved in signaling new or surprising stimuli. One of the early major figures in this field, Gary Aston-Jones, published a series of studies in primates recording from the LC. He found that these neurons respond to sudden, surprising stimuli, but as these stimuli become predictable, the response ceases (Aston-jones, 1994; Aston-jones et al., 1999). The LC exhibits two major firing patterns: tonic, where it is active at a certain firing rate during waking and attentive states, and phasic, a brief, large increase in activity causing a sudden increase in the

release of norepinephrine. These phasic bursts are the type of signal that occurs in response to surprising or startling stimuli.

LC neurons are more active during waking, and less active during sleep (Swift et al., 2018). The LC is also more active during in novel environments (Takeuchi et al., 2016). Unlike the VTA, the LC does not appear to signal a reward prediction error. However, it does seem to predict the delivery of rewards in certain circumstances (Sara and Bouret, 2012). The LC may be involved in learning; LC projections to the amygdala are required for fear conditioning, while LC projections to the prefrontal cortex are required for extinction of the same fear response (Uematsu et al., 2017) LC neurons also may be involved in neurodegenerative disease; they are some of the first neurons to degenerate in Alzheimer's, chemogenetic rescue of LC neuronal activity improves learning in an Alzheimer's rat model (Rorabaugh et al., 2017; Weinshenker, 2018), and the integrity of the LC in humans predicts performance on certain memory tasks (Mather and Harley, 2016).

There are several types of adrenergic receptors, all metabotropic (Foote et al., 1983). In the brain, the beta receptors can initiate LTP (O'Dell et al., 2015). $\alpha 1$ adrenergic receptors act through Gq signaling, while $\alpha 2$ adrenergic receptors are inhibitory, and are expressed at LC terminals to provide negative feedback (Foote et al., 1983).

Projections from the LC have recently been found to release not only norepinephrine, but a small amount of dopamine (Beas et al., 2018; Kempadoo et al., 2016; Smith and Greene, 2012; Takeuchi et al., 2016). This makes sense, since norepinephrine is synthesized from dopamine within the synaptic vesicle. Faster release may change the balance between norepinephrine and dopamine, if vesicles are released before dopamine is converted to norepinephrine. This added role of the LC in providing both dopaminergic and noradrenergic signals provides a vital new avenue

of study, and the ways in which the LC and VTA may act separately or synergistically have yet to be clarified.

Neuromodulation in the hippocampus

The hippocampus receives many types of neuromodulatory input, with a wide variety of effects (Palacios-filardo and Mellor, 2019).

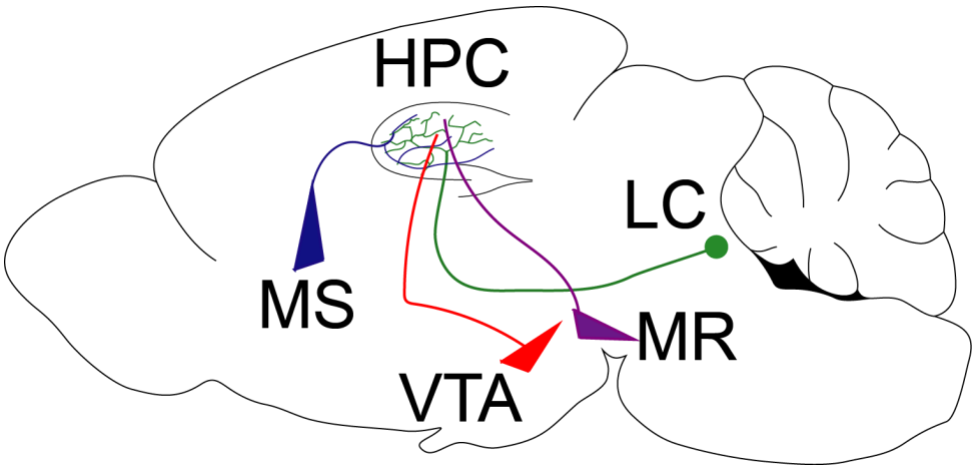

Figure 3. Major neuromodulatory projections to the hippocampus. The hippocampus (HPC) receives neuromodulatory input from multiple structures. The medial septum (MS) sends cholinergic, while the ventral tegmental area (VTA) sends dopaminergic projections, the median raphe (MR) sends serotoninergic projections, and the locus coeruleus (LC) sends noradrenergic projections that can also release a small amount of dopamine.

The effects of dopamine may be the best understood of all the neuromodulatory influences on the hippocampus. Dopamine is required for LTP, and the synaptic tag and capture hypothesis states that dopamine marks specific synapses for strengthening, implicating it in memory formation (Wang et al., 2010). Given the role of dopamine in reward signaling, and the role of the hippocampus in spatial learning, it follows that hippocampal dopamine would be involved in spatial reward learning. The VTA is active near rewarded locations, and its activation improves

performance on spatial memory tasks (Gomperts et al., 2015; McNamara et al., 2014). Blocking D1/D5 dopamine receptors prevents learning of a new rule for finding rewards (Retailleau and Morris, 2018).

The LC is also involved in spatial learning, as described earlier. LC stimulation improves performance on a sandwell digging task, as well as a Barnes maze (Kempadoo et al., 2016; Takeuchi et al., 2016). Both of these publications found that this effect could by blocked by pharmacological inhibition of D1/D5 receptors, but not beta 1 adrenergic receptors, indicating that the LC effect is mediated via dopamine. However, one caveat of this interpretation is that the authors did not block other types of adrenergic receptors.

The LC strongly innervates the dentate gyrus (DG), and its activation causes LTP in dentate neurons (Walling and Harley, 2004). One recent study found that LC neurons show a specific activity pattern in relation to sharp wave ripples. Additionally, when the LC was activated abnormally during sleep (at a rate that did not cause the animals to wake up), animals had trouble learning a novel location of a reward, while they still remembered the old location they had already learned (Swift et al., 2018). Neuromodulatory influences on the hippocampus, and throughout the brain, has many important and varied effects, but these effects and the mechanisms by which they happen have yet to be fully understood (Palacios-filardo and Mellor, 2019).

Astrocytes

In the field of neuroscience, often the first focus is on the principal cells of each region, what kind of information they process, and how they connect with other regions to form circuits. Additional players have begun to be considered, such as inhibitory interneurons and neuromodulators. Another crucial, yet too often overlooked component of the brain are glial cells.

Glia, which means “glue” in Greek, were initially thought just to provide a structural component of the brain. However, they have many vital functions (Barres, 2008).

There are different classes of glial cells. Microglia are immune cells of the brain, similar to macrophages, and they play a crucial role in responding to invasion, but also a crucial role in development and adulthood, due to the fact that they engulf unnecessary synapses (Stevens et al., 2007). Astrocytes seem to participate in a very wide variety of processes. I chose to focus on astrocytes because they respond to neuromodulatory input with large increases in intracellular calcium, and thus may affect neural responses to neuromodulators (Bazargani and Attwell, 2016; Hirase et al., 2014).

Major roles of astrocytes

Astrocytes evenly tile the entire central nervous system with nonoverlapping territories of branches that end in fine processes. These fine processes surround synapses, taking up potassium to maintain ionic balance and restore it after an action potential, preventing spillover of neurotransmitter to maintain synaptic specificity, and taking up neurotransmitter to maintain temporal specificity of signals, as well as to break down transmitters and shuttle the components back to neurons (Liddelow and Barres, 2015). They do not depolarize the way that neurons do, rather they sit at a low resting membrane potential due to the presence of potassium leak channels. They express excitatory amino acid transporters 1 and 2 (EAAT1, EAAT2), which take up glutamate, and GAT, which takes up GABA (Barres, 2008).

Among the roles that astrocytes play, some vital ones are releasing signaling molecules during development for synapse formation (Kucukdereli et al., 2011), engulfing synapses during development (Chung et al., 2013; Clarke and Barres, 2013), helping form the blood brain barrier

and regulating blood flow (Attwell et al., 2010; Gordon et al., 2011; Liddelow and Barres, 2015). During sleep, astrocytes clear waste from the brain. They express water channels, such as Aquaporin 4 (Aqp4), which are required for this function (Iliff et al., 2012). They may also be involved in regulating sleep pressure (Florian et al., 2011; Halassa et al., 2009).

Astrocytes also respond to injury by going into a reactive state. If there is a direct central nervous system mechanical insult, they form what is known as a glial scar, which serves a protective function (Anderson et al., 2014, 2019). There is also a range of types of reactivity; Ben Barres's lab published a series of papers describing two major types of reactive astrocytes, A1 and A2. After an ischemic insult, astrocytes develop an A1 phenotype, which tends to be more neuroprotective, while after an intraperitoneal injection of lipopolysaccharide, a sugar found on the surface of bacteria, astrocytes develop an A2 reactive phenotype, which results in neurotoxicity (Liddelow et al., 2017; Zamanian et al., 2012). The adaptive function of this neurotoxicity is not understood, but it is known that microglia instruct the astrocytes to kill neurons (Liddelow et al., 2017). Astrocytes also develop a reactive phenotype during normal aging, making this a possible target to ameliorate problems associated with aging (Boisvert et al., 2018).

Astrocytes may play a role in learning. They release lactate, which provides energy for neurons, and is required for long term memory formation (Suzuki et al., 2011). Additionally, when astrocytes are activated via an optically activateable Gq-coupled receptor, it causes neural potentiation and improved performance on a contextual fear conditioning task (Adamsky et al., 2018).

Astrocytic calcium signals

One of the most salient, yet still poorly understood properties of astrocytes are the large calcium signals that they exhibit in response to neuromodulators and some neurotransmitters (Bazargani and Attwell, 2016). Although all the receptors that astrocytes express has not yet fully been described, it is known that they express receptors for acetylcholine, norepinephrine, and dopamine. These may also be regionally specific, perhaps depending on the surrounding circuitry (Molofsky et al., 2012; Zhang and Barres, 2010).

There are different types of astrocyte calcium signals that may have different sources. One type is the large, somatic calcium signals, while another is the smaller, more localized signals that occur in the fine processes (Haustein et al., 2014; Shigetomi et al., 2016; Srinivasan et al., 2016). The larger signals appear to be caused by activation of the inositol triphosphate receptor (IP3R), which is downstream of metabotropic receptors, usually G-protein coupled receptors (GPCRs) that signal through Gq. They have been shown to occur in response to glutamate (earlier in development), norepinephrine, acetylcholine, and dopamine (Agulhon et al., 2008; Bazargani and Attwell, 2016; Bekar et al., 2008; Hirase et al., 2014; Paukert et al., 2014; Takata et al., 2011; Wang et al., 2012). The smaller signals can also occur in response to norepinephrine (Srinivasan et al., 2015), and their source could be from external calcium (Shigetomi et al., 2016) or from the brief opening of the mitochondrial transitional membrane pore, which fluxes a small amount of calcium (Agarwal et al., 2017).

The function of either of these types of signals is still unknown. One earlier set of studies performed a battery of behavioral tests on mice missing the IP3R2, the subtype selectively found in astrocytes. Both a developmental and inducible knockout did not show any differences in any of the behaviors assayed, including spatial learning and reversal learning (Petravicz et al., 2014, 2008). Other studies, however, have begun to tease apart possible roles for these signals using the

same knockout mice. In one set of studies, stimulation of the NB caused LTP in the barrel cortex when paired with whisker stimulation, but this was abolished with IP3R2 knockout (Takata et al., 2011). Astrocyte calcium signals may also have a relationship with neural oscillations; increasing astrocyte calcium using halorhodopsin increased the power of the gamma frequency band in visual cortex (Poskanzer and Yuste, 2016, 2011).

What happens after these calcium signals occur in astrocytes? One elegant study from Maiken Nedergaard's lab showed that astrocyte calcium increases cause more Na^+/Ca^{2+} exchange, increasing the sodium concentration and increasing activity of the Na^+/K^+ ATPase. An increase in K^+ uptake by astrocytes would cause a decrease in extracellular potassium, causing an efflux of potassium from neurons and thus lowering their resting membrane potential. This lowered membrane potential would increase the signal to noise ratio of neuronal responses to inputs by making them less responsive to small inputs, but more responsive to large inputs (Wang et al., 2012).

Astrocyte calcium signals are also conserved across species, implying that they serve an important function. In drosophila larvae, astrocyte calcium signals occur in response to octopamine, the fly analog of norepinephrine, activating a TRP channel and causing the astrocytes to increase the activity of dopaminergic neurons (Ma et al., 2016). Zebrafish larvae also exhibit astrocyte calcium signals, which tend to occur after repeated behavioral mismatches between motor action and surrounding stimuli that cause them to give up swimming (Mu et al., 2019). Astrocyte calcium signals in mice appear to increase in magnitude when the surrounding cortex is presumed to be active, such as V1 astrocytes in visual cortex, but only in combination with a startle response. This may allow astrocytes to respond differently to their surrounding circuit (Paukert et al., 2014).

Conclusion

The hippocampus is an excellent brain area to study experience dependent changes in circuit dynamics, neural plasticity, as well as the relationship between neuromodulators, astrocytes and neural circuit function. This is due to its relatively well-characterized circuitry, its inputs from neuromodulatory regions, and the presence of place cells, a cellular readout that corresponds well to behavior and is known to change during learning. Area CA1 of the hippocampus has a laminar structure, with the cell bodies and dendrites of pyramidal neurons in separate locations, permitting the study of astrocytes near different cellular compartments.

Thus far, the mechanisms for place field plasticity around rewards, and the relationship between neuromodulators, astrocytes and neural plasticity are not fully understood. This study was able to provide a link between neuromodulation from the LC and place field plasticity, and to describe differences between astrocytes in different lamina of the hippocampus. Future studies can help clarify the relationship between neuromodulation, astrocyte function, and place fields.

Chapter 1: A role for the locus coeruleus in place cell reorganization during spatial reward learning[1]

We investigated the activity of CA1-projecting LC fibers (LC-CA1) in a head-fixed goal-oriented spatial learning (GOL) task (Danielson et al., 2016b; Turi et al., 2019; Zaremba et al., 2017) and tested their contribution to the reorganization of HPC CA1 place cells. We found that LC-CA1 projections exhibited increased activity near a new reward location, where CA1 place

[1] This Chapter was adapted from a publication in *Neuron* (Kaufman, Geiller and Losonczy, 2020).

cells normally become enriched. Optogenetic activation of LC-CA1 axons near the reward induced place cell overrepresentation of a familiar rewarded location, enhancing reward-related place cell plasticity, while optogenetic inhibition of LC-CA1 axons suppressed place cell overrepresentation. LC stimulation only affected place fields near rewarded locations; in a paradigm where animals did not learn goal locations, LC activation had no effect, and neither did conjunctive activation of multiple GOL-supporting circuits, indicating a task-dependent nature for this mechanism. We conclude that the LC is a key player in inducing place cell reorganization, and that it likely acts in conjunction with other factors that are differentially active near rewards. All work in this chapter was performed in collaboration with Dr. Tristan Geiller. We both performed surgeries, trained the mice, and collected the data. Dr. Geiller did a large part of the analysis using the lab code base that was written by previous graduate students, and I assisted with analysis.

1.1 Methods

Viruses

Recombinant adeno-associated viruses (rAAVs) were used for GCaMP6 and optogenetic channel expression. Cre-dependent bReaChes, a red-excitation shifted variant of channelrhodopsin (Rajasethupathy et al., 2015), expression was achieved with rAAV2/9:Ef1α-(bReaChes-tdTomato)$_{Cre}$ (obtained from Dr. Boris Zemelman, UT Texas, Austin), GCaMP6s expression in the LC with rAAV 2/9:Ef1α-(GCaMP6s)$_{Cre}$ (Dr. Boris Zemelman, UT Texas, Austin). For expression in HPC CA1 pyramidal neurons, rAAV2/1:hSyn-GCaMP6f and rAAV2/1:CaMKII-GCaMP6f were used (see Tables of Reagents and Resources, Viruses). For experiments with viral mixtures, viruses were mixed in a 1:1 ratio. If animals were used for multiple experiments, they were trained on a burlap belt between paradigms.

Viral injection and hippocampal window/headpost implant

Viral injections were performed with a Nanoject syringe, as previously described (Lovett-Barron et al., 2014). Briefly, mice were anesthetized with isofluorane and treated with buprenorphine or meloxicam to minimize postoperative discomfort. The skull was exposed and a hole was drilled, and a sterile glass capillary containing viral mixtures was lowered into the brain. After injections, the skin was sutured and mice were allowed to recover. The LC was injected bilaterally at coordinates AP -5.45 mm, ML ±1.28 mm, and DV -3.65 mm with 150 – 300 nL of virus. The dorsal HPC area CA1 was injected in the left hemisphere at coordinates from Bregma AP -2.1 or -2.2, ML -1.5 or -1.75, and DV -1.2, -1.1, and -1.0 with 50-64 nL of virus at each DV site. Mice were implanted with an imaging window (diameter 3.0 mm, height 1.5 mm) over the left dorsal-intermediate hippocampus with a stainless-steel or brass headpost. Imaging cannulas were constructed by adhering (Norland optical adhesive) a 3-mm glass coverslip (64-0720, Warner) to the steel cannula (Ziggy's tubes and wires). The surgical procedure has been described previously (Lovett-Barron et al., 2014). Briefly, mice were anesthetized and treated with buprenorphine or meloxicam, the skull was exposed and a 3 mm hole was made in the skull. Bone, dura and cortical layers were removed, while flushing with ice-cold cortex buffer. The cannula was inserted into the hole, secured with Vetbond, and a headpost was affixed to the skull with dental cement. Mice recovered in their home cage, and were monitored for three days post-surgery.

***In vivo* calcium two-photon imaging and optogenetics**

Imaging was conducted using a two-photon 8 kHz resonant scanner (Bruker). A piezoelectric crystal was coupled to the objective as described previously (Danielson et al., 2016b) in order to allow fast displacement along the Z-axis. The objective was a Nikon 40x NIR water

immersion, 0.8 NA, 3.5 mm working distance. The excitation laser was 920 nm (50-100 mW, Coherent Ultra II). For some structural images in red, the laser was 1070 nm (Coherent Fidelity), and scanning was interlaced with the 920 nm laser for green excitation. Red (tdTomato) and green (GCaMP6) channels were separated by emission cubes as described previously (Danielson et al., 2016b). Fluorescence signals were collected using photon multiplier tubes (PMT, GaAsP PMT, Hamamatsu R3896). A preamp (1.4 x 105 dB, Bruker) was used to amplify signals before digitization. Pockels cells were used to regulate the power of the LED reaching the tissue. Images were acquired at 1x digital zoom, 1.2, or 1.4, with 512 x 512 pixels. For pyramidal neurons, two separate planes were acquired from 20 μm and up to 30 μm apart, with the piezo waiting to settle at each plane for 35ms, such that the frame rate was about 8 Hz. For axons, 2-5 planes 2 μm apart were acquired to maintain the axon in the z plane.

For optogenetic experiments, a dichroic mirror was used to allow red light to pass through into the brain, and green light to be reflected into the PMT. The stimulation was performed with an ultrafast and high-power collimated LED, at 625 nm (Prizmatix, 625 nm). It was triggered using an Arduino board that gated the inverse photostimulation signal of the Pockels cell, which turns off briefly between mirror turnaround, as well as when the piezo reverses direction. The average power of the LED was 35-70 mW measured under the objective. This approach allowed us to protect our PMTs from the high intensity illumination but still take the advantage of the fast, full frame resonant galvo scanning without losing frames during photostimulation.

Behavioral experiments

Mice were trained on a cue-free burlap belt. 3-4 days after the implantation surgery, they were water deprived. First, they were habituated to head fixation for several 10-minute sessions.

Then they were allowed to lick freely for water, which was delivered initially at 15 locations on the belt. Then the animals were required to lick initially to receive the water reward, and each day the reward schedule was gradually dropped to 3 rewards per two meter burlap belt. Training took approximately 10 days. During imaging, mice ran on an unfamiliar cued belt, with multiple types of fabric and cues. For HPC CA1 pyramidal cells imaging, we used multisensory cues, including a constant stream of pinene-scented air, a blinking ultraviolet LED, and a constant tone. For the LC imaging, since LC axons are sensitive to multisensory stimuli, and we wanted to examine signals in response to behavioral factors, these additional stimuli were not used. The mice ran three 10-minute sessions per day, separated by at least forty-five minutes. The mice were required to lick initially for the reward, and rewards were available in the location for a maximum of two seconds.

For random foraging during pyramidal cell recordings and LED stimulation, animals were habituated to the belt 3x for 1 day to have stable place fields, then they ran 3 x 10-minute sessions per day for three days. LED stimulation began on the third session of the first imaging day, and continued for 5-6 sessions. Behavioral performance was assessed by the proportion of licks in the area immediately preceding the reward zone, beginning 35 cm before the reward. All behavioral training and experiments were done using software developed in the lab by another graduate student, Jack Bowler.

Calcium imaging data preprocessing

The preprocessing steps for the raw fluorescence signal have been described elsewhere (Danielson et al., 2016b). Briefly, the imaging data was motion corrected using the SIMA software package (Kaifosh et al., 2014). Frames where the motion correction failed were discarded if they

were below a certain threshold of similarity to the time-averaged image of the entire calcium video. Pyramidal neurons or LC-CA1 axons were hand-segmented using a data visualization server program developed in the lab. The same LC-CA1 axons and pyramidal neurons were transferred across sessions wherever possible, and identified with a unique ID, so that their activity across sessions could be tracked. Relative fluorescence changes in pyramidal neurons ($\Delta F/F$) were computed with a baseline calculation method adapted from Jia et al.(Jia et al., 2011), with uniform smoothing window $t_1 = 3s$ and baseline size $t_2 = 60s$. For pyramidal cells, we detected statistically significant transients as described previously (Danielson et al., 2016b) to use for place field calculations. More analyses were implemented using Python using custom written scripts.

For axons, the details are located in **Figure 1.S1**. We first determined that the axons were synchronous by looking at the mean pairwise correlation coefficient in each session for each ROI (axon segment). A shuffle distribution of pairwise correlation coefficients was generated by taking the same axon at different sessions in time. The 99th percentile of the shuffle distribution constituted the threshold for each animal above which ROIs were included in the analyses. For each session, the remaining axons were simplified as a single trace by taking the first principal component of the signal. We finally removed any linear trends in the resulting trace over chunks of 80s of data (in case the bleaching process occurred exponentially), and smoothed using a Savitzky-Golay filter (sliding window of 21 frames, polynomial degree 6).

Place cell metrics

Detailed methods for determining statistically significant place cells and their place fields, and the enrichment of the place fields around the reward zone are described (Danielson et al., 2016b; Zaremba et al., 2017). Briefly, for each pyramidal cell, calcium transients with onsets

during running bouts of at least 1 s in duration were used to calculate the spatial information of the cell (Skaggs et al., 1993). Transients were randomly shuffled to different times during the running events, and the spatial information was recalculated. One thousand iterations were performed to create a null distribution for spatial information, and the cell was considered to be a place cell if its spatial information was above the 95th percentile of the null distribution. The belt was evenly divided into 100 spatial bins, and the place field was calculated from its transient rate map over these bins. The rate map was the number of transients in a given spatial bin normalized by the animal's occupancy in that spatial bin, which was then smoothed with a Gaussian kernel (s = 3 spatial bins). To detect individual place fields, each local maximum of the smoothed rate map was fitted with a Gaussian curve centered at that location. For each smoothed rate map, the place fields where the associated Gaussian was smaller than 50% of the largest Gaussian (by measuring the total area under the curve) were discarded. The remaining Gaussians were considered place fields. The centroid of each place field was determined by the location of the peak of the Gaussian, and the location of the centroid of the largest place field was used for enrichment analysis.

Enrichment was determined by the proportion of place fields with centroids in the area beginning 25 cm before the reward zone spanning to the end of the zone. The transient frequency was calculated as the rate of significant transients detected by the method described above. The duration of the transient was taken as the beginning and end of the transient, normalized by the frame rate. The amplitude was the peak of the $\Delta F/F$ signal. For each statistically significant transient of a place cell, the area under the curve (**Figure 1.S3A**) was computed as the sum of the calcium fluorescence signal during the transient duration, normalized by the frame rate.

For **Figure 1.S3C**, the place cells with place fields outside the reward zone on session 1 were plotted according to the location of their centroids on subsequent sessions. Place fields within

the reward zone on session 5 were plotted on previous and subsequent sessions as well. The proportion of place cells inside the reward zone compared with cells outside the reward zone was averaged across sessions before the LED (sessions 1-4, LED off), and across sessions with the LED (**Figure 1.S3D**, LED on). Recurrence probability (**Figure 1.S3B**) was calculated by taking the place fields within the reward zone on day 9 in control and experimental groups, and determining the proportion of those cells that were place cells on previous days.

Generalized linear model

We use a generalized linear model to re-generate the calcium activity as a linear function of behavioral variables (Allen et al., 2017; Pinto and Dan, 2015; Turi et al., 2019). Fitting the GLM coefficients entails finding the linear combination of behavioral covariates which optimally predicts the calcium signal of LC axons. The following behavior variables were used: velocity, licking, and position. All the variables (except position) were smoothed with a Gaussian kernel (σ = 50ms). For the position signal, we divided the treadmill into 100 non-overlapping bins, which were represented in the model by 100 corresponding binary variables that were equal to one during times when the animal occupied that spatial bin and zero otherwise (**Figure 1.S1G**). These behavior variables were fitted to the calcium activity using ridge regression, to manage potential collinearity of predictors and avoid overfitting.

For cross-validation, the calcium activity was divided into blocks corresponding to the number of laps in the session. We trained the model on (*n-1*) laps and then tested on the held-out lap. The testing lap was then rotated to cover all the *n* laps of the session. Finally, we concatenated all the tested laps to have the cross-validated predicted trace of the entire session. The regularization penalty was optimized separately through cross-validation on the training set, before

fitting the final model on the full training set and evaluating prediction quality on the test set. To assess fit quality, we calculated the coefficient of determination (R_2) between the model's predicted axonal calcium activity and the actual axonal calcium activity. To estimate the specific contribution of each category of behavior variables, we also trained a reduced model which contained all variables except the variable of interest. We then calculated the (base-2) log-likelihood ratio between the full model and the reduced model, normalized by the number of time samples, to estimate the information gained (in bits/sample) by including the missing variable. This measure was also estimated only from the held-out test data in the cross-validation procedure.

Linear regression between speed and fluorescence signal in LC

In order to assess the amplitude of the overshoot of activity seen in the LC signal in the second phase of the goal-oriented task when the animal approaches the reward zone, we looked at the linear relationship between the velocity of the animal and the calcium trace (**Figure 1.2G**). The rationale behind this analysis is that it is impractical to estimate a baseline to generate ΔF/F values (either static or dynamic) since the activity tracks velocity (as seen in the GLM analysis, **Figure 1.2C**), and differences in ΔF/F are small. The relationship between velocity and the calcium trace was the best measure to detect changes in LC signal without altering or transforming the data to get rid of the velocity component. We computed a linear regression between the two variables in the window -35 to 0 cm before the reward, and extracted the slope of the fit.

Histology and immunohistochemistry

After the last imaging sessions mice were put under deep isoflurane anesthesia and transcardially perfused with 0.1 M PBS followed by 4% paraformaldehyde in 0.1 M PBS. After

overnight post-fixation in the same solution the brains were transferred to PBS. The LC was sliced with a vibratome into 50 μm slices, while the hippocampus was sliced into 50-70 μm slices. Slices were washed 3x with 0.1 M PB, then washed in tris-buffered saline (TBS) with 0.3% triton (TBST) several times, incubated in 10% normal donkey serum in TBS for 45 minutes, then incubated for 1 hour at room temperature and for ~2 days in primary antibodies: slices were incubated with the following antibodies (for details see Tables of Reagents and Resources: Antibodies): anti-GFP, anti-dsRed, or anti-Th (either chicken or rabbit). The slices were then washed with TBS several times and incubated with the appropriate secondary antibodies. The slices were rinsed, mounted with Aquamount, and imaged on a confocal microscope.

Statistics

No statistical methods were used to predetermine sample sizes, but our sample sizes are similar to those reported in previous publications. For all the analyses, if data points followed a normal distribution (confirmed using the Kolmogorov-Smirnov test), depending on the type of comparison, a two-tailed paired sample or unpaired t-test was applied. For non-normal distributions, depending on the type of comparison, the non-parametric two-tailed paired-sample Wilcoxon signed rank test or two-tailed unpaired Mann-Whitney U test was used. If a sample had fewer than five data points, a non-parametric test was used as we did not have enough statistical power to test for normality. *, $p < 0.05$, **, $p < 0.01$, ***, $p < 0.001$.

1.2 Results

In order to assess the activity of place cells during GOL, mice were intracranially injected with a recombinant adeno-associated virus (rAAV) expressing GCaMP6f under a CaMKII

promoter, and a cannula was implanted over dorsal CA1. Under the two-photon microscope, the mice performed the GOL task on a 2-meter treadmill belt containing tactile cues (**Figure 1.1A**, see **Methods**). During GOL, an operantly delivered water reward was given in one location for three days (reward zone 1, RZ1), and was then moved to a second location for the last three days (reward zone 2, RZ2, **Figure 1.1A**) (Danielson et al., 2016b; Turi et al., 2019; Zaremba et al., 2017). Learning was assessed by the proportion of licks inside the reward zone (**Figure 1.1B, C**) (Danielson et al., 2016b; Turi et al., 2019; Zaremba et al., 2017). Pyramidal cells located in the CA1 pyramidal layer (CA1PCs) were imaged, and a subset of these was determined to be place cells based upon their spatially tuned activity (**Fig. 1.1D, Methods**). Previous studies have shown that place fields of CA1PCs become enriched around a new reward location, but not the first location, thus remapping around a translocated reward (Danielson et al., 2016b; Turi et al., 2019; Zaremba et al., 2017). We analyzed the degree of reward overrepresentation in all the control mice we used in this study, and found that reward overrepresentation was absent during the first reward portion of the task, and pronounced in the last session of the second reward zone (**Figure 1.1E, F**). We hypothesized that this enrichment could be caused by differential activity of LC-CA1 projections around the translocated reward.

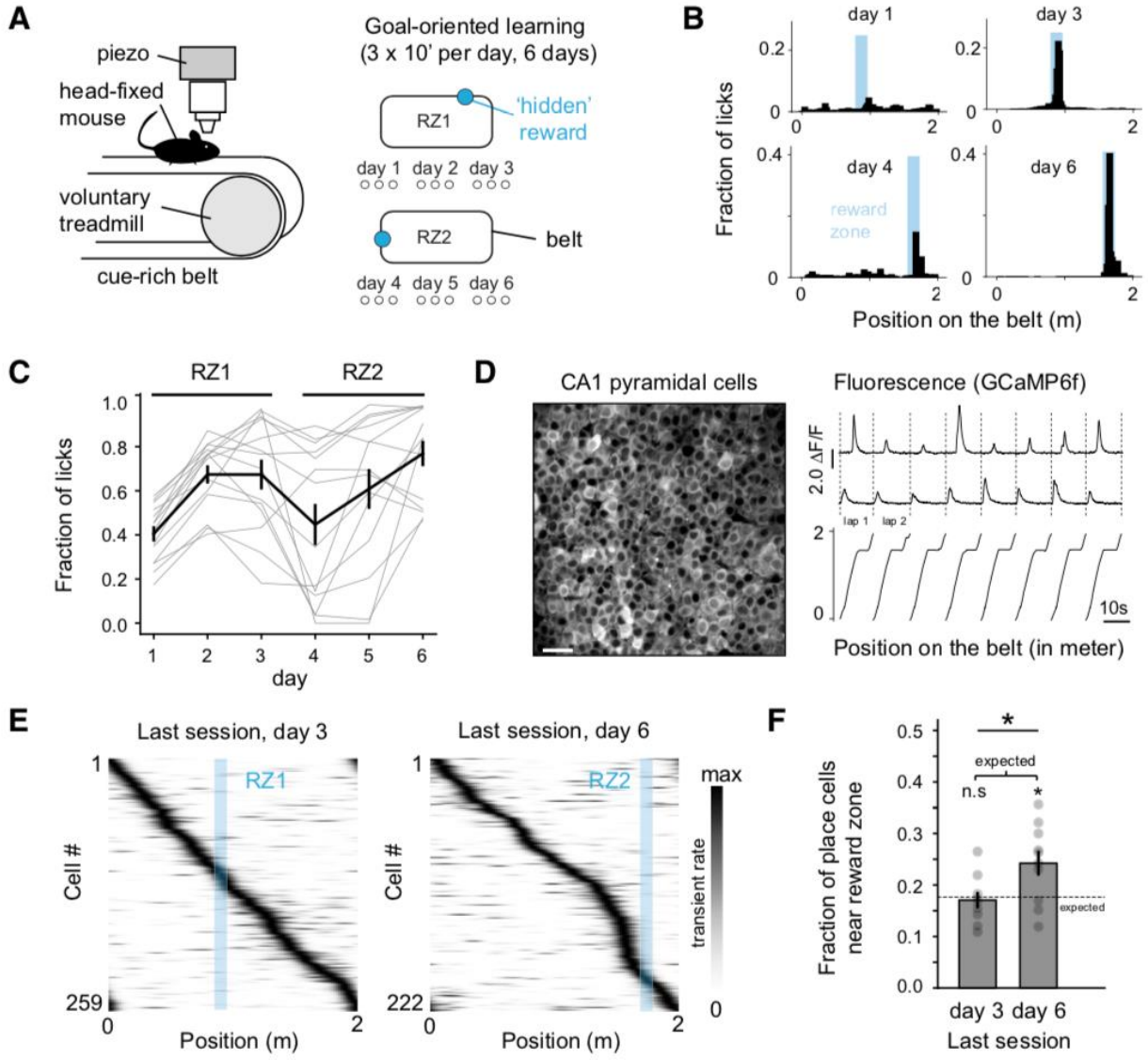

Figure 1.1. Place Cells Are Enriched at a Translocated Reward Site during GOL (A) The goal-oriented learning (GOL) task. Mice searched for an unmarked reward zone (RZ), and water rewards were delivered operantly within the fixed 10-cm zone. The RZ was at the same location for 3 days and then moved to a new location. (B) Representative licking from one mouse. Histograms: fraction of total number of licks in each position bin (n = 100). Blue shaded areas: RZs. (C) Fraction of licks within the RZ aggregated by session and plotted by day (thick line and bars: mean ± SEM; thin gray lines: individual animals). (D) Left: time-averaged image from a representative recording session with 2p GCaMP6f imaging in CA1PCs. Right: relative GCaMP-calcium fluorescence (Δ*F*/*F*) traces from two example place cells. Scale bar: 50 μm.

(E) Example place cell tuning curves in the last session of RZ1 and RZ2. Rows: average tuning curves for individual cells along the linearized belt, normalized by peak activity. Blue shaded area: RZ location. (F) Percentage of place cells (mean ± SEM) in the peri-reward zone (pRZ) defined as the RZ + 25 cm preceding the zone. The last session of day6 (RZ2) shows enrichment compared with day3 (RZ1). Dashed line: percentage of place cells expected from a uniform distribution along the belt (day3: 0.17 ± 0.045, day6: 0.242 ± 0.07, unpaired two- tailed t test; $t_{(18)} = 2.4$, $p = 0.02$. One-sample two- tailed t test for expected value derived from the uniform distribution; day3: $t_{(8)} = 0.36$, $p = 0.72$, day 6: $t_{(9)} = 2.72$, $p = 0.02$). See also Figure 1.S2-1.S4.

To assess the activity of LC-CA1 projections, we injected a Cre-dependent rAAV into the LC of Th-IRES-Cre$^{+/-}$ mice to express GCaMP6s in tyrosine hydroxylase (Th)-positive LC neurons, and implanted an imaging cannula over dorsal CA1 (**Figure 1.2A**). We tracked the same LC-CA1 fibers in mice performing the GOL task (**Figure 1.2B**). LC-CA1 fiber activity in each field of view was highly synchronous, with a small subset of inactive fibers (**Figure 1.S1**, **Methods**).

We first determined how different behavioral variables contributed to LC-CA1 activity during GOL by training a generalized linear model (GLM) (Turi et al., 2019) on three different covariates: position, velocity, and licking (**Figure 1.1G**, **Methods**). We assessed the quality of the model by computing the cross-validated coefficient of determination R^2 on the held-out test data (**Figure 1.2C**, **Methods**). We observed that R^2 values were higher in RZ2 than RZ1 (**Figure 1.2D**). To determine the contribution of the different variables in each zone, we computed the log-likelihood ratio between the full and reduced models, in which a given variable was omitted (**Figure 1.S1H,I**, **Methods**). The contribution of position significantly increased in the second zone while velocity and licking remained constant (**Figure 1.2D**). We reasoned that the increase was due to differences in LC-CA1 activity at specific locations, and so we decided to examine the calcium signals around each RZ.

When the mouse approached RZ1, the LC-CA1 signal rose and fell with velocity (**Figure 1.2E, F**). After translocation of the reward, when the mouse approached RZ2, LC-CA1 activity was less correlated with velocity, manifested in a dip, followed by an overshoot (**Figure 1.2E, F**). This overshoot preceded the reward, and developed on the first day of the second zone, consistent with a predictive reward signal (Bouret and Sara, 2004). We quantified the degree of the overshoot using a linear regression between the velocity and the axonal calcium traces just before the reward onset (**Methods**), and found that LC activity became gradually decorrelated from velocity after the reward zone was moved (**Figure 1.2G**, **Methods**). The less LC-CA1 activity was correlated with velocity, the better the mice performed on the task (**Figure 1.2H**), and in mice that did not learn the second reward location, LC activity remained correlated with velocity (**Figure 1.2G**, non-learning). The decorrelation from velocity began in the first few sessions of the second reward zone, while in the first zone, velocity and the LC-CA1 signal remained correlated (**Figure 1.2A**). The correlation began to decrease even during the first few laps of the first session, decreasing during the first few laps each day (**Figure 1.2A**). We pooled place cell enrichment data from two previous publications in the lab (Danielson et al., 2016b; Zaremba et al., 2017), which showed that the place field enrichment also gradually increased across sessions in the second zone (**Figure 1.S2C**). The decorrelation of the LC signal begins before the place cell enrichment, and is maintained over time while enrichment increases (**Figure 1.S2D**). We did not see an LC-CA1 response near the old reward zone after the reward was moved, nor did we see an increased LC-CA1 response near the new reward zone before it was moved (**Figure 1.S2E**).

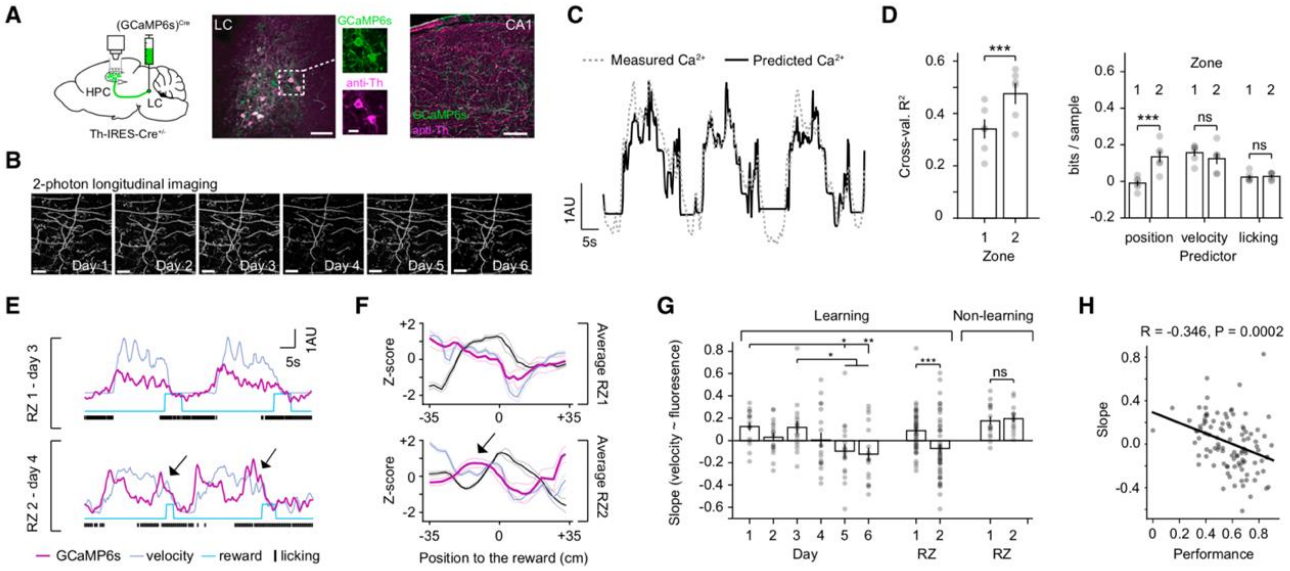

Figure 1.2. Locus Coeruleus Activity Changes during GOL. A. Left: LC-CA1 axon labeling strategy. Cre-dependent virus [rAAV2/9:EF1a-(GCaMP6s)^{Cre}] was injected into the locus coeruleus (LC) of Th-IRES-Cre$^{+/}$ mice. LC axons in hippocampal (HPC) CA1 were imaged through a cannula. Middle and right: post hoc immunofluorescent staining with antibodies against tyrosine- hydroxylase (anti-Th) and GCaMP (anti-GFP) in LC and HPC to confirm labeling strategy. Scale bar: LC: 50 mm; inset: 20 mm, HPC: 100 mm. B. Example of multi-day 2p imaging of LC-CA1 axons in CA1 stratum oriens (SO). Scale bar: 50 mm. C. A generalized linear model (GLM) trained with three covariates (position, velocity, and licking) to predict LC-CA1 activity. Example trace of LC-CA1 calcium activity (dashed line) and predicted by the GLM (solid line). D. Left: cross-validated R^2 calculated on the held-out test data in RZ1 sessions and RZ2 sessions (mean ± SEM, RZ1: 0.34 ± 0.04; RZ2: 0.48 ± 0.04; n = 6 mice, two-tailed paired t test, $t_{(5)} = 5.97$, p = 0.004). Right: contribution of different variables estimated by the amount of information gained by including each variable during RZ1 and RZ2 (mean ± SEM; position in RZ1: 0.01 ± 0.013; position in RZ2: 0.14 ± 0.03; velocity in RZ1: 0.15 ± 0.03; velocity in RZ2: 0.12 ± 0.03; licking in RZ1: 0.02 ± 0.01; licking in RZ2: 0.03 ± 0.01; n = 6 mice, two-tailed paired t tests between RZ1 and RZ2 for: velocity, $t_{(5)} = 4.84$, p = 0.005; position, $t_{(5)} = 1.49$, p = 0.196; licking, $t_{(5)} = 0.63$, p = 0.556). E. Example traces of LC-CA1 activity (dark magenta) and behavioral variables in RZ1 and RZ2 for 2 consecutive laps. In RZ1, axons are correlated with velocity, while in RZ2, there is a decorrelation between LC-CA1 activity and velocity (arrows). 1 arbitrary unit (AU) refers to 1 sigma of the Z-score trace for the fluorescence *F* (GCaMP6s) and speed in cm/s (velocity). F. Average peri-stimulus activity histogram of the LC-CA1 signal (dark magenta), velocity (lavender), and licking (black) in RZ1 and RZ2, centered on reward. The overshoot in LC-CA1 activity is only visible in RZ2 (arrow) (n = 6 mice, mean: darker colors, SEM:

lighter colors). It preceded the reward by an average of 24.33 ± 2.02 cm. G. Slope of the linear fit between velocity and LC-CA1 signals. The signals are less correlated over the course of learning. Data are in mean ± SEM for sessions in a given day collected from n = 6 mice (Learning day1: 0.126 ± 0.038; day2: 0.03 ± 0.036; day3: 0.118 ± 0.056; day4: 0.006 ± 0.067; day5:-0.093 ± 0.061; day6:-0.121 ± 0.059. One-way mixed-effects model ANOVA $F(5, 82) = 4.28$, p = 0.0017. Post hoc Tukey test, day1 versus day5, p = 0.026. day1 versus day6, p = 0.008. day2 versus day5, p = 0.047. day2 versus day6, p = 0.016) and are correlated in RZ1 but decorrelated in RZ2 (Learning RZ1: 0.09 ± 0.026; RZ2: 0.069 ± 0.036. Two-tailed unpaired t test, $n_1 = 51$ sessions, $n_2 = 54$ sessions, $t(104) = 3.57$, p = 0.0005). Two mice that did not learn the task showed signals correlated with velocity in both RZs (Non-learning RZ1: 0.175 ± 0.037, RZ2: 0.194 ± 0.03. Two-tailed unpaired t test, $n_1 = 15$ sessions, $n_2 = 16$ sessions, $t(30) = 0.399$, p = 0.693).H. The slope of the relationship between speed and fluorescence was correlated with behavioral performance, as measured by the fraction of licks in the RZ (Pearson's R test, n = 105 points, R = 0.346, p = 0.0002). Each point is the average performance as a function of the average correlation coefficient for each session and each mouse. See also Figure 1.S1-1.S4.

We then performed a control experiment to confirm that this increase in activity was not related to improved performance on the task over time by imaging LC-CA1 axonal activity for six days without moving the reward (**Figure 1.S3A**). Over six days of the same reward zone, LC-CA1 activity did not develop an overshoot of activity near the reward, and the correlation between velocity and LC-A1 activity rather increased over time (**Figure 1.S3B**). We also imaged CA1PC activity during the second three days of the first reward zone, and enrichment did not occur around the first reward, even after six days. We then moved the reward, and observed place field enrichment around the translocated reward (**Figure 1.S3C**). These results show that upon learning a new reward location, LC-CA1 axons develop a spatially localized increase in activity just before the new reward, and place field reorganization and enrichment in CA1PCs follows this increase (Danielson et al., 2016b; Turi et al., 2019; Zaremba et al., 2017) (**Figure 1.1E,F, Figure 1.S2E**). Therefore, we next aimed to test whether activation of LC-CA1 fibers could generate reward-related enrichment of CA1 place cells.

We used an all-optical system to simultaneously stimulate optogenetically and image through the glass window of the cannula (Turi et al., 2019) (**Figure 1.3A**, **Methods**). We confirmed that we could activate LC-CA1 axons by co-expressing a red-shifted excitatory opsin (bReaChes) (Rajasethupathy et al., 2015; Turi et al., 2019) and GCaMP6s (**Figure 1.3A-C**) in LC-CA1 axons. Next, we simultaneously activated LC-CA1 axons with bReaChes and imaged CA1PCs with GCaMP6f (**Figure 1.3D**). Optogenetic activation of LC-CA1 axons did not acutely affect GCaMP-calcium signals in CA1PCs (**Figure 1.3E**).

Since both the overshoot of LC-CA1 activity and reward-related place cell enrichment occur preferentially around the translocated reward (RZ2) during the second phase of the GOL task, we next aimed to optogenetically recapitulate the LC-CA1-overshoot in the first phase of the learning task, near the first reward (RZ1), where enrichment normally does not occur (**Figure 1.1E, F**). Using the LC-bReaChes, CA1PC-GCaMP strategy, we stimulated LC-CA1 fibers prior to the reward, beginning in the fifth session of the task (**Figure 1.3F,** top). For analysis of place cell activity near reward, we included the area preceding the reward and spanning the entire RZ, hereafter referred to as the peri-reward zone (PRZ) (**Figure 1.3F,** top). This local, unilateral LC-CA1 stimulation, beginning partway through the learning paradigm, did not alter behavioral performance (**Figure 1.3F**, bottom), or the overall properties of place cells in the PRZ compared to controls (**Figure 1.3D**). Strikingly, however, we observed a robust enrichment of place cells near the reward in the last session that was not present in control animals (**Figure 1.3G-H**).

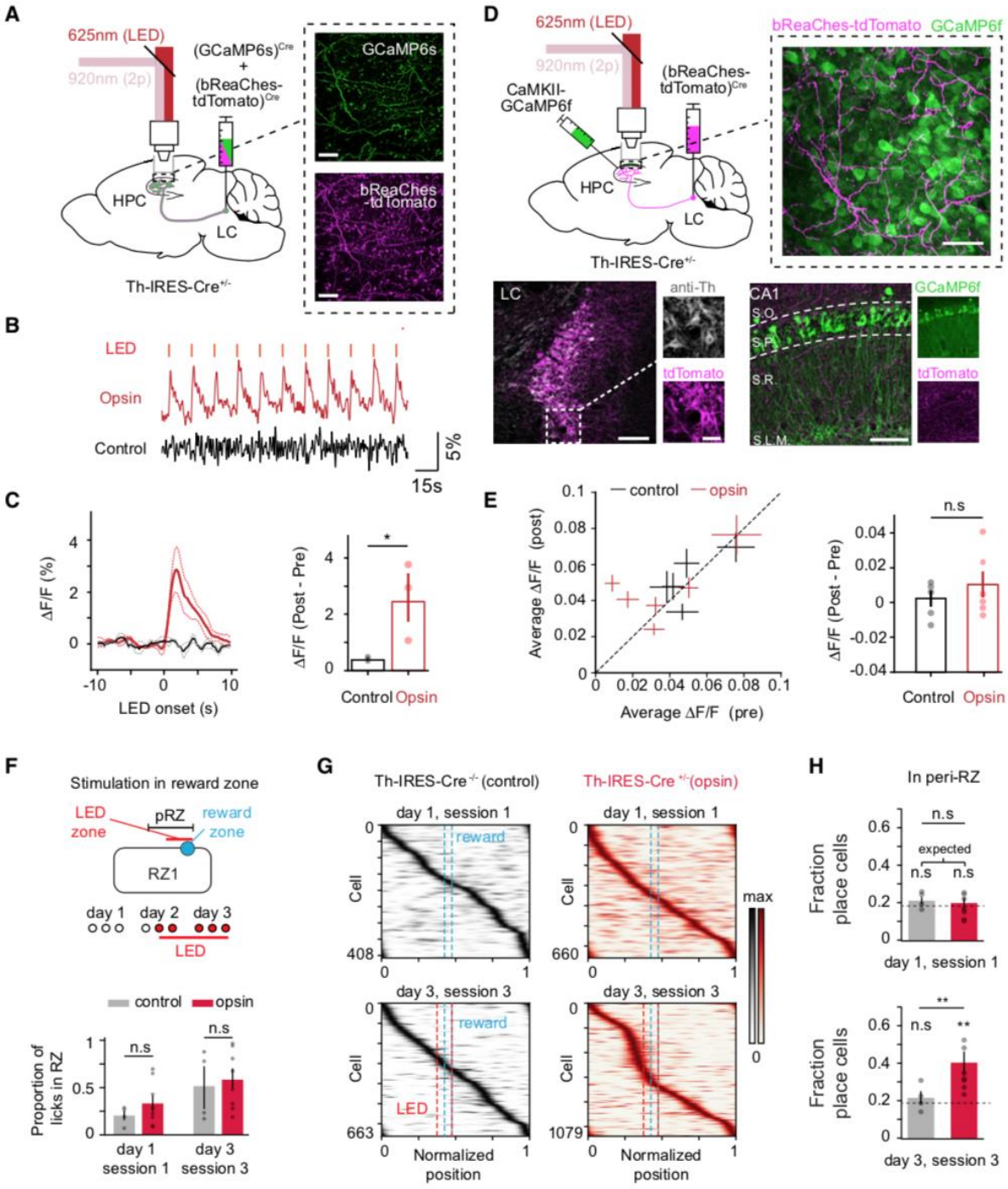

Figure 1.3. Stimulating LC-CA1 Axons Induces CA1 Place Cell Enrichment near a Rewarded Location during GOL

A. Left: labeling strategy for optogenetic stimulation and imaging of LC-CA1 axons. The LC was injected with rAAV2/9:EF1a-(GCaMP6s)^{Cre} and rAAV2/9:EF1a- (bReaChes-

tdTomato)^{Cre}. Right: time-averaged 2p images of GCaMP6s and bReaChes-tdTomato in CA1 *in vivo*, showing overlap between the two. Scale bar: 50 mm. B. Δ*F/F* traces of LC-CA1 axons expressing either GCaMP6s and bReaChes (opsin) or GCaMP6s only (control). Photostimulation: 1-s pulse every 20 s. C. Left: average Δ*F/F* traces in control and opsin mice (n = 3 mice per condition). Dotted line: SEM. Right: difference of Δ*F/F* between post- and pre-stimulation was higher for opsin mice (mean ± SEM, control: $2x10^4 \pm 4x10^4$; opsin: 0.0246 ± 0.008. Two-tailed unpaired t test, $t_{(5)} = 2.9$, p = 0.044). D. Top left: labeling strategy for optogenetic stimulation of LC-CA1 axons and imaging of CA1PCs. rAAV2/9:EF1a-(bReaChes-tdTomato)^{Cre} was injected in the LC, and rAAV2/1:CaMKII-GCaMP6f was injected in CA1. Top right: averaged 2p Z stack of CA1PCs and LC-CA1 axons. Scale bar: 50 mm. Bottom left: example LC injected with bReaChes-tdTomato and stained for tyrosine hydroxylase (anti-Th). Bottom right: example HPC stained for td-Tomato. LC-CA1 axons labeled with bReaChes-tdTomato can be seen in all layers (S.O., *stratum oriens*; S.P., *str. pyramidale*; S.R., *str. radiatum*; S.L.M., *str. lacunosum-moleculare*). Scale bars: LC and CA1,100 mm; LC inset, 20 mm. E. Stimulating LC-CA1 axons does not acutely affect CA1PC activity. Difference in D*F/F* during pre- versus post-light stimulation. Left: each cross is one mouse, size of the cross is SEM. Right: average difference post- minus pre-light stimulation (mean ± SEM, control: 0.0015 ± 0.0047, opsin: 0.0097 ± 0.0075. Two-tailed unpaired t test, $t_{(11)} = 0.88$, p = 0.403; control, n = 5 mice; opsin, n = 6 mice). Red: Th-IRES-Cre$^{+/}$ mice injected with bReaChes-tdTomato in the LC (opsin). Black: Th-IRES-Cre$^{/}$ (control). Each dot is one mouse. F. Top: optogenetic stimulation of LC-CA1 axons in RZ1 of the GOL task. The LED stimulation began 10 cm before reward and spanned the whole RZ. The peri-reward zone (pRZ) began 25 cm before the LED zone. Bottom: opsin (Th-IRES-Cre$^{+/}$, n = 8 mice) and control (Th-IRES-Cre$^{/}$, n = 4 mice) animals showed the same behavioral learning dynamics (mean ± SEM, session1, control: 0.203 ± 0.048; opsin: 0.332 ± 0.083. session9, control: 0.514 ± 0.182; opsin: 0.583 ± 0.108. Mann-Whitney U test. sesion1, $z_{(11)} = 12.0$, p = 0.28, session 9, $z_{(11)} = 12.0$, p = 0.28). G. Heatmaps of place cells in the first and last sessions of control and opsin mice. Opsin mice show a large degree of enrichment before the light stimulation zone in the last session (session9). H. Percentage of place fields in the pRZ in session1 (top) and session9 (bottom). Session9 of opsin mice shows enrichment compared with control (mean ± SEM, session1, control: 0.216 ± 0.019; opsin: 0.199 ± 0.028. session9, control: 0.216 ± 0.035; opsin: 0.402 ± 0.059. Mann-Whitney U test. Session1, $z_{(11)} = 12.0$, p = 0.276, session9, $z_{(11)} = 3.0$, p = 0.017. Session1, control versus expected distribution: $t_{(3)} = 1.3$, p = 0.28; opsin versus expected distribution: $t_{(7)} = 1.21$, 0.26. session9, control versus expected $t_{(3)} = 1.95$, p = 0.14; opsin versus expected: $t_{(7)} = 4.11$, 0.004). See also Figure 1.S4.

This enrichment could stem from recruitment of *de-novo* place cells, a shift of place fields toward the reward, or a dedicated population of reward-representing cells (Gauthier and Tank,

2018). To determine the source of the enrichment, we looked at the place cells in the PRZ during the last session, and examined their recurrence probability in previous sessions (Zaremba et al., 2017). We observed similar recurrence dynamics between experimental and control groups, indicating that LC-CA1 activation likely did not induce new place fields (**Figure 1.S3E**). However, in the experimental group, some place cells in the PRZ in the last session were active outside the PRZ in sessions before LC stimulation (**Figure 1.S3F**). In addition, place cells that were inside the PRZ after LC stimulation were more stable than place cells outside it (**Figure 1.S3G**) Thus, LC activation shifts existing place cells toward the reward, and stabilizes place cells around the reward, but likely does not preferentially recruit new place cells.

We next sought to determine whether LC-CA1 activity was necessary for place field enrichment normally observed around the translocated reward. We hypothesized that chronic spatially and temporally local reduction of LC-CA1 activity could alter the number of place cells overrepresenting the rewarded location. We used an LC-archaerhodopsin (ArchT), CA1PC-GCaMP strategy to inhibit LC-CA1 activity through the imaging cannula (**Figure 1.4A**), and inhibited the LC-CA1 axons around the second reward zone (**Figure 1.4B**). We imaged CA1PCs during the last session to assess enrichment. As with excitation, local, unilateral inhibition of LC-CA1 fibers did not affect behavioral performance, as the mice were able to learn the location of both rewarded sites (**Figure 1.4C**). However, inhibiting the LC-CA1 axons near the second reward decreased the degree of place field enrichment we observed in this zone (**Figure 1.4D**).

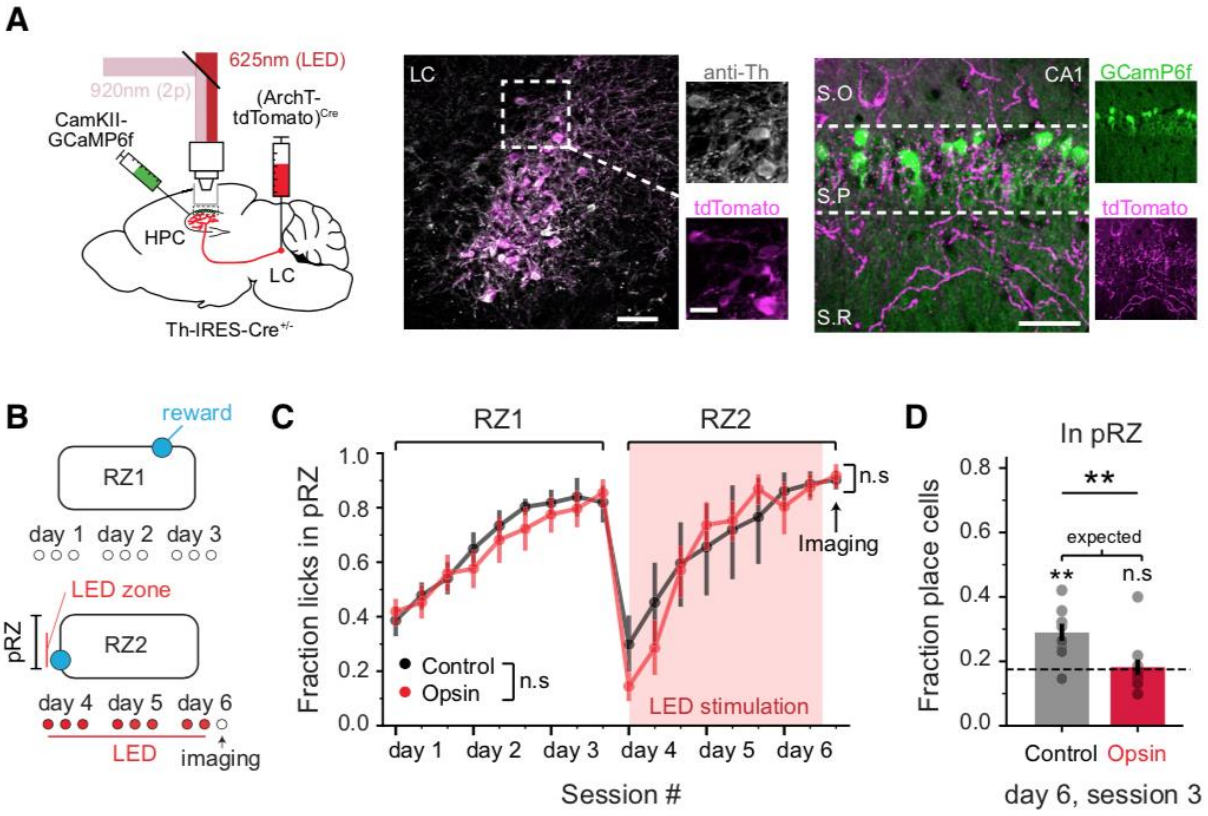

Figure 1.4. Inhibition of LC-CA1 Axons De- creases CA1 Place Field Enrichment A. Left: labeling strategy for LC-CA1 optogenetic inhibition and imaging of CA1PCs. The LC was injected with rAAV2/9:EF1a-(ArchT-tdTomato)^{Cre}, and rAAV2/1:CaMKII-GCaMP6f was injected in CA1. Middle: example LC injected with ArchT- tdTomato and stained for tyrosine hydroxylase (anti-Th). Right: example HPC section. LC-CA1 axons labeled with ArchT-tdTomato can be seen in all layers. Scale bars: LC and CA1: 50 mm; LC inset: 20 mm. B. Optogenetic inhibition of LC-CA1 axons star- ted on the session1 of RZ2 of the GOL task. The LED stimulation zone began 10 cm before the reward and spanned the whole RZ. C. Left: opsin (Th-IRES-Cre$^{+/}$, n = 11 mice) and control (Th-IRES-Cre$^{/}$, n = 9 mice) animals showed the same behavioral learning dynamics (mean ± SEM, repeated-measures ANOVA, opsin versus control, within-subject factor of session, $F_{1,17} = 1.89$, p = 0.17). Opsin and control mice showed the same behavioral performance in the last session of RZ2 (unpaired two-tailed t test, $t_{(19)} = 0.35$, p = 0.72). D. Percentage of place cells in the peri-reward zone (pRZ) for control and opsin mice (mean ± SEM). Dashed line: percentage of place cells expected from a uniform distribution (expected = 0.176. control: 0.29 ± 0.03, opsin: 0.18 ± 0.02. Opsin versus control, unpaired two-tailed t test, $t_{(19)} = 3.02$, p = 0.007.

One-sample two-tailed t test for expected value, control: $t_{(8)} = 4.32$, $p = 0.003$, opsin: $t_{(10)} = 0.28$, $p = 0.77$).

Next, we asked whether optogenetic activation of LC-CA1 fibers was sufficient to drive place field overrepresentation when the stimulation was not paired with a reward location. To answer this question, we used two different approaches. For the first approach, mice performed the GOL task and the stimulation was kept in an unrewarded area during the learning of the first reward zone. This protocol produced no effect on the number of place cells in the stimulated area or in the dynamics of enrichment of the first zone (**Figure 1.S4A,B**). To test for putative interactive or competitive effects between stimulation and learning the zone, we used a second approach in which we performed LC-CA1 stimulation in a constant location during a non-spatial task, where the animal is delivered rewards at randomized locations on the belt (Danielson et al., 2016b; Turi et al., 2019; Zaremba et al., 2017), and did not see enrichment around the stimulated zone (**Figure 1.4C-E**). In a subset of experiments, we combined optogenetic LC-CA1 stimulation with addition of a novel cue on the belt, which also did not suffice to cause place field reorganization (**Figure 1.S4H**).

Finally, we examined whether the LC-CA1 could act in conjunction with other members of reward-related HPC microcircuits to influence place cell plasticity independently from the reward. In particular, we have recently demonstrated that disinhibition conveyed by Vasoactive Intestinal Polypeptide (VIP)-expressing interneurons plays a role in regulating reward-related place cell representations in CA1 (Turi et al., 2019). We crossed VIP-IRES-Cre and Th-IRES-Cre mice, and injected both the LC and the HPC with an rAAV expressing bReaChes in a Cre-dependent manner. This allowed us to simultaneously stimulate VIP-expressing interneurons and LC axons in the HPC CA1 (**Figure 1.S4F**). We stimulated at a constant location during the random foraging paradigm, to decouple stimulation from reward. The combined VIP and LC-CA1

stimulation did not lead to a shift in place fields toward the stimulated site (**Figure 1.S4G**). Since LC stimulation caused place field enrichment only at a rewarded site, and only during a spatial learning task, we conclude that the LC acts in conjunction with other signals that occur around rewards in a task-dependent manner.

1.3 Discussion

It has been suggested that each CA1PC is equally competent to become a place cell (Bittner et al., 2017, 2015), implying that all cells receive the requisite inputs for all locations, and thus could remap or stabilize when the cell's response to a specific input is altered. Our data show that LC activity increases before reward delivery, which, together with evidence of place field enrichment before the reward zone, may indicate the opening of a plasticity window allowing for the potentiation of inputs that predict rewards (Stachenfeld et al., 2017). Optogenetic stimulation mimicking this change in LC-CA1 activity induced goal-directed reorganization of CA1 place cells, but only near a reward, primarily through a goal-directed shift toward and stabilization of place cells near the reward.

The structure of the GOL task in this study was such that when the mouse was first exposed to RZ1, the context was novel. Other studies examining goal-directed reorganization around rewards were performed in a familiar environment (Breese et al., 1989; Dupret et al., 2010; Fyhn et al., 2002; Hok et al., 2007; Hollup et al., 2001; Kobayashi et al., 1997). Changes in reward representation tend to occur when patterns of reinforcement are changed in the same environment (Breese et al., 1989; Kobayashi et al., 1997). Therefore, one explanation for place cell enrichment occurring in RZ2, rather than RZ1, is that goal-directed place cell dynamics are obscured by conflicting demands related to the formation of stable contextual representations. Once a stable

representation is established, changes could result in goal-related overrepresentation of place fields. A recent study described “reward cells” that track rewarded locations, which we did not see, perhaps due to the fact that the reward was moved once rather than multiple times (Gauthier and Tank, 2018). While reward-related enrichment was not explicitly described in recent papers imaging CA1 pyramidal neurons, there does appear to be some enrichment near the reward, even in a familiar environment (Dombeck et al., 2010; Hainmueller and Bartos, 2018; Ziv et al., 2013). This may be due to differences in task structure. Our task is operant (mice have to lick in order to receive water rewards) to ensure the mice learn the location, while to our best understanding the tasks in the referenced papers may have used non-operant reward paradigms, which reduces learning demands.

The finding that LC-CA1 activity increases specifically near a new rewarded location is consistent with a role for the LC in orienting toward unexpected or surprising salient stimuli (Aston-Jones and Waterhouse, 2016); these stimuli could be relevant for behavior, and merit overrepresentation within the cognitive map. Additionally, the time course of place cell reorganization was slower than that of the reward-related LC signal. There could be effects related to offline consolidation that may occur between sessions or during sleep that helps the plasticity to peak.

The signaling mechanism for LC-activation induced place cell reorganization is unknown. Thus far, the major effects of the LC on HPC learning appear to be mediated through D1/D5 dopamine receptors, and not through β-adrenergic receptors (Kempadoo et al., 2016; Takeuchi et al., 2016), although α1 receptors can accelerate perceptual learning (Glennon et al., 2019). Norepinephrine, dopamine, or both could be responsible for both the native and induced

enrichment we observed. Future experiments could determine the source of the enrichment by blocking these receptor types.

To avoid spurious changes to HPC representations of the environment, simultaneous engagement of multiple systems may be required for plasticity induction. Consistent with this model, LC-CA1 stimulation was only sufficient to drive place field enrichment when paired with a rewarded goal location, a highly salient and complex stimulus. This could also explain why neither local, unilateral LC-CA1 activation or inhibition led to a strong behavioral effect. Some factors known to be differentially active for spatially-guided reward learning include local disinhibitory circuits (Turi et al., 2019) and other neuromodulatory transmitter actions, such as serotonergic (Teixeira et al., 2018) and cholinergic activity (Hangya et al., 2015; Palacios-filardo and Mellor, 2019). In addition, the ventral tegmental area (VTA) may act together with the LC to influence place field plasticity, possibly during different brain states (Duszkiewicz et al., 2019; Gomperts et al., 2015b; McNamara et al., 2014), or via synergistic release of dopamine from the VTA and norepinephrine from the LC. Other cellular participants in neural transmission, such as astrocytes, could also be involved, since astrocytes respond to neuromodulatory input with large calcium increases that may affect circuit function (Bazargani and Attwell, 2016).

We combined LC stimulation with VIP-expressing interneuron-mediated disinhibition of pyramidal neurons, to engage two possible systems involved in goal-oriented learning, or at the very least combine LC stimulation with pyramidal cell disinhibition (Turi et al., 2019). The coactivation of these circuit motifs did not lead to place field enrichment in a random foraging task, where animals do not learn a goal location. This suggests that either VIP-expressing interneurons and the LC do not work together, or that place field plasticity depends on the cognitive load of the task. In fact, task-related demands affect the stability of HPC place representations in

a dopamine-dependent manner (Kentros et al., 2004), with place fields being more stable during spatial as opposed to non-spatial tasks. We found that LC stimulation outside of the goal location, even in a goal-oriented learning task, did not induce place field reorganization. The most parsimonious explanation for our data may be that that task demands lead to a higher baseline neuromodulatory tone, upon which multiple reward-related systems, including the LC, can act to induce plasticity.

High baseline LC activity may increase place fields' stability during their formation by altering the noradrenergic or dopaminergic tone of the neural environment, creating a favorable state for pyramidal neurons to strengthen their responses to inputs. The LC is highly active in novel environments (Takeuchi et al., 2016), when place cells are formed. In addition, inhibiting the LC during initial context exposure prevents contextual learning and causes CA3 place cells to become unstable upon re-exposure to a familiar environment (Wagatsuma et al., 2018). Additionally, as measured by immediate early gene RNA cellular localization within cells in the HPC, activation of the LC caused remapping in a familiar environment (Grella et al., 2019). Our results are compatible with a role for the LC in adjusting, strengthening, or altering the responses of CA1 pyramidal cells to their inputs.

High neuromodulatory activity seems to be a trademark signal during locomotion and arousal. While we have not seen studies examining these signals within the dorsal HPC, one study imaged axons from the VTA in the striatum, and found some to be correlated with movement, while others were correlated with reward (Howe and Dombeck, 2016). The activity of cholinergic axons is also correlated with movement onset in the striatum and changes in movement state (Howe et al., 2019), and LC axon activity in the cortex is correlated with pupil dilation, which is correlated with movement (Breton-Provencher and Sur, 2019). While we see initially that the LC

is correlated with movement, its relationship with velocity changes once the learning paradigm changes. Future experiments could determine if activity of other neuromodulatory projections during GOL tasks also exhibit learning related changes so that conjunctive effects of different neuromodulators can tune the network to differentially respond to inputs.

Our results support a working model where a balance of differential neuromodulatory, local inhibitory and astrocyte calcium activity that act on top of task-related brain states to alter the cognitive map. We found that LC-CA1 stimulation could tip the balance toward place cell reorganization when other ingredients were in place due to the presence of a reward. Future studies are needed to untangle the precise identities of these ingredients and how they interact with each other, but our findings show that the LC is a key player in HPC population dynamics supporting goal-directed spatial learning.

Supplementary Figures for Chapter 1 (Figures 1.S1 – 1.S4)

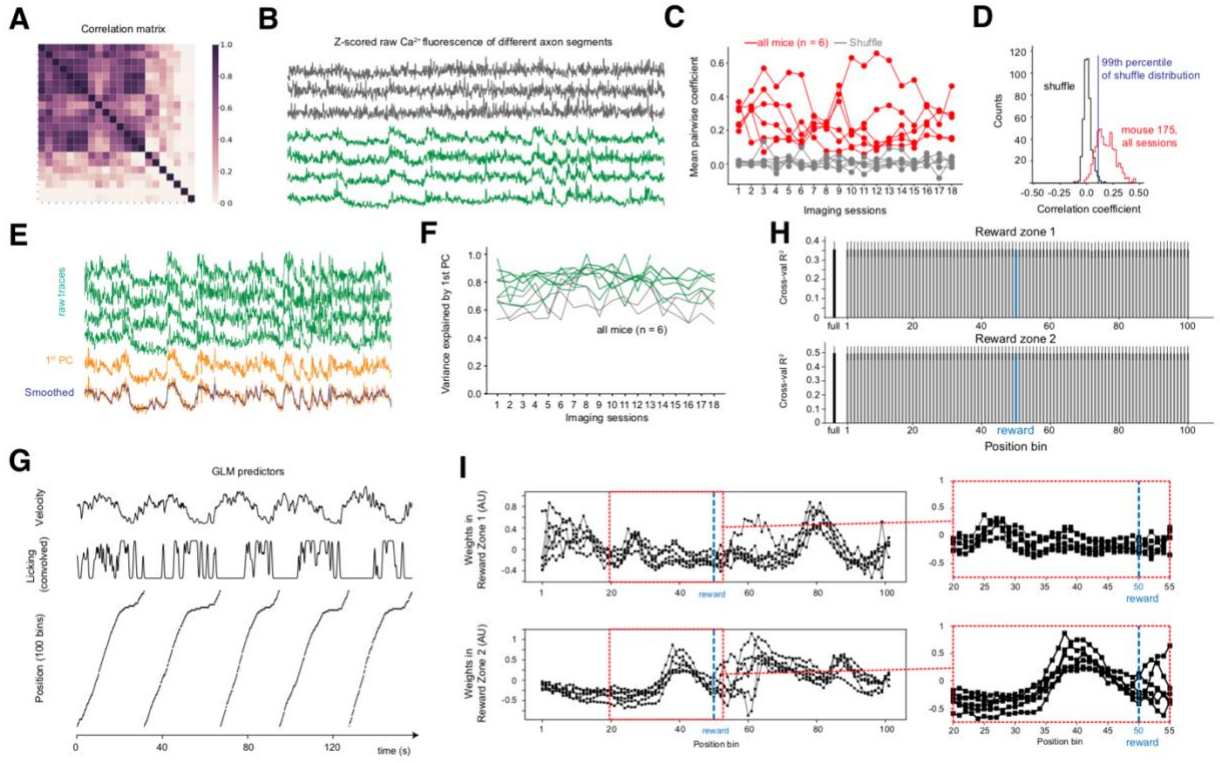

Figure 1.S1 - LC axons signal processing and GLM predictors of LC activity

Related to Figure 1.2

A. The Pearson's pairwise correlation matrix of the calcium traces from all the axons in one session. Most axons are correlated with each other. B. Example calcium traces from four ROIs that are highly correlated with each other, and three that are not. Traces shown in green have a good signal to noise ratio, while the axons in grey have poor signal and are not useable for analysis. C. The mean pairwise correlation coefficient of all the axons remains consistent over days (red lines), compared to a shuffle distribution (grey). The shuffle distribution was computed using the mean pairwise correlation coefficient of a given axon in a session with all the axons taken from a different session. D. Distribution of the mean pairwise correlation coefficient for all the axons in all the sessions (red) and the shuffle distribu- tion as described in c (grey). The 99th percentile of the shuffle distribution (blue line) was used as the threshold to define axons with poor pairwise correlations and thus poor signal to noise ratio. E. After discarding the uncorrelated axons, the signal from the remaining axons (green) was reduced to a single trace by taking the first principal component of the raw calcium traces (yellow), and smoothing with a Savitsky-Golay filter with a sliding window of 21 frames and polynomial degree of 6 (smoothed, blue). F. The

variance in the calcium signal explained by the first principal component was consistent across days, and consis- tently high. The variance explained by the first principal component shown in green do not include discarded axons, while those shown in gray include the uncorrelated axons. G. Factors used as predictors for the GLM plotted in time. Velocity, licking and position (binned into 100 2 cm segments) were used as predictors for the calcium signal. See methods for more details H. The cross validated R2 value of the reduced model without each position bin, compared to the full model, left, full. I. The weights of each position bin in reward zones 1 and 2. Each line is one mouse, and each square is one position bin plotted across the whole belt. In reward zone 2 (inset), the weights of the positions are higher 10 bins (or 20 cm), before the reward. This is not seen in reward zone 1 (top left, top inset).

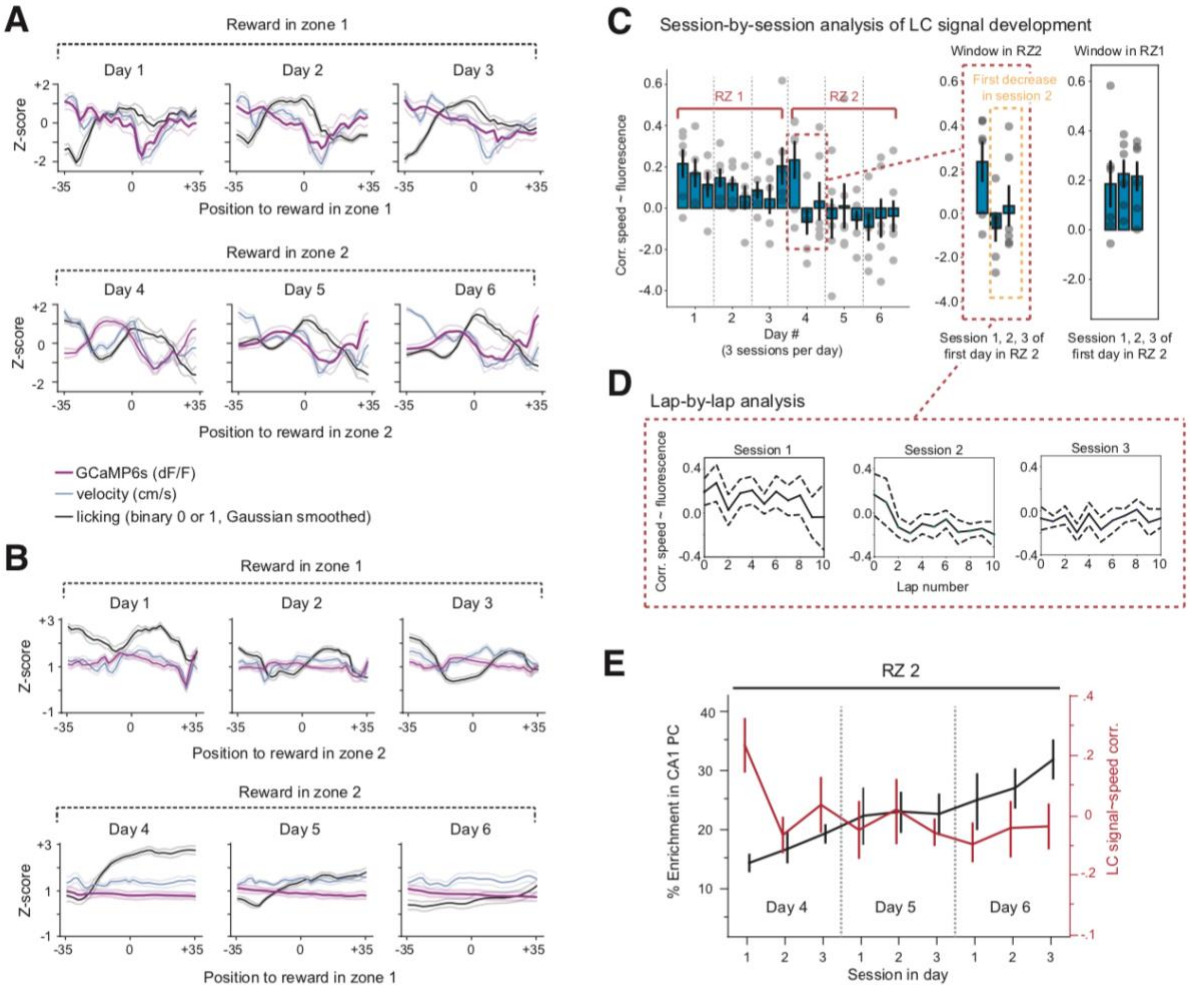

Figure 1.S2 - Dynamics of LC signal development and CA1 reward enrichment in the GOL task

Related to Figures 1.1-1.2

A. The GCaMP signal, velocity, and licking averaged across each day and aligned around the reward zone (0 cm). The decorrelation between velocity and GCaMP appears as a bump in the GCaMP6s signal, and is visible on days 4-6 but not on days 1-3 (corre- sponding to RZ2 and RZ1). B. On days 1-3, this plot shows the GCaMP signal, velocity, and licking aligned to reward zone 2 (the future reward zone) in the first three days of the paradigm, when the reward was in zone 1. On days 1-4, reward zone 1 is set at zero, and the actual reward position is in zone 2. The GCaMP signal shows no discernible changes in reward zone 1 when the reward is in zone 2 C. Session-by-session analysis of the correlation between speed and fluorescence of LC axons. Inset, left: first three sessions of first day in RZ2. Right, first three sessions of the location of RZ1, during the first day in RZ2 (n = 6 mice). D. Traversal-by-traversal analysis of the LC signal versus velocity. Average of 6 mice +/- SEM on the first day of RZ2 (3 sessions per day). Laps are averaged in non-overlapping blocks of two (n = 6 mice). E. Session-by-session analysis of reward enrichment in CA1 pyramidal cells (black) overlaid with LC signal~speed correlation (red, same data as in C) in the 3 days of RZ2 (day 4, 5, 6 of the GOL task) (LC, n = 6 mice; CA1, n = 9 mice).

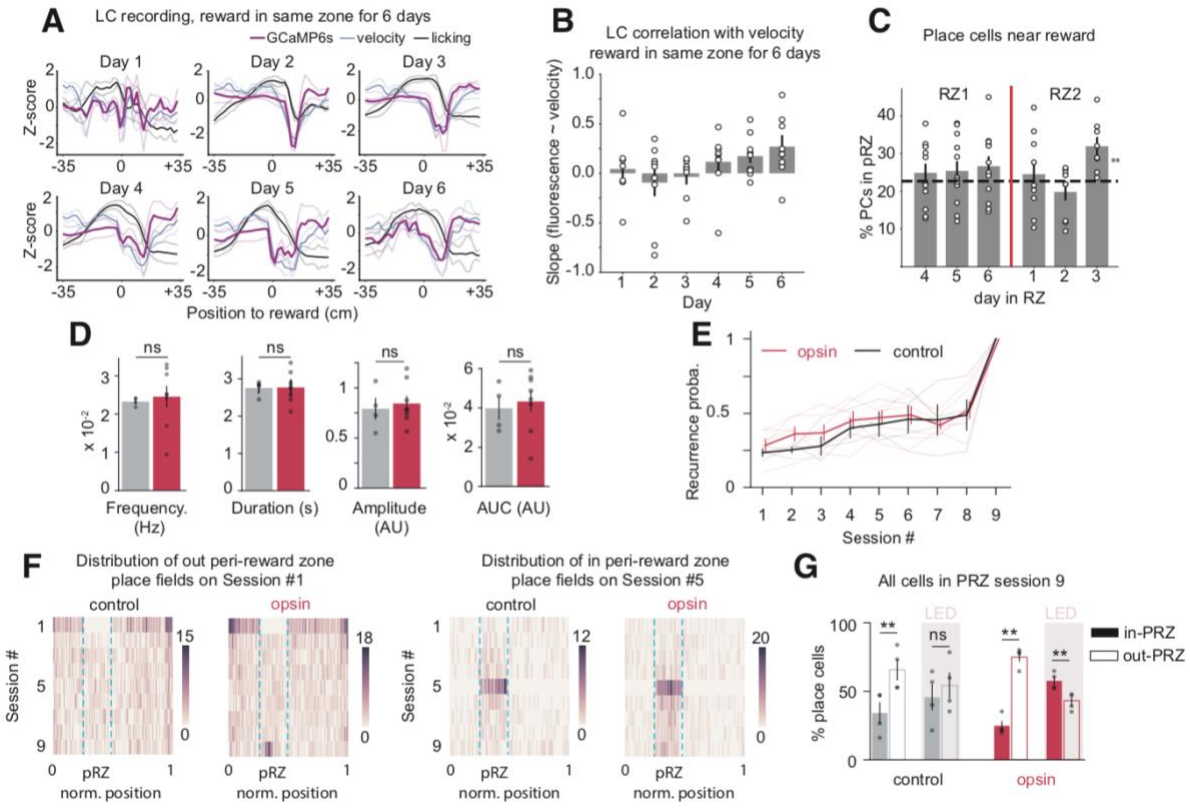

Figure 1.S3 - Locus coeruleus signal and CA1-PCs do not change in the same reward zone. Place field enrichment comes from cells shifting from outside the reward zone, and a stabilization of cells in the reward zone

Related to Figures 1.1-1.2

A. LC activity, GCaMP, and velocity over 6 days of the same reward zone. Velocity and LC activity remain correlated. n= 3 mice. B. LC GCaMP6f and velocity remain correlated over six days of the same reward zone. Mean ± SEM. across days, 0.04 ± 0.12, -0.09 ± 0.14, -0.04 + 0.08, 0.12 ± 0.10, 0.17 ± 0.07, 0.27 ± 0.12. Circles represent individual sessions. n = 3 mice. C. Place cells do not enrich over the second three days (6 total days) of the same reward zone, but are enriched around a new zone compared with a uniform distribution. Mean ± SEM, **, p = 0.0067, one-tailed t-test compared to the expected distribution. pRZ, peri-reward zone. Circles represent individual sessions. D. Transient properties of place fields in the PRZ on session 9 in control and opsin mice (Mean ± SEM and compared with Mann-Whitney U tests. Frequency, control: 0.023 ± 5x10-4; opsin: 0.024 ± 0.0028; z(11)= 8.0, P=0.101. Duration, control: 2.75 ± 0.103; opsin: 2.77 ± 0.146, z(11)= 14.0, P=0.399. Amplitude, control: 0.792 ± 0.108; opsin: 0.846 ± 0.074, z(11)=13.0, P=0.336. AUC, area under the curve, control: 0.039 ± 0.006; opsin: 0.043 ± 0.005, z(11)=13.0, P=0.336; control n = 4; opsin, n = 8 mice). E. Recurrence probability of place cells with fields in PRZ on session 9. There is no difference between opsin and control groups (Holm-Sidak method, with α = 0.05. Computations assume sessions are from populations with the same standard deviation. Control, n = 4 mice; opsin, n = 8 mice. None of the days were significantly different, all p-values > 0.9). F. Distribution of place fields along the belt across different sessions. The same cells were tracked over all the imaging sessions. Left, distribution across sessions 1-9 of cells outside the PRZ on session 1. Right, of cells with fields inside the PRZ on session 5. G. Origin of PRZ place cells. We restricted this analysis to place cells in the PRZ on session 9 and determined where their place fields were on previous sessions - inside (in-PRZ), or outside the PRZ (out-PRZ). The number of cells was averaged across pre-LED (sessions 1-4) and LED-on sessions (LED, sessions 5-8). Pre-LED stimulation, in-PRZ session 9 cells for both groups had place fields outside the PRZ. After LED, cells main- tained fields in-PRZ in opsin animals (Mean ± SEM, compared with Mann-Whitney U tests. Control mice, n = 4. pre-LED, in-PRZ: 0.34 ± 0.08, out-PRZ: 0.66 ± 0.08, in-PRZ vs out-PRZ, z(4) = 0.0, p = 0.01. LED on, in-PRZ: 0.46 ± 0.09, out-PRZ: 0.54 ± 0.09, in-PRZ vs out-PRZ, z(4) = 6.0, p = 0.33. Opsin mice, n = 8; pre-LED, in-PRZ: 0.25 ± 0.04, out-PRZ: 0.75 ± 0.04, in-PRZ vs out-PRZ, z(7) = 0.0, p = 0.01. LED on, in-PRZ: 0.57 ± 0.04, out-PRZ: 0.43 ± 0.04, in-PRZ vs out-PRZ, z(7) = 0.0, p = 0.01).

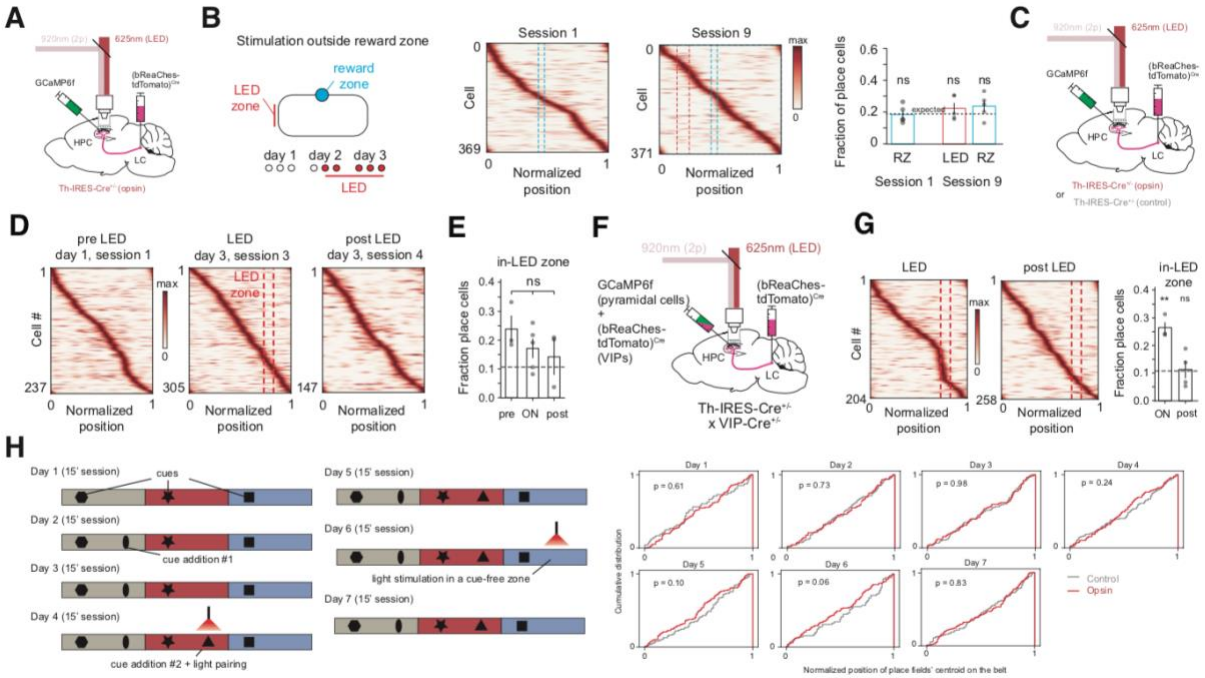

Figure 1.S4 - LED stimulation of LC axons during random foraging, random foraging paired with addition of novel cues, and random foraging with VIP interneuron stimulation Related to Figures 1.1-1.3

A. Labeling protocol with bReaChes expressed in the LC, and pyramidal neurons labeled with GCaMP. B. LC fibers were stimulated outside the reward zone, using the same behavioral paradigm as for LC stimulation in the reward zone (left). Heatmaps of place fields shows that there was no place field enrichment near the LED stimulation zone or near the reward (center), quantified as the fraction of place fields in session 1 and session 9 (right) (mean ± sem, reward session 1: 0.18 ± 0.02, session 9: 0.22 ± 0.03, LED session 9: 0.24 ± 0.04). Percentage of place fields around the reward zone and LED zone were not different on any sessions from an expected uniform distribution, showing no enrichment around those 2 zones (Reward session 1: , $t_{(3)}$=0.32, p = 0.4; session 9, $t_{(4)}$ = 0.76, p = 0.24; LED session 9, $t_{(4)}$ = 1.28, p = 0.13) C. Labeling protocol with bReaChes expressed in the LC, and pyramidal neurons labeled with GCaMP. D. The rewards moved each lap, and the LED zone was fixed. Mice ran 3 x 10-minute sessions per day, and the LED was present from the third session of day 1 to the third session of day 3. The mice ran one more session to determine whether any potential enrichment remained. Heatmaps of place fields before the LED (n = 3 mice), on the last LED session (n = 5 mice), and post LED (n = 3 mice). E. There was no difference across days in the proportion of place fields in the LED zone (mixed-effects model F(2, 8) = 1.022, p = 0.4024). Data presented in mean ± sem; pre-LED: 0.29 ± 0.047, LED-ON: 0.22 ± 0.034, post-LED: 0.19 ± 0.062. F. Labeling strategy to stimulate LC axons and VIP interneurons while imaging CA1 pyramidal cells. In a Th-IRES-Cre+/- crossed with a VIP-Cre+/-, the LC

and the HPC were injected with a rAAV expressing bReaChes-tdTomato [rAAV2/9:EF1a-(bReaChes-tdTomato)Cre] in a Cre-dependent manner, and a non-Cre dependent GCaMP6f (rAAV2/1:CaMKII-GCaMP6f) was also injected in dorsal CA1. G. Left, Heatmaps of place fields during the last LED stimulation session (n = 3 mice), and post LED (n = 4 mice). Enrichment occurs during VIP stimulation, likely due to direct disinhibition of pyramidal cells, but it is not present in the session after stimulation. Right, quan- tification of place fields number near the LED zone. Data presented in mean ± sem; LED-ON: 0.26 ± 0.02, post: 0.11± 0.032 (one-sample two-tailed t-test for expected value derived from a uniform distribution of 0.11, control: t(2) = 9.8, p = 0.01, opsin: t(3) 1.62, p = 0.24). H. Pairing cues with LED stimulation. Mice ran one 15-minute session per day for 7 consecutive days, and the reward delivery positions were randomized each lap (random foraging).The belt contained a few sparse cues. First, we habituated the mice to the belt for one day (day 0, not shown). We then added a succession of stimuli, including cues and LED light to stimulate the axons (Day 2, cue 1, day 3 cue 1 post, day 4 cue 2 + LED, day 5 cue 2 alone, day 6 LED, day 7 post LED). The cumulative proportion of place field centroids on the belt on each day was not different between opsin mice with bReaChes and control mice without bReaChes (opsin, n = 5 mice; control, n = 5 mice for each day. Day 1: Two-sided Kolmogorov-Smirnov test, n1 = 48, n2 = 117, z(164) = 0.126, p = 0.617. Day 2: Two-sided Kolmogorov-Smirnov test, n1 = 94, n2 = 91, z(184) = 0.098, p = 0.735. Day 3: Two-sided Kolmogorov-Smirnov test, n1 = 103, n2 = 84, z(186) = 0.0067, p = 0.983. Day 4: Two-sided Kolmogorov-Smirnov test, n1 = 97, n2 = 97, z(193) = 0.144, p = 0.244. Day 5: Two-sided Kolmogorov-Smirnov test, n1 = 86, n2 = 106, z(191) = 0.173, p = 0.102. Day 6: Two-sided Kolmogorov-Smirnov test, n1 = 58, n2 = 116, z(173) = 0.207, p = 0.063. Day 7: Two-sided Kolmogorov-Smirnov test, n1 = 102, n2 = 115, z(216) = 0.082, p = 0.836).

Chapter 2: Calcium signals in hippocampal astrocytes during behavior

Astrocytes are studied for their many functions in the brain, including participation in forming the blood brain barrier, removing waste from the brain during sleep, uptake of ions, and surrounding synapses to maintain fidelity of synaptic signaling in time and space. However, they are rarely thought of as participants in circuits that could affect neuronal function. While some researchers believe that astrocytes release neuroactive substances (such as adenosine), astrocytes

could influence neurons simply by performing their normal functions, particularly ion or transmitter uptake, differently under certain specific circumstances.

Although astrocytes are not electrically active, like many types of cells, they use calcium as an internal signal. This calcium has multiple sources – mostly from internal stores such as the endoplasmic reticulum (ER) or mitochondria (Agarwal et al., 2017). It could also be due to influx across the membrane, but the literature is not conclusive on this point (Agulhon et al., 2008; Shigetomi et al., 2016). There are different types of astrocyte calcium signals that are defined by their location and size. The large, somatic calcium signals are mostly due to release of calcium from the ER, mostly as a result of metabotropic G-protein coupled receptor signaling from neuromodulatory receptors through the IP3R, the subtype of which expressed in astrocytes is the IP3R2 (Srinivasan et al., 2015). The source of the smaller signals that occur in the fine processes of the astrocytes is somewhat unclear, but these signals can occur when the IP3R2 is knocked out, in response to neuromodulatory input (Srinivasan et al., 2015).

As described in the introduction, the downstream effects of astrocyte IP3R2 signaling are unclear, and they have not been shown to grossly affect behavior (Petravicz et al., 2014, 2008), but they may affect neural potentiation (Takata et al., 2011), and they may affect the gain of neurons' responses to input via increased potassium uptake (Wang et al., 2012).

We chose to focus on the large, somatic calcium signals for several reasons. First, they are easy to measure and observe. Second, there are tools to abolish them. Third, the function and cause of the smaller calcium signals is also unknown, as are the expected size and location of these signals. Thus, these large, somatic signals seem like an appropriate signal to begin to examine, particularly since astrocyte calcium signals have not yet been studied in the hippocampus by two-photon microscopy during behavior.

We examined astrocytes in three different layers of the hippocampus, the strata oriens (SO), radiatum (SR) and pyramidale (SP). We found that astrocytes in SR are more synchronous and more frequently active than astrocytes in SP and SO during running on a cued belt, either in a spatial or non-spatial task. However, during a behavioral paradigm where the animals were exposed to stimuli of different modalities and valences, astrocytes responded synchronously and at a high frequency in all the hippocampal layers we examined.

Finally, we generated mice to knock out the IP3R2, the major source of these somatic calcium signals, inducibly and selectively in astrocytes. We confirmed that the IP3R2 is absent from mice with active Cre recombinase. These mice can be used to determine whether IP3R-mediated astrocyte calcium signals are necessary for spatial learning and place field shifts toward rewards.

2.1 Methods

Viruses

Recombinant adeno-associated viruses (rAAVs) were used for GCaMP6f expression. For labeling astrocytes, an rAAV 2/5: GFAP-GCaMP6f virus, generated by Dr. Baljit Khakh's lab, was purchased from the UPenn Viral core, and subsequently from Addgene. This virus was injected into wildtype mice (C57Bl6J), 6-12 weeks old. For simultaneous astrocyte and LC labeling, the same astrocyte specific virus was injected into the hippocampus, while another virus expressing GCaMP6f was injected into the LC of Th-IRES-Cre mice. This virus, rAAV 2/9:Ef1a-$(GCaMP6f)_{Cre}$, was obtained from Dr. Boris Zemelman, UT Texas, Austin. Thus far, these mice have only been used to analyze astrocyte activity, rather than LC activity, because GCaMP6s showed an improved signal to noise ratio in LC axons compared with GCaMP6f, and since both astrocytes and axons were labelled with a green fluorophore, LC axons passing through the fine

processes of astrocytes will need signal separation in order to be processed. If animals were used for multiple experiments, they were trained on a burlap belt between paradigms.

Viral injection and hippocampal window/headpost implant

Viral injections were performed with a Nanoject syringe, as previously described in methods in Chapter 1, and Lovett-Barron et al. (2014). Briefly, mice were anesthetized with isofluorane and treated with buprenorphine or meloxicam. The skull was exposed a hole was drilled, and a sterile glass capillary containing viral mixtures was lowered into the brain. After injections, the skin was sutured and mice were allowed to recover. The LC was injected bilaterally at coordinates AP -5.45 mm, ML ±1.28 mm, and DV -3.65 mm with 150 – 300 nL of virus. The dorsal HPC area CA1 was injected in the left hemisphere at coordinates from Bregma AP -2.1 or -2.2, ML -1.5 or -1.75, and DV -1.2, -1.1, and -1.0 with 50-64 nL of virus at each DV site. Mice were implanted with an imaging window (diameter 3.0 mm, height 1.5 mm) over the left dorsal-intermediate hippocampus with a stainless-steel or brass headpost. Imaging cannulas were constructed by adhering (Norland optical adhesive) a 3-mm glass coverslip (64-0720, Warner) to the steel cannula (Ziggy's tubes and wires). The surgical procedure has been described previously (Lovett-Barron et al., 2014). Briefly, mice were anesthetized and treated with buprenorphine or meloxicam, the skull was exposed and a 3 mm hole was made in the skull. Bone, dura and cortical layers were removed, while flushing with ice-cold cortex buffer. The cannula was inserted into the hole, secured with Vetbond, and a headpost was affixed to the skull with dental cement. Mice recovered in their home cage, and were monitored for three days post-surgery.

***In vivo* calcium two-photon imaging**

Imaging was conducted using a two-photon 8 kHz resonant scanner (Bruker). A piezoelectric crystal was coupled to the objective as described previously (Danielson et al., 2016b) in order to allow fast displacement along the Z-axis. The objective was a Nikon 40x NIR water immersion, 0.8 NA, 3.5 mm working distance. The excitation laser was 920 nm (50-100 mW, Coherent Ultra II). For some structural images in red, the laser was 1070 nm (Coherent Fidelity), and scanning was interlaced with the 920 nm laser for green excitation. Red (tdTomato) and green (GCaMP6) channels were separated by emission cubes as described previously (Danielson et al., 2016b). Fluorescence signals were collected using photon multiplier tubes (PMT, GaAsP PMT, Hamamatsu R3896). A preamp (1.4 x 105 dB, Bruker) was used to amplify signals before digitization. Pockels cells were used to regulate the power of the LED reaching the tissue. Images were acquired at 1x digital zoom, 1.2, or 1.4, with 512 x 512 pixels. For astrocytes, the first experiments were captured at approximately 1 Hz, with one imaging plane, with stratum pyramidale and stratum radiatum of the hippocampus acquired in separate imaging sessions, with radiatum 90-150 μm below the imaging plane of the pyramidale. Astrocytes in stratum pyramidale and radiatum were acquired in separate imaging sessions of the same mice, while astrocytes in stratum oriens were taken just above the pyramidal layer, in a separate cohort of mice. For mice with concurrently labeled astrocytes and axons, 5 imaging planes 2 μm apart were acquired with a piezo to maintain the axon in the z plane.

Behavioral experiments

Mice were trained on a cue-free burlap belt. 3-4 days after the implantation surgery, they were water deprived. First, they were habituated to head fixation for several 10-minute sessions. Then they were allowed to lick freely for water, which was delivered initially at 15 locations on

the belt. Then the animals were required to lick initially to receive the water reward, and each day the reward schedule was gradually dropped to 3 rewards per two meter burlap belt. Training took approximately 10 days. During imaging, mice ran on an initially unfamiliar cued belt, with multiple types of fabric and cues. We also used multisensory cues, including a constant stream of pinene or limonene-scented air, a blinking ultraviolet LED, and a constant or regularly beeping tone. For rewarded intervals experiment, animals ran on an uncued burlap belt, with rewards delivered non-operantly at regular intervals. For the random foraging paradigm, animals were given three operantly delivered or non-operantly delivered rewards on a cued belt that changed locations every lap. For the hidden rewards paradigm, rewards were delivered at locations tied to the location of spatial cues on the belt, as in LC experiments (**Chapter 1, Fig 1.1, 1.2**). For salience experiments, the animal was allowed to run on a burlap belt while cues in different sensory modalities, including an odor, light, and tone, a water reward, and an aversive airpuff were delivered in a randomized order, 5-10 times each, also randomized in time within a several second interval in order to make the stimuli unpredictable.

Calcium imaging data preprocessing

The preprocessing steps for the raw fluorescence signal have been described elsewhere (Danielson et al., 2016b). Briefly, the imaging data was motion corrected using the SIMA software package (Kaifosh et al., 2014). Frames where the motion correction failed were discarded if they were below a certain threshold of similarity to the time-averaged image of the entire calcium video. Axons were hand-segmented using a data visualization server program developed in the lab. The same astrocytes were transferred across sessions wherever possible, and identified with a unique ID.

Relative fluorescence changes in astrocytes ($\Delta F/F$) were computed using a rolling median of varying window sizes, adjusted according to each session. Since astrocytes are active relatively infrequently, the median was an appropriate baseline to use, and it effectively corrected for slow changes in the level of calcium fluorescence, usually a slow decrease, that was occasionally observed during a session. The raw signal was smoothed with a gaussian filter of varying size depending on the frame rate at which the data was collected. Frames that were blanked by the motion correction or that had been discarded due to poor motion correction of those frames were interpolated from the surrounding frames using a gaussian. The baseline was subtracted from the raw signal, and the result was divided by the baseline, in order to calculate the $\Delta F/F$.

If the $\Delta F/F$ did not reach a certain threshold (0.3), traces were assumed to have poor signal to noise ratio, and they were discarded. Additionally, if the largest z-scored positive deflection in the calcium signal was equivalent to the largest z-scored negative signal, or the negative signal was larger than the positive signal, the trace was also discarded. Very occasionally, a few noisy traces with large negative and positive deflections were manually discarded, as was one trace with a very large and long (nearly two minutes) individual astrocyte event. Only approximately 3-4 traces out of over a thousand traces were manually discarded.

For event detection, the derivative of the signal was calculated to capture the rise and fall of the astrocyte calcium. Events began when the calcium began to rise as a certain speed, measured by the derivative reaching a certain cutoff. They were determined to end after the derivative reached a certain negative threshold since this indicates a fall in the calcium signal. The end was set as the point after the calcium fell, that was close to the value of the signal at the beginning of the event, below that initial value, or close to the baseline. The calcium signal was required to

reach a certain threshold in order to qualify as an event. The thresholds for peak size, rise speed, and fall speed were all adjusted manually for each session in order to optimally detect events.

Synchronicity and Principal Component Analysis (PCA)

To determine whether astrocytes were synchronously active, the Pearson's R correlation coefficient was computed on both the raw and *ΔF/F* signal of the entire session, comparing every astrocyte to every other astrocyte in the same session. The *ΔF/F* was used for subsequent analyses. The average of the upper triangle of the R values in the correlation matrix for each session was used as a measure of synchronicity to capture the entire session, since correlation values were rarely large and negative, they would not negate the large positive correlation values.

Principal component analysis (PCA) was performed on the *ΔF/F* in order to determine how many components accounted for most of the variance in the astrocyte calcium signals.

Generation of Astrocyte specific inducible IP3R2 knockout mice

Heterozygous IP3R2$^{+/fl}$ mice were obtained from Dr. Martin Paukert (UT San Antonio). These mice were bred to be homozygous and crossed with Aldh1L1-CreER mice, generated by Dr. Baljit Khakh's lab and purchased from Jackson labs. These mice express Cre specifically in astrocytes, and the Cre can be inducibly activated by tamoxifen injection. Homozygous IP3R2$^{fl/fl}$ were bred to Aldh1L1-CreER mice, then backcrossed in order to obtain littermates that were all homozygous for IP3R2$^{fl/fl}$ with half the litter expressing Cre in astrocytes, and half the litter not expressing Cre, so that all the mice could be injected with tamoxifen for the best possible control. Cre-positive and Cre-negative littermates were injected with 75 mg/kg of tamoxifen for five days, and sacrificed two weeks later. IP3R2 knockout was confirmed in littermates by immunohistochemistry (**Figure 5**).

Histology and immunohistochemistry

After the last imaging sessions mice were put under deep isoflurane anesthesia and transcardially perfused with 0.1 M PBS followed by 4% paraformaldehyde in 0.1 M PBS. After overnight post-fixation in the same solution the brains were transferred to PBS. The hippocampus was sliced into 50-70 μm slices. Slices were washed 3x with 0.1 M PB, then washed in tris-buffered saline (TBS) with 0.3% triton (TBST) several times, incubated in 10% normal donkey serum in TBS for 45 minutes, then incubated for 1 hour at room temperature and for ~2 days in primary antibodies: slices were incubated with the following antibodies: anti-GFAP, anti-GFP, anti-NeuN, anti-Iba1, or anti-IP3R2 (see Tables of Reagents and Resources, Antibodies). For anti-IP3R2, slices were incubated in ice cold methanol for 5 minutes before the staining protocol in order to permeate the endoplasmic reticular membrane to access the epitope. The slices were then washed with TBS several times and incubated with the appropriate secondary antibodies. The slices were rinsed, mounted with Aquamount, and imaged on a confocal microscope.

Statistics

No statistical methods were used to predetermine sample sizes, but our sample sizes are similar to those reported in previous publications. A one-way ANOVA was used, followed by post-hoc t-tests with a Bonferroni correction for multiple comparisons. For Figure 4, a mixed effects model was used, since some mice were not recorded in all experiments. *, $p < 0.05$, **, $p < 0.01$, ***, $p < 0.001$.

2.2 Results

Astrocytes and microglia transiently respond to the cannula implant

Since astrocytes are known to respond to injury, confirming that they recover after the cannula implant was an important control. Astrocyte reactivity was measured by degree of GFAP expression, since GFAP is known to increase its expression in reactive astrocytes. Mice were implanted and sacrificed at different timepoints after the implant, brains were sliced at 50 μm, in two separate cohorts. Each cohort was stained in parallel with the same antibody solution, then images were acquired on the confocal using the same acquisition settings. A region of interest was drawn around the hippocampus ipsilateral and contralateral to the implant. 2-4 slices from 2-4 mice per cohort were used for quantification. The average fluorescence in the hippocampus was quantified and normalized to the average fluorescence from several unimplanted mice. Astrocyte reactivity, and microglial activation, as measured by expression levels of Iba1 quantified the same way as GFAP. Between two and three weeks, astrocyte reactivity and microglial activation return to baseline (**Figure 2.1**).

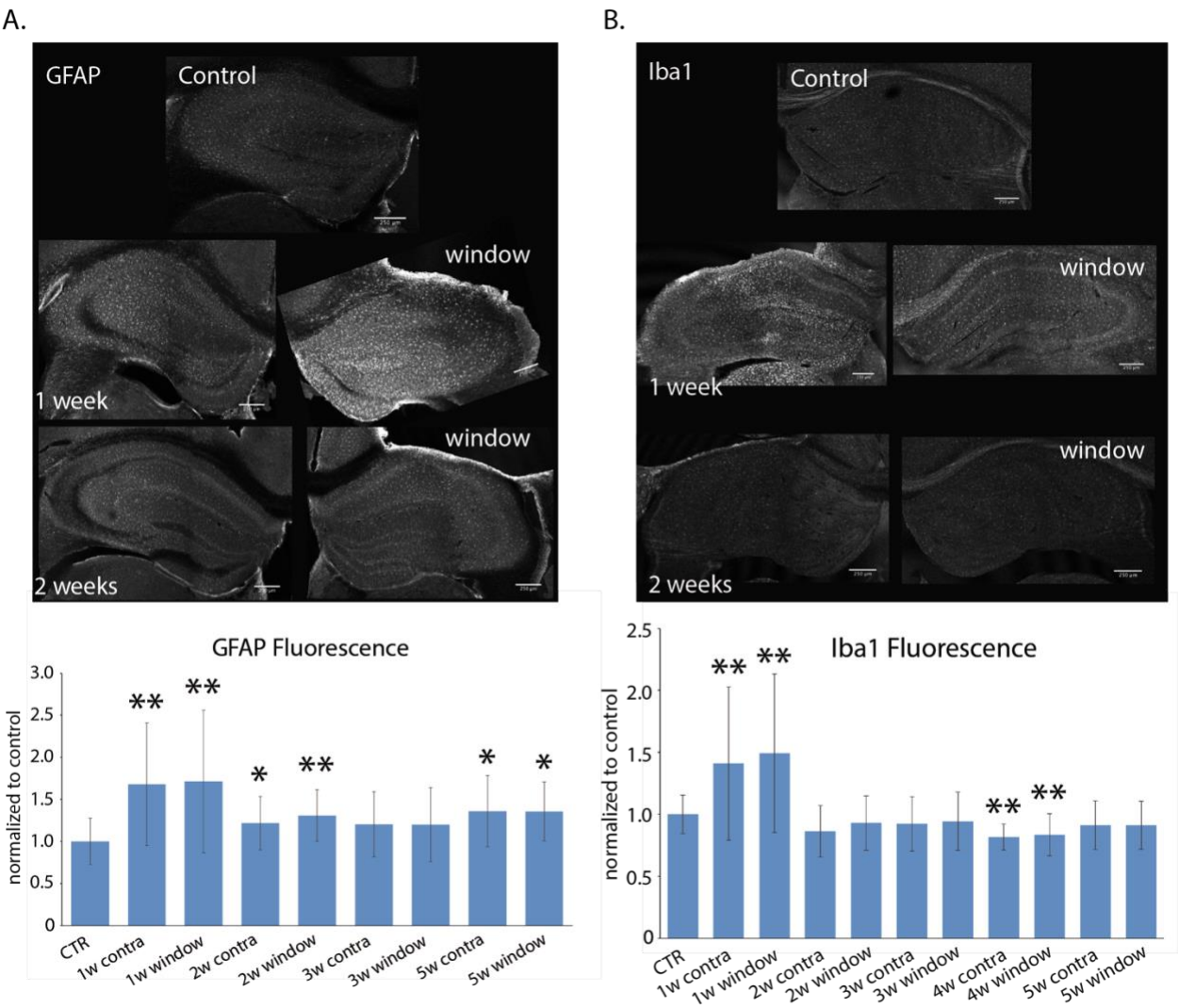

Figure 2.1. Astrocyte and microglial response to cannula implant.

Animals were implanted with a cannula (window) over the left hippocampus, then sacrificed at different time points after the implant, from 1 week (1w) to 5 weeks (5w). They were concurrently sacrificed with an unimplanted mouse (CTR). Two cohorts of mice were used, and 11-20 slices per condition were used. For each cohort, slices were stained in parallel with the same antibody solution, with images acquired on a confocal microscope with identical imaging settings for each cohort. Mean fluorescence in a region of interest drawn around the hippocampus were normalized to the average fluorescence of several control mice. Contra, side contralateral to the implant. A. Example confocal images and fluorescence quantification from control mice and both sides of the hippocampus at 1 week and 2 weeks, stained for GFAP to indicate astrocyte reactivity. B. Examples of brain slices stained for Iba1 to mark activated microglia. Groups were compared with a t-test to control mice. N = 11-20 slices from 3-6 mice per condition. * $p < 0.05$, ** $p < 0.01$. Scale bars, 500 μm.

Astrocytes are selectively labeled with GCaMP

To examine hippocampal astrocyte calcium signals, mice were injected with an rAAV into dorsal hippocampal area CA1 to express GCaMP6f under a GFAP promoter for selective expression in astrocytes (**Figure 2.2A**). Example fields of view *in vivo* are shown in **Figure 2.2B**. Brains that had been injected with the rAAV 2/5: GFAP-GCaMP6f were stained for GFAP and NeuN. The cells that were labeled with the virus expressed GFAP, which selectively labels astrocytes (and radial glia) in the adult brain, but not labeled with NeuN, which selectively labels neuronal nuclei (**Figure 2.2C**). Another group of mice, that expressed Cre recombinase in catecholaminergic cells (Th-IRES-Cre) were simultaneously injected with rAAV 2/5: GFAP-GCaMP6f to label astrocytes, and also injected with Cre-dependent GCaMP6f in the LC, similar to Chapter 1. Some of these mice were also crossed with a mouse expressing td-tomato, a red indicator, in a Cre dependent manner (Ai9 mice, see Tables of Reagents and Resources, Mice). *In vivo* images from mice with both LC axons and astrocytes labeled in the hippocampus are shown in **Figure 2E**. While both LC axons and astrocytes are labeled with the same fluorophore, they are expected to have dramatically different morphologies as demonstrated in **Figure 2E**, as well as different time courses of calcium activity, due to the different types of calcium signaling that each is thought to use, namely calcium entry due to ionotropic receptors or voltage-gated calcium channels in axons, versus metabotropic receptor activated calcium release from internal stores in astrocytes, which should be much slower than ionotropic and calcium channel mediated calcium signals. However, axons pass through the fine processes of astrocytes, resulting in some bleedthrough into the axon signals. Since we have adequately characterized the dynamics of LC axon activity in Chapter 1 during behavior, we decided to focus on characterizing astrocyte

calcium for current analyses. However, the simultaneously recorded LC axon data is available to be analyzed as well, once a sufficient method to segregate the astrocyte and axon calcium can be identified.

We decided to measure large, somatic astrocyte calcium signals. Regions of interest were drawn manually around astrocyte somata, and wherever possible, transferred across imaging sessions so that their identity could be maintained for further characterization.

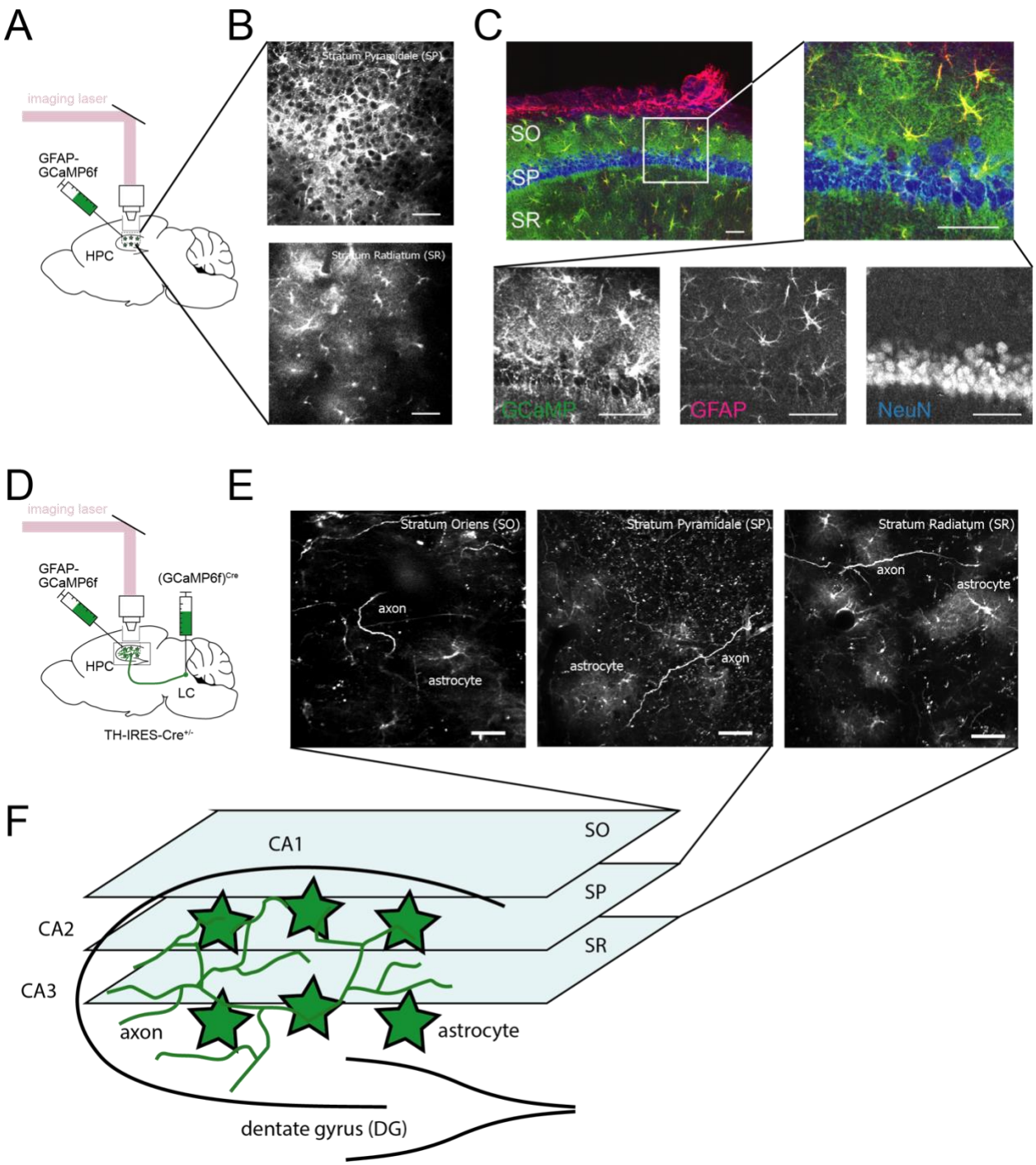

Figure 2.2. Astrocyte labeling strategy.

A. Schematic of the injection site and imaging setup. Mice were injected with an rAAV expressing GCaMP6f on a GFAP promoter, a cannula was implanted over the hippocampus through which the cells could be imaged. B. Example in vivo images acquired with a two-photon microscope of the stratum pyramidale (SP) and stratum radiatum (SR). Scale bar,

50 μm. C. A confocal image of a hippocampal brain slice, with different layers labeled (stratum oriens, SO, SP, SR). The slice was stained for GFP to better visualize GCaMP expression (green, GCaMP, for GFAP to confirm that GCaMP was expressed in astrocytes (magenta), and stained for NeuN to mark neuronal nuclei (blue). GCaMP and GFAP labeling overlap, while GCaMP and NeuN do not, indicating that the virus selectively labels astrocytes. Scale bar, 50 μm. D. Some mice were concurrently labeled with GCaMP in both astrocytes and the LC, as in Chapter 1. Th-IRES-Cre mice were injected with a Cre-dependent rAAV expressing GCaMP6f into the LC. Both axons and astrocytes are visible in the hippocampus. E. Example images *in vivo* from different layers of the hippocampus, SO, SP and SR. Scale bar, 50 μm. F. Schematic showing the different layers of CA1, and simultaneous labeling of astrocytes and HPC-LC axons.

Astrocytes in SR are more active, the SP contains astrocytes without any calcium events

Astrocytes were imaged in three layers of area CA1 of the hippocampus: the stratum oriens, stratum pyramidale, where the cell bodies of pyramidal neurons are located, and the stratum radiatum, where axons from area CA3 synapse onto pyramidal neurons in CA1 (**Figure 2.2E, F**). Examples of calcium signals from astrocytes recorded in different layers of CA1 are shown in **Figure 2.3A**. Astrocyte calcium events were identified using the derivative of the calcium signal (red, **Figure 2.3A**). We noticed several qualities of astrocyte calcium signals immediately. First, as expected based on the literature from other brain areas (Bekar et al., 2008; Paukert et al., 2014; Srinivasan et al., 2016, 2015; Takata et al., 2011), large somatic astrocyte calcium signals were mostly synchronous across different cells. However, as can be seen in some traces in figure 3A, there are occasional instances where some astrocytes do not participate in a large event, as well as the reverse, where individual or a few cells will exhibit a large calcium signal when the other cells are not active.

The number of events in each cell was counted, and this was averaged across cells per imaging session. Astrocytes in the stratum radiatum had a higher rate of events than in the stratum oriens and stratum pyramidale (**Figure 2.3B**). However, when astrocytes with no transients in a

session were excluded, the SR still had a higher event rate than SO, but was no longer significantly different from SP.

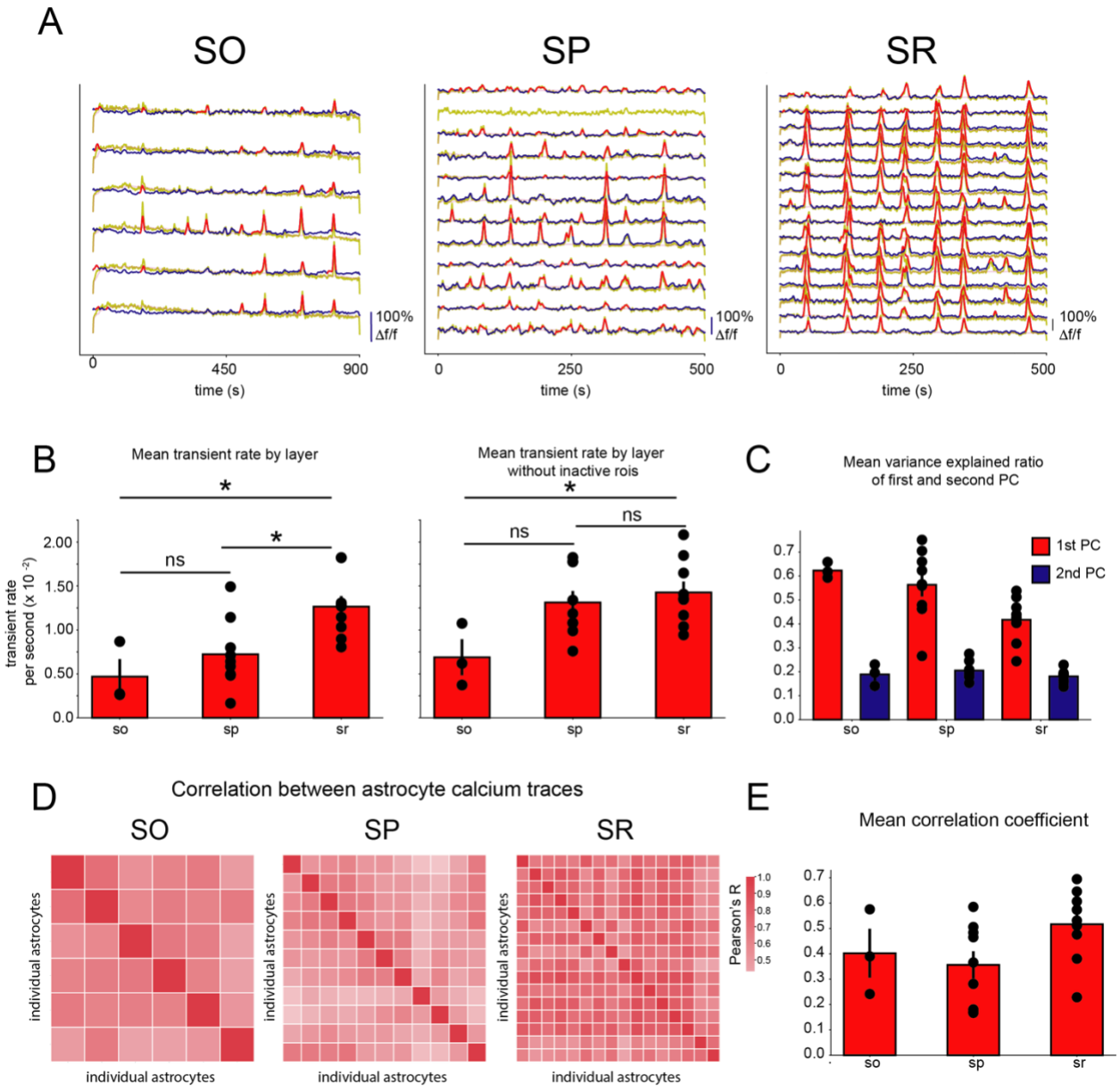

Figure 2.3. Hippocampal astrocytes show differences in activity across hippocampal layers. A. Example calcium signals from regions of interest (ROIs) drawn around astrocyte somata. Each figure is one entire imaging session from one layer of the hippocampus (SO, left; SP, middle; SR, right). The smoothed raw calcium signal is in yellow, baseline in light pink, and ΔF/F in dark blue. Calcium events, or transients, are overlaid over the ΔF/F in red. Some ROIs with a poor signal to noise ratio were discarded, and the smoothed raw calcium signal is presented in yellow without a baseline or ΔF/F, second trace from the top in SP. B.

Transients were detected in in all imaging sessions. The average number of transients from all ROIs was calculated per imaging session. Each data point is the average transient rate per session in an imaging layer for, averaged across sessions for each mouse. Left, the average transient rate from all ROIs. Right, astrocytes with no transients were excluded. SO, n = 3 mice, SP, n = 9 mice, SR, n = 9 mice. Left, significant by one way ANOVA, F = 7.33, p = 0.0047. Post-hoc t-tests were performed, SO vs SR, p = 0.0074; SP vs SR, p = 0.0075; SO vs SP, p = 0.34. To test for multiple comparisons, a Bonferroni correction was performed, making the required threshold for significance 0.0167. Right, significant by one way ANOVA, F = 4.32, p = 0.029. Post-hoc t-tests were performed, SO vs SR, p = 0.014; SO vs SP, p = 0.036; SP vs SR, p = 0.54. C. Principal component analysis was performed on the ΔF/F of all ROIs for each session, and the variance explained ratio (normalized so the total variance explained is 1) was averaged across sessions from each layer. Points are mean values of the variance explained ratio for each mouse, from the first and second principal component. Two-way mixed effects ANOVA, significant main effect of layer, F (2, 18) = 5.44 p = 0.014; significant main effect of 1st or 2nd PC, F (1, 18) = 144.0, p<0.0001; significant interaction between HPC layer and principal component, F(2, 18) = 4.34, p = 0.029. D. Pearson's R correlation coefficient between ΔF/F of each astrocyte with every other astrocyte. E. The mean of the upper triangle of the correlation matrix of each session was taken. Each data point is the mean of these values for each mouse. One-way ANOVA, F = 2.49, p = 0.11.

Astrocyte calcium activity is correlated

To determine whether there were different patterns of astrocyte activity that accounted for the variance in the observed calcium, we performed principal component analysis (PCA) on the ΔF/F of the calcium trace, with astrocytes with a poor signal to noise ratio excluded (see methods). The variance accounted for by the first principal component was high across all layers, and a small amount of variance was accounted for by the second PC (**Figure 2.3C**). We interpreted this to mean that the astrocyte calcium signals were synchronous.

To measure astrocyte synchronicity more directly, the Pearson's correlation coefficient between the ΔF/F of the calcium trace of each astrocyte was computed against all the other astrocytes (**Figure 2.3D**). We occasionally observed astrocytes that were not strongly correlated with other astrocytes, but did not generally observe astrocytes that were strongly anticorrelated

with other astrocytes. The average correlation coefficient per session was grouped by mice, and presented in **Figure 3E**. While not significant, SR is slightly more correlated than SO and SP.

Astrocyte calcium signals differ across layers in different behavioral paradigms

All the analyses described so far were grouped by layer across different behavioral paradigms. Mice ran under the microscope in a variety of behavioral paradigms, similar to Chapter 1 and described in detail in the methods (**Figure 2.4A**). The first set of two mice with labeled astrocytes were recorded in a very simple paradigm that we called the "rewarded intervals" paradigm. Here, the mice ran on an uncued, plain, burlap belt, with water rewards delivered at equal spatial intervals that increased as the mice improved on their performance of the task. We recorded the stratum radiatum and stratum pyramidale in these mice in separate sessions. Since there were only two mice recorded in this paradigm, we did not include them in statistical analyses comparing different behaviors, but different metrics of astrocyte activity are still presented in **Figure 2.4**.

The second behavioral task was the random foraging paradigm, where mice ran on a treadmill belt with tactile cues in a multisensory context. The mice ran in two different contexts, which are grouped together for these analyses. The mice also ran in the hidden rewards task, where a water reward is presented in a specific location relative to tactile cues, and the mouse learns the location of the reward, which can be measured by the percentage of licks in the reward zone. The mice learned one reward zone, and then the reward was moved. For these analyses, the two reward zones are grouped together. Finally, to determine which types of stimuli hippocampal astrocytes responded to, mice underwent the salience protocol. These mice were allowed to run on an uncued burlap belt, and stimuli in different sensory modalities (light, tone, odor) and of different

behavioral valences (water reward, aversive airpuff) were presented in a randomized order and a variable time window so that they would not become predictable.

Astrocytes in SR showed a higher average correlation coefficient than other layers, except during the salience experiment, where all layers showed highly correlated astrocyte activity. This is consistent with the literature, which describes large, synchronous astrocyte responses to startling stimuli, thought to be due to noradrenergic signaling through the α1a adrenergic receptor thought to be located directly on the astrocytes (Bekar et al., 2008; Paukert et al., 2014; Zhang et al., 2014). Since the stimuli in the salience protocol were randomized in time and in the order they were presented, we would expect them to be startling, and recruit many astrocytes in calcium events, causing them to appear more synchronous (**Figure 2.4B**).

While the activity of astrocytes in SR was highly correlated compared to other layers, the variance accounted for by the first principal component was lower in the random foraging and hidden rewards paradigms compared to the other layers (**Figure 2.4C**). We do not know if this is due to the fact that these signals were perhaps less noisy than the other layers, and therefore the first component contains some noise in those experiments, or for some other reason. This remains to be determined.

Similarly to the grouped data, the average transient rate in SR was higher in the random foraging and hidden rewards paradigms, but all layers were similar in the salience paradigm (**Figure 2.4D**). However, when inactive astrocytes without any transients were excluded from this analysis, SP and SR were similar. This indicates that SP contains many inactive astrocytes (**Figure 2.4E**).

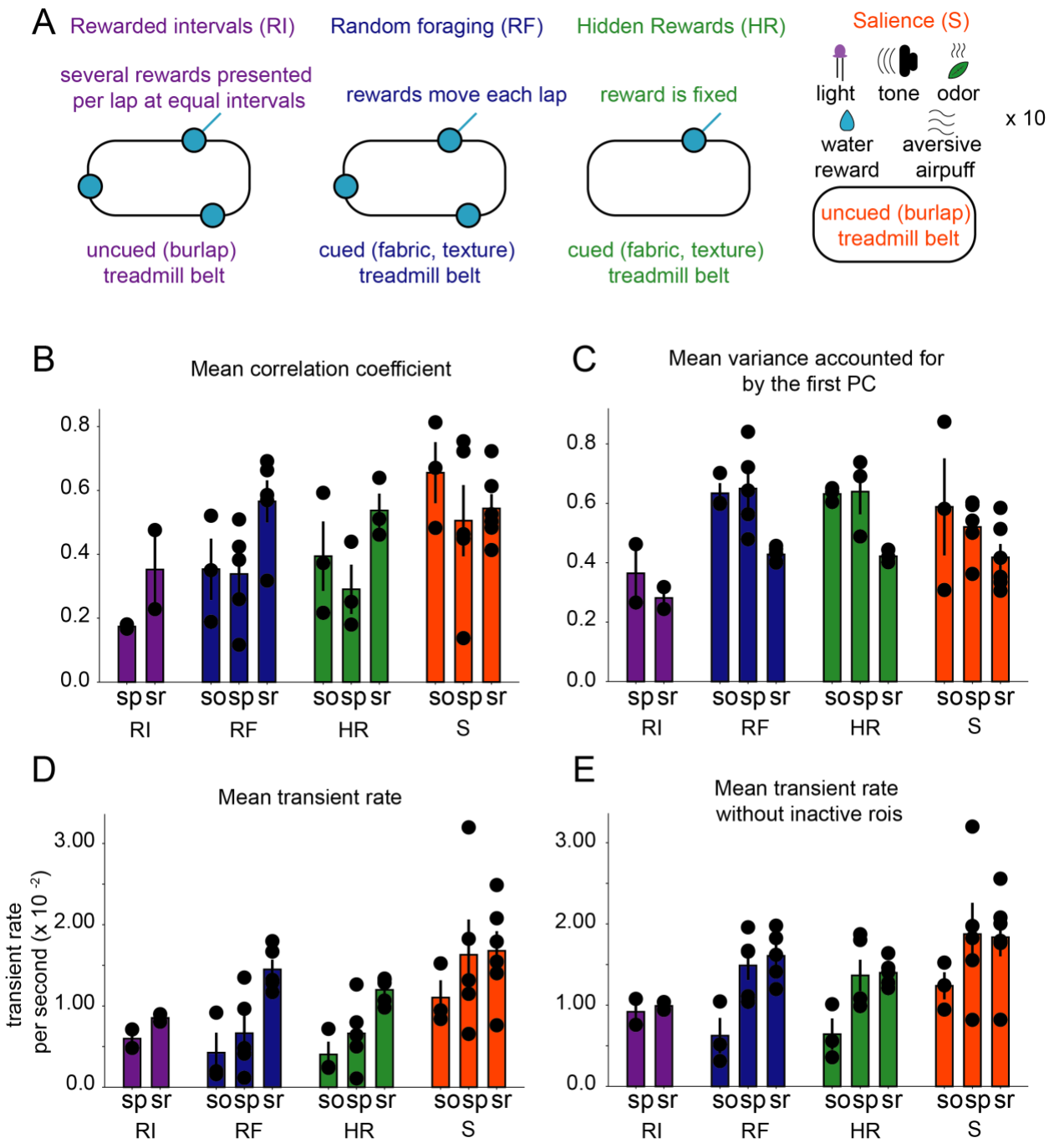

Figure 2.4. Metrics of astrocyte activity during different behavioral paradigms.
A. Schematics of behavioral paradigms, or experiment types. Rewarded intervals (RI), random foraging (RF), hidden rewards (HR), and salience (Sal). For B-D, RI mice were not included in analysis since there were only two mice, but are shown for comparison purposes. B. Mean correlation coefficient, calculated the same way as in Figure 3, but separated by experiment type. SR appears consistently higher than SP and SP, except during the salience experiments. Mixed effects model, significant effect of experiment type, F (2, 27) = 3.56, p =

0.042; significant effect of layer, F (1.950, 26.33) = 3.42, p = 0.049. C. Variance accounted for by the first principal component in different layers by experiment type. Mixed effects model, significant effect of layer, F (2, 27) = 9.86, p = 0.0006; nonsignificant effect of experiment type, F (1.844, 24.90) = 0.98, p = 0.38, nonsignificant interaction between layer and experiment type, F (4, 27) = 0.40, p = 0.80. D. Mean transient rate across different layers by experiment type. Mixed effects model, significant effect of experiment type, F (1.533, 15.33) = 7.86, p = 0.007, significant effect of layer, F (2, 11) = 6.01, p = 0.017. E. Mean transient rate without inactive ROIs. Only cells that had at least one transient per session were included in this analysis. Significant effect of experiment type, F (1.441, 22.33) = 4.02, p = 0.044, significant effect of layer, F (2, 31) = 8.72, p = 0.0010, no significant interaction between experiment type and layer, F (4, 31) = 0.16, p = 0.96.

Group metrics of astrocyte calcium activity do not change with learning

To determine whether any of these metrics of astrocyte activity changed with learning, we used the percentage of licks in the reward zone (plus an area 25 cm preceding the reward, together known as the peri-reward zone, or PRZ, as in Chapter 1) as a learning metric. This value was included in a linear regression against the average correlation coefficient, variance accounted for by the first PC, and average transient rate with and without inactive ROIs. None of these values were significant in any of the hippocampal layers we measured (data not shown). By these measures, which are averaged across all ROIs in a session, astrocyte activity does not appear to change with learning.

Astrocyte IP3R2 receptors are knocked out in transgenic mice

After generating the inducible IP3R2 knockout mice (Aldh1L1-CreER x IP3R2$^{fl/fl}$), littermates were treated with tamoxifen for five days, and sacrificed two weeks later. Cre positive littermates do not show IP3R2 staining in astrocytes (colocalized with GFAP), while Cre negative littermates stained in parallel for the virus do (Figure 5).

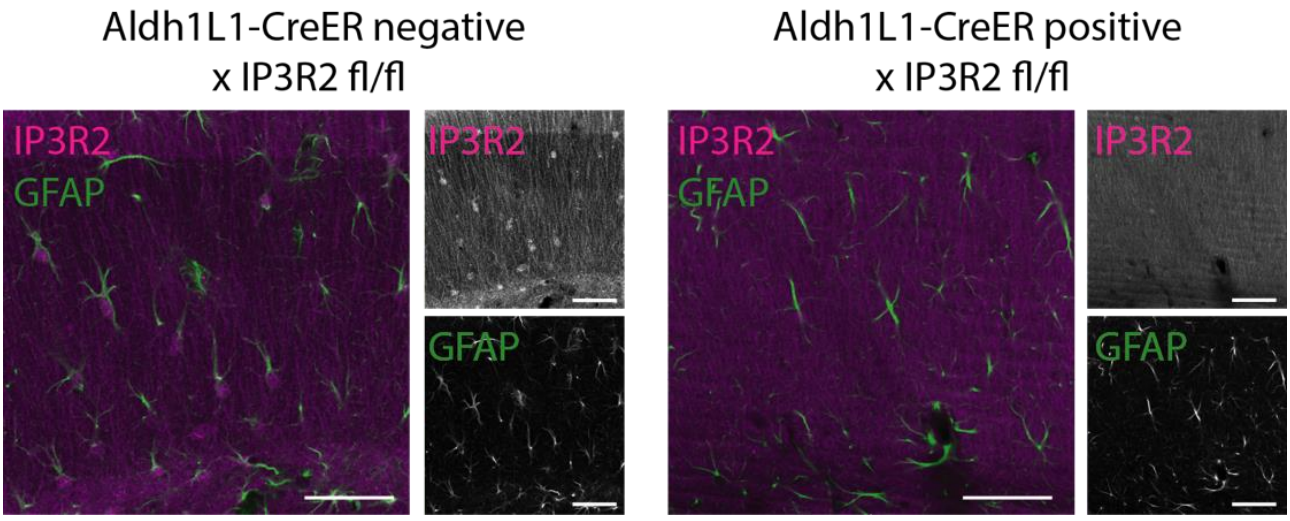

Figure 2.5. Aldh1L1-CreER positive x IP3R2$^{fl/fl}$ mice do not express the IP3R2 after treatment with tamoxifen.

Example confocal images from an Aldh1L1-CreER negative x IP3R2$^{fl/fl}$ mouse (left) and a Aldh1L1-CreER positive x IP3R2$^{fl/fl}$ littermate (right). Both mice were treated with 75 mg/kg of tamoxifen for five days, sacrificed two weeks later, and brain tissue was stained for IP3R2 and GFAP to confirm IP3R2 knockout in astrocytes. Astrocytes are clearly labeled in both mice, but IP3R2 are missing from the Cre positive mouse. Scale bars, 50 μm.

2.3 Discussion

To our knowledge, this is the first study using two-photon calcium imaging to examine astrocytes in the hippocampus of awake, behaving mice. We observed large, synchronous calcium signals in three different layers of the hippocampus, with some differences between layers. SR was more highly corelated, as well as more active, compared with the SO and SP. However, SP contained astrocytes that did not exhibit any calcium events, and the active astrocytes exhibited a similar event rate to SR.

SO was less active than SR, showing fewer calcium events. However, during the salience paradigm, in which mice were presented with a set of presumably startling stimuli, there were no differences observed between the different layers, indicating that SO astrocytes are capable of calcium events, but were less active during the other behavioral paradigms.

It is unknown why there are differences between the layers of the hippocampus in terms of event rate or level of correlation. These differences could be due to several factors, including differences in the astrocytes themselves, perhaps expression of different receptors or different levels of receptor expression, or morphological differences, or even differences in astrocytic coupling by gap junctions. It could also be due to levels of innervation by neuromodulatory projections that the astrocytes respond to, or astrocyte proximity to these projections. The differences observed in the stratum radiatum could also be due to the fact that the stratum pyramidale contains all inhibitory synapses, while the radiatum contains primarily excitatory synapses, creating a different mixture of surrounding neurotransmitters.

The function of these differences is even less clear, given that the function of astrocyte calcium signals has yet to be determined (Adamsky et al., 2018; Agulhon et al., 2008; Petravicz et al., 2014, 2008). We hypothesize that astrocytes may contribute to the gain in pyramidal neuron responses to inputs that occurs with LC activation. This could be determined using the astrocyte specific IP3R2 inducible knockout mice we generated in the lab, by recording place cell reorganization around rewards without astrocyte calcium release from the ER. A particularly good next experiment would be to perform the LC stimulation around the first rewarded location that we performed in Chapter 1, in the presence or absence of intact astrocyte calcium signaling, in order to determine whether place field reorganization around rewards due to LC innervation is mediated at least partially through astrocytes.

Further analyses should describe more specific metrics of astrocyte activity, such as event peak, area under the curve, and event length. Additionally, the proportion of astrocytes that participate in each calcium event should be quantified as a further measure of synchronicity. Differences in astrocyte responses to behavioral events should be determined as well. We should

perform analyses to determine whether more astrocytes respond to certain types of behavioral events. Perhaps more astrocytes participate in events that occur around rewards, for example. While the current measures we used to characterize astrocyte activity during behavior did not show differences with learning, other metrics of astrocyte activity may show differences, either occurring during or after learning, or at the unfamiliar rewarded location, as with the LC axon activity.

The relationship between LC activity and astrocyte calcium activity could be clarified as well. As in Paukert et al (2014), astrocytes tend to respond during behavioral stimuli such as running, but not every time. In Paukert et al (2014), the authors put forth the hypothesis that this was due to differences in neuromodulatory activity. However, in chapter 1, we found that LC axons responded quite consistently to running, suggesting that this may not be the case. However, we did not measure the rate of LC axon events, and the GCaMP6s indicator used in Chapter 1 is not able to resolve fast signals. A recent paper from Hajime Hirase's lab determined that astrocyte calcium signals occurred in response to multiple LC axon events in a row (Oe et al., 2020), which could be consistent with our data. If we develop a satisfactory method to segregate LC axon calcium recorded simultaneously with astrocytes, we may be able to further understand the relationship between these two signals. Additionally, optogenetic activation of LC axons while recording astrocyte calcium would be informative in clarifying the relationship between LC axon activity and astrocyte calcium signals. Optogenetic inhibition of the LC, combined with the salience paradigm, could also help determine the relationship between LC activity and astrocyte activation in response to these stimuli.

While there are many analyses that can still be performed, this is the first time differences in hippocampal astrocytes across layers in terms of their calcium activity has been described. There

are some caveats, particularly that the layers were not recorded in the same sessions, and the stratum oriens was recorded in a different set of mice, while the stratum radiatum and stratum pyramidale were recorded in the same mice. However, we believe that it is an important step in laying the foundation to understand the role of astrocytes in circuit function during behavior.

Conclusion

The hippocampus is well-studied with respect to its circuitry, and its role in spatial learning and memory, as well as neural plasticity. The advent of two-photon microscopy has provided a method to chronically study hippocampal neurons at a population level, allowing for an understanding of neural changes that accompany spatial learning. Given the well-established behavioral paradigms for assessing hippocampal learning, and that place cell activity is a good readout of brain activity during complex behavior, we used the hippocampus as a model to study neural plasticity during learning, and the role of neuromodulatory input and calcium activity in astrocytes, via two-photon imaging and optogenetic manipulation of circuits.

A better understanding of hippocampal function, incorporating neuromodulation and astrocytes, these somewhat non-canonical participants in circuits, will lead to a better understanding of principles of neural plasticity and the interactions between different cell types in the brain.

References

Adamsky, A., Kol, A., Kreisel, T., Doron, A., Ozeri-engelhard, N., Melcer, T., Refaeli, R., Horn, H., Regev, L., Groysman, M., London, M., Goshen, I., 2018. Astrocytic Activation Generates De Novo Neuronal Potentiation and Memory Enhancement Article Astrocytic Activation Generates De Novo Neuronal Potentiation and Memory Enhancement. Cell 174, 1–13. https://doi.org/10.1016/j.cell.2018.05.002

Agarwal, A., Wu, P.-H., Hughes, E.G., Fukaya, M., Tischfield, M.A., Langseth, A.J., Wirtz, D., Bergles, D.E., 2017. Transient Opening of the Mitochondrial Permeability Transition Pore Induces Microdomain Calcium Transients in Astrocyte Processes. Neuron 1–19. https://doi.org/10.1016/j.neuron.2016.12.034

Agulhon, C., Petravicz, J., McMullen, A.B., Sweger, E.J., Minton, S.K., Taves, S.R., Casper, K.B., Fiacco, T. a., McCarthy, K.D., 2008. What Is the Role of Astrocyte Calcium in Neurophysiology? Neuron 59, 932–946. https://doi.org/10.1016/j.neuron.2008.09.004

Akerboom, J., Chen, T.-W., Wardill, T.J., Tian, L., Marvin, J.S., Mutlu, S., Carreras Caldéron, N., Esposti, F., Borghuis, B.G., Sun, X.R., Gordus, A., Orger, M.B., Portugues, R., Engert, F., Macklin, J.J., Filosa, A., Aggarwal, A., Kerr, R.A., Takagi, R., Kracun, S., Shigetomi, E., Khakh, B.S., Baier, H., Lagnado, L., Wang, S.S.-H., Bargmann, C.I., Kimmel, B.E., Jayaraman, V., Svoboda, K., Kim, D.S., Schreiter, E.R., Looger, L.L., 2012. Optimization of a GCaMP Calcium Indicator for Neural Activity Imaging. J. Neurosci. 32, 13819–13840. https://doi.org/10.1523/JNEUROSCI.2601-12.2012

Allen, W.E., Kauvar, I. V., Chen, M.Z., Richman, E.B., Yang, S.J., Chan, K., Gradinaru, V., Deverman, B.E., Luo, L., Deisseroth, K., 2017. Global Representations of Goal-Directed Behavior in Distinct Cell Types of Mouse Neocortex. Neuron 94, 891-907.e6.

https://doi.org/10.1016/j.neuron.2017.04.017

Amilhon, B., Huh, C.Y.L., Manseau, F., Ducharme, G., Nichol, H., Adamantidis, A., Williams, S., 2015. Parvalbumin Interneurons of Hippocampus Tune Population Activity at Theta Frequency. Neuron 86, 1277–1289. https://doi.org/10.1016/j.neuron.2015.05.027

Andersen, P., Morris, R., Amaral, D., Bliss, T., O'Keefe, J. (Eds.), 2007. The hippocampus book. Oxford University Press, New York.

Anderson, M. a., Ao, Y., Sofroniew, M. V., 2014. Heterogeneity of reactive astrocytes. Neurosci. Lett. 565, 23–29. https://doi.org/10.1016/j.neulet.2013.12.030

Anderson, M.A., Shea, T.M.O., Burda, J.E., Ao, Y., Barlatey, S.L., Bernstein, A.M., Kim, J.H., James, N.D., Rogers, A., Kato, B., Wollenberg, A.L., Kawaguchi, R., Coppola, G., Wang, C., Deming, T.J., He, Z., Courtine, G., Sofroniew, M. V, 2019. Required growth facilitators propel axon regeneration across complete spinal cord injury. Nature 561, 396–400. https://doi.org/10.1038/s41586-018-0467-6

Aronov, D., Nevers, R., Tank, D.W., 2017. Mapping of a non-spatial dimension by the hippocampal–entorhinal circuit. Nat. Publ. Gr. 543, 719–722. https://doi.org/10.1038/nature21692

Asok, A., Leroy, F., Rayman, J.B., Kandel, E.R., 2019. Molecular Mechanisms of the Memory Trace. Trends Neurosci. 42, 14–22. https://doi.org/10.1016/j.tins.2018.10.005

Aston-jones, G., 1994. Locus Coeruleus Neurons in Monkey Are Selectively Activated by Attended Cues in a Vigilance Task J. Neurosci 14(7), 4467-4480.

Aston-jones, G., Rajkowski, J., Cohen, J., 1999. Role of Locus Coeruleus in Attention and Behavioral Flexibility 3223.

Aston-jones, G., Waterhouse, B., 2016. Locus coeruleus : From global projection system to

adaptive regulation of behavior. Brain Res. 1645, 75–78. https://doi.org/10.1016/j.brainres.2016.03.001

Attwell, D., Buchan, A.M., Charpak, S., Lauritzen, M., Macvicar, B. a, Newman, E. a, 2010. Glial and neuronal control of brain blood flow. Nature 468, 232–243. https://doi.org/10.1038/nature09613

Barnes, C.A., 1979. Memory Deficits Associated With Senescence : A Neurophysiological and Behavioral Study in the Rat. J. Comp. Physiol. Psychol. 93, 74–104.

Barres, B.A., 2008. The Mystery and Magic of Glia: A Perspective on Their Roles in Health and Disease. Neuron 60, 430–440. https://doi.org/10.1016/j.neuron.2008.10.013

Basu, J., Siegelbaum, S.A., 2015. The corticohippocampal circuit, synaptic plasticity, and memory. Cold Spring Harb. Perspect. Biol. 7, 1–26.

Basu, J., Zaremba, J.D., Cheung, S.K., Hitti, F.L., Zemelman, B. V, Losonczy, A., Siegelbaum, S.A., 2016. Gating of hippocampal activity, plasticity, and memory by entorhinal cortex long-range inhibition. https://doi.org/10.1126/science.aaa5694

Bazargani, N., Attwell, D., 2016. Astrocyte calcium signaling: the third wave. Nat. Neurosci. 19, 182–189. https://doi.org/10.1038/nn.4201

Beas, B.S., Wright, B.J., Skirzewski, M., Leng, Y., Hyun, J.H., Koita, O., Ringelberg, N., Kwon, H.B., Buonanno, A., Penzo, M.A., 2018. The locus coeruleus drives disinhibition in the midline thalamus via a dopaminergic mechanism. Nat. Neurosci. 21, 1–11. https://doi.org/10.1038/s41593-018-0167-4

Bekar, L.K., He, W., Nedergaard, M., 2008. Locus coeruleus a-adrenergic-mediated activation of cortical astrocytes in vivo. Cereb. Cortex 18, 2789–2795. https://doi.org/10.1093/cercor/bhn040

Bittner, K.C., Grienberger, C., Vaidya, S.P., Milstein, A.D., John, J., Suh, J., Tonegawa, S., Magee, J.C., 2015. Conjunctive input processing drives feature selectivity in hippocampal CA1 neurons. Nat. Neurosci. 18, 1133–1142.

Bittner, K.C., Milstein, A.D., Grienberger, C., Romani, S., Magee, J.C., 2017. Behavioral time scale synaptic plasticity underlies CA1 place fields. Science 357, 1033–1036.

Bliss, T.V.P., Lomo, T., 1973. Long-lasting potentiation of synaptic transmission in the dentate area of the anaesthetized rabbit following stimulation fo the perforant path. J. Physiol. 232, 331–356.

Boisvert, M.M., Erikson, G.A., Shokhirev, M.N., Allen, N.J., Boisvert, M.M., Erikson, G.A., Shokhirev, M.N., Allen, N.J., 2018. The Aging Astrocyte Transcriptome from Multiple Regions of the Mouse Brain. Cell Rep. 22, 269–285. https://doi.org/10.1016/j.celrep.2017.12.039

Bouret, S., Sara, S.J., 2004. Reward expectation, orientation of attention and locus coeruleus-medial frontal cortex interplay during learning. Eur. J. Neurosci. 20, 791–802. https://doi.org/10.1111/j.1460-9568.2004.03526.x

Brandon, M.P., Koenig, J., Leutgeb, J.K., Leutgeb, S., 2015. New and distinct hippocampal place codes are generated in a new environment during septal inactivation. Neuron 82, 789–796. https://doi.org/10.1016/j.neuron.2014.04.013.New

Braun, E.K., Wimmer, G.E., Shohamy, D., 2018. Retroactive and graded prioritization of memory by reward. Nat. Commun. 1–12. https://doi.org/10.1038/s41467-018-07280-0

Breese, C.R., Hampson, R.E., Deadwyler, S.A., 1989. Hippocampal Place Cells : Stereotypy and Plasticity. J Neurosci 9, 1097–1111.

Breton-Provencher, V., Sur, M., 2019. Active control of arousal by a locus coeruleus

GABAergic circuit. Nat. Neurosci. 22, 218–228. https://doi.org/10.1101/412338

Bush, D., Barry, C., Burgess, N., 2014. What do grid cells contribute to place cell firing? Trends Neurosci. 37, 136–145. https://doi.org/10.1016/j.tins.2013.12.003

Butler, W.N., Hardcastle, K., Giocomo, L.M., 2019. Remembered reward locations restructure entorhinal spatial maps. Science 363, 1447–1452.

Buzsáki, G., 2015. Hippocampal sharp wave-ripple: A cognitive biomarker for episodic memory and planning. Hippocampus 25, 1073–1188. https://doi.org/10.1002/hipo.22488

Buzsáki, G., Anastassiou, C.A., Koch, C., 2016. The origin of extracellular fields and currents — EEG, ECoG, LFP and spikes. Nat Rev Neurosci 13, 407–420. https://doi.org/10.1038/nrn3241.The

Buzsáki, G., Schomburg, E.W., 2016. What does gamma coherence tell us about inter-regional neural communication? Nat Neurosci 18, 484–489. https://doi.org/10.1038/nn.3952.What

Buzsáki, G., Tingley, D., 2019. Space and time: The hippocampus as a sequence generator. Trends Cogn. Sci. 22, 853–869. https://doi.org/10.1016/j.tics.2018.07.006.Space

Cai, D.J., Aharoni, D., Shuman, T., Shobe, J., Biane, J., Song, W., Wei, B., Veshkini, M., La-vu, M., Lou, J., Flores, S.E., Kim, I., Sano, Y., Zhou, M., Baumgaertel, K., Lavi, A., Kamata, M., Tuszynski, M., Mayford, M., Golshani, P., Silva, A.J., 2016. A shared neural ensemble links distinct contextual memories encoded close in time. Nature 534, 115–118. https://doi.org/10.1038/nature17955

Chung, W.-S., Clarke, L.E., Wang, G.X., Stafford, B.K., Sher, A., Chakraborty, C., Joung, J., Foo, L.C., Thompson, A., Chen, C., Smith, S.J., Barres, B. a, 2013. Astrocytes mediate synapse elimination through MEGF10 and MERTK pathways. Nature 504, 394–400. https://doi.org/10.1038/nature12776

Clarke, L.E., Barres, B. a, 2013. Emerging roles of astrocytes in neural circuit development. Nat. Rev. Neurosci. 14, 311–21. https://doi.org/10.1038/nrn3484

Colgin, L.L., 2016. Rhythms of the hippocampal network. Nat. Rev. Neurosci. 17, 239–249. https://doi.org/10.1038/nrn.2016.21

Colgin, L.L., Moser, E.I., Moser, M.B., 2008. Understanding memory through hippocampal remapping. Trends Neurosci.

Danielson, N.B., Kaifosh, P., Zaremba, J.D., Lovett-Barron, M., Tsai, J., Denny, C.A., Balough, E.M., Goldberg, A.R., Drew, L.J., Hen, R., Losonczy, A., Kheirbek, M.A., 2016a. Distinct Contribution of Adult-Born Hippocampal Granule Cells to Context Encoding. Neuron 90, 101–112. https://doi.org/10.1016/j.neuron.2016.02.019

Danielson, N.B., Zaremba, J.D., Kaifosh, P., Bowler, J., Ladow, M., Losonczy, A., 2016b. Sublayer-Specific Coding Dynamics during Spatial Navigation and Learning in Hippocampal Area CA1. Neuron 91, 652–665. https://doi.org/10.1016/j.neuron.2016.06.020

Deisseroth, K., 2015. Optogenetics : 10 years of microbial opsins in neuroscience. Nat. Neurosci. 18, 1213–1225.

Denk, W., Strickler, J.H., Webb, W.W., 1990. Two-Photon Laser Scanning Fluorescence Microscopy. Science 248, 73–76.

Diamantaki, M., Coletta, S., Nasr, K., Zeraati, R., Laturnus, S., Berens, P., Preston-Ferrer, P., Burgalossi, A., 2018. Manipulating Hippocampal Place Cell Activity by Single-Cell Stimulation in Freely Moving Mice. Cell Rep. 23, 32–38. https://doi.org/10.1016/j.celrep.2018.03.031

Dombeck, D. a., Khabbaz, A.N., Collman, F., Adelman, T.L., Tank, D.W., 2007. Imaging Large-Scale Neural Activity with Cellular Resolution in Awake, Mobile Mice. Neuron 56, 43–57.

https://doi.org/10.1016/j.neuron.2007.08.003

Dombeck, D. a, Harvey, C.D., Tian, L., Looger, L.L., Tank, D.W., 2010. Functional imaging of hippocampal place cells at cellular resolution during virtual navigation. Nat. Neurosci. 13, 1433–1440. https://doi.org/10.1038/nn.2648

Donegan, M., Stefanini, F., Meira, T., Gordon, J.A., Fusi, S., Siegelbaum, S.A., 2019. Coding of social novelty in the hippocampal CA2 region and its disruption and rescue in a mouse model of schizophrenia. bioRxiv.

Donita, L., Jill, B., Heien, M.L.A. V, Wightman, M.R., 2003. Detecting subsecond dopamine release with fast-scan cyclic voltammetry in vivo. Clin. Chem. 49, 1763–1773.

Dragoi, G., Tonegawa, S., 2011. Preplay of future place cell sequences by hippocampal cellular assemblies. Nature 469, 397–401. https://doi.org/10.1038/nature09633.Preplay

Dupret, D., Neill, J.O., Csicsvari, J., 2013. Dynamic Reconfiguration of Hippocampal Interneuron Circuits during Spatial Learning. Neuron 78, 166–180. https://doi.org/10.1016/j.neuron.2013.01.033

Dupret, D., O'Neill, J., Pleydell-bouverie, B., Csicsvari, J., 2010. The reorganization and reactivation of hippocampal maps predict spatial memory performance. Nat. Neurosci. 13, 995–1002. https://doi.org/10.1038/nn.2599

Duszkiewicz, A.J., Mcnamara, C.G., Takeuchi, T., Genzel, L., 2019. Novelty and Dopaminergic Modulation of Memory Persistence: A Tale of Two Systems. Trends Neurosci. 42, 102–114. https://doi.org/10.1016/j.tins.2018.10.002

Eichenbaum, H., 2017. Perspective On the Integration of Space , Time , and Memory. Neuron 95, 1007–1018. https://doi.org/10.1016/j.neuron.2017.06.036

Fischler, W.M., Joshi, N.R., Devi-chou, V., Kitch, L.J., Schnitzer, M.J., Abbott, L., Axel, R.,

2019. Olfactory Landmarks and Path Integration Converge to Form a Cognitive Spatial Map. bioRxiv.

Flavell, S.W., Pokala, N., Macosko, E.Z., Albrecht, D.R., Larsch, J., Bargmann, C.I., 2013. Serotonin and the Neuropeptide PDF Initiate and Extend Opposing Behavioral States in C . elegans. Cell 154, 1023–1035.

Florian, C., Vecsey, C.G., Halassa, M.M., Haydon, P.G., Abel, T., 2011. Astrocyte-derived adenosine and A1 receptor activity contribute to sleep loss-induced deficits in hippocampal synaptic plasticity and memory in mice. J. Neurosci. 31, 6956–6962. https://doi.org/10.1523/JNEUROSCI.5761-10.2011

Foote, S.L., Bloom, F.E., Aston-Jones, G., 1983. Nucleus locus ceruleus: new evidence of anatomical and physiological specificity. Physiol. Rev. 63, 844–914.

Francavilla, R., Villette, V., Luo, X., Chamberland, S., Muñoz-pino, E., Camiré, O., Wagner, K., Kis, V., Somogyi, P., Topolnik, L., 2018. Connectivity and network state-dependent recruitment of long-range VIP-GABAergic neurons in the mouse hippocampus. Nat. Commun. 1–17. https://doi.org/10.1038/s41467-018-07162-5

Fyhn, M., Molden, S., Hollup, S., Moser, M., Moser, E.I., 2002. Hippocampal Neurons Responding to First-Time Dislocation of a Target Object. Neuron 35, 555–566.

Gauthier, J.L., Tank, D.W., 2018a. A Dedicated Population for Reward Coding in the Hippocampus. Neuron 99, 179-193.e7. https://doi.org/10.1016/j.neuron.2018.06.008

Gauthier, J.L., Tank, D.W., 2018b. A Dedicated Population for Reward Coding in the Hippocampus. Neuron 99, 1–15. https://doi.org/10.1016/j.neuron.2018.06.008

Glennon, E., Carcea, I., Martins, A.R.O., Multani, J., Shehu, I., Svirsky, M.A., Froemke, R.C., 2019. Locus coeruleus activation accelerates perceptual learning. Brain Res. 1709, 39–49.

https://doi.org/10.1016/j.brainres.2018.05.048

Gomperts, S.N., Kloosterman, F., Wilson, M.A., 2015a. VTA neurons coordinate with the hippocampal reactivation of spatial experience 1–22. https://doi.org/10.7554/eLife.05360

Gomperts, S.N., Kloosterman, F., Wilson, M.A., 2015b. VTA neurons coordinate with the hippocampal reactivation of spatial experience. Elife 1–22.

Gordon, G.R.J., Howarth, C., MacVicar, B. a, 2011. Bidirectional control of arteriole diameter by astrocytes. Exp. Physiol. 96, 393–399. https://doi.org/10.1113/expphysiol.2010.053132

Grella, S.L., Neil, J.M., Edison, H.T., Strong, V.D., Odintsova, I. V, Walling, S.G., Martin, G.M., Marrone, X.D.F., Harley, X.C.W., 2019. Locus Coeruleus Phasic , But Not Tonic , Activation Initiates Global Remapping in a Familiar Environment. J Neurosci 39, 445–455.

Grosmark, A.D., Buzsáki, G., 2016. Diversity in neural firing dynamics supports both rigid and learned hippocampal sequences. Science 351, 1440–1443. https://doi.org/10.1126/science.aad1935

Hafting, T., Fyhn, M., Molden, S., Moser, M.-B., Moser, E.I., 2005. Microstructure of a spatial map in the entorhinal cortex. Nature 436, 801–806. https://doi.org/10.1038/nature03721

Hainmueller, T., Bartos, M., 2018. Parallel emergence of stable and dynamic memory engrams in the hippocampus. Nature 558, 292–296.

Halassa, M.M., Florian, C., Fellin, T., Munoz, J.R., Lee, S.Y., Abel, T., Haydon, P.G., Frank, M.G., 2009. Astrocytic Modulation of Sleep Homeostasis and Cognitive Consequences of Sleep Loss. Neuron 61, 213–219. https://doi.org/10.1016/j.neuron.2008.11.024

Handler, A., Graham, T.G.W., Cohn, R., Morantte, I., Siliciano, A.F., Zeng, J., Li, Y., Ruta, V., 2019. Distinct Dopamine Receptor Pathways Underlie the Temporal Sensitivity of Associative Learning. Cell 178, 60–75. https://doi.org/10.1016/j.cell.2019.05.040

Hangya, B., Ranade, S.P., Lorenc, M., Kepecs, A., 2015. Central Cholinergic Neurons Are Rapidly Recruited by Reinforcement Feedback. Cell 162, 1155–1168. https://doi.org/10.1016/j.cell.2015.07.057

Harris, K.D., Csicsvari, J., Hirase, H., Dragoi, G., Buzsáki, G., 2003. Organization of cell assemblies in the hippocampus. Nature 424, 552–556. https://doi.org/10.1038/nature01834

Hasselmo, M.E., 2006. The role of acetylcholine in learning and memory. Curr. Opin. Neurobiol. 16, 710–715. https://doi.org/10.1016/j.conb.2006.09.002

Haustein, M.D., Kracun, S., Lu, X.-H., Shih, T., Jackson-Weaver, O., Tong, X., Xu, J., Yang, X.W., O'Dell, T.J., Marvin, J.S., Ellisman, M.H., Bushong, E.A., Looger, L.L., Khakh, B.S., 2014. Conditions and Constraints for Astrocyte Calcium Signaling in the Hippocampal Mossy Fiber Pathway. Neuron 82, 413–429. https://doi.org/10.1016/j.neuron.2014.02.041

Hebb, D.O., 1949. The Organization of Behavior. John WIley & Sons Inc, New York.

Hirase, H., Iwai, Y., Takata, N., Shinohara, Y., Mishima, T., 2014. Volume transmission signalling via astrocytes. Philos. Trans. R. Soc. Lond. B. Biol. Sci. 369, 20130604. https://doi.org/10.1098/rstb.2013.0604

Hitti, F.L., Siegelbaum, S.A., 2014. The hippocampal CA2 region is essential for social memory. Nature 508, 88–92. https://doi.org/10.1038/nature13028

Hoffman, K.L., Dragan, M.C., Leonard, T.K., Micheli, C., Montefusco-Siegmund, R., Valiante, T.A., 2013. Saccades during visual exploration align hippocampal 3 – 8 Hz rhythms in human and non-human primates. Front. Syst. Neurosci. 7, 1–10. https://doi.org/10.3389/fnsys.2013.00043

Hok, V., Lenck-Santini, P.-P., Roux, S., Save, E., Muller, R.U., Poucet, B., 2007. Goal-Related

Activity in Hippocampal Place Cells. J Neurosci 27, 472–482. https://doi.org/10.1523/JNEUROSCI.2864-06.2007

Hollup, S.A., Molden, S., Donnett, J.G., Moser, M., Moser, E.I., 2001. Accumulation of Hippocampal Place Fields at the Goal Location in an Annular Watermaze Task. J Neurosci 21, 1635–1644.

Howard, C.E., Chen, C., Tabachnik, T., Hormigo, R., Ramdya, P., Mann, R.S., 2019. Serotonergic Modulation of Walking in Drosophila. Curr. Biol. 29, 4218–4230. https://doi.org/10.1016/j.cub.2019.10.042

Howard, M.W., Eichenbaum, H., 2015. Time and space in the hippocampus. Brain Res. 1621, 345–354. https://doi.org/10.1016/j.brainres.2014.10.069

Howe, M., Ridouh, I., Letizia, A., Mascaro, A., Larios, A., Azcorra, M., Dombeck, D.A., 2019. Coordination of rapid cholinergic and dopaminergic signaling in striatum during spontaneous movement. Elife 1–24.

Howe, M.W., Dombeck, D.A., 2016. Rapid signalling in distinct dopaminergic axons during locomotion and reward. Nature 535, 505–510. https://doi.org/10.1038/nature18942

Iliff, J.J., Wang, M., Liao, Y., Plogg, B.A., Peng, W., Gundersen, G.A., Benveniste, H., Vates, G.E., Deane, R., Goldman, S.A., Nagelhus, E.A., Nedergaard, M., 2012. A paravascular pathway facilitates CSF flow through the brain parenchyma and the clearance of interstitial solutes, including amyloid β. Sci. Transl. Med. 4, 147ra111. https://doi.org/10.1126/scitranslmed.3003748

Jia, H., Rochefort, N.L., Chen, X., Konnerth, A., 2011. In vivo two-photon imaging of sensory-evoked dendritic calcium signals in cortical neurons. Nat. Protoc. 6, 28–35. https://doi.org/10.1038/nprot.2010.169

Jimenez, J.C., Su, K., Goldberg, A.R., Luna, V.M., Bian, J.S., Ordek, G., Zhou, P., Ong, S.K., Wright, M.A., Zweifel, L., Paninski, L., Hen, R., Kheirbek, M.A., 2018. Anxiety Cells in a Hippocampal-Hypothalamic Circuit. Neuron 97, 670–683. https://doi.org/10.1016/j.neuron.2018.01.016

Jutras, M.J., Fries, P., Buffalo, E.A., 2013. Oscillatory activity in the monkey hippocampus during visual exploration and memory formation. Proc. Natl. Acad. Sci. 110, 13144–13149. https://doi.org/10.1073/pnas.1302351110/-/DCSupplemental.www.pnas.org/cgi/doi/10.1073/pnas.1302351110

Kaifosh, P., Lovett-barron, M., Turi, G.F., Reardon, T.R., Losonczy, A., 2013. Septo-hippocampal GABAergic signaling across multiple modalities in awake mice. Nat. Neurosci. 16, 1182–1187. https://doi.org/10.1038/nn.3482

Kaifosh, P., Zaremba, J.D., Danielson, N.B., Losonczy, A., 2014. SIMA: Python software for analysis of dynamic fluorescence imaging data. Front. Neuroinform. 8, 80. https://doi.org/10.3389/fninf.2014.00080

Kandel, E.R., Schwartz, J.H., Jessell, T.M., Siegelbaum, S.A., Hudspeth, A.J. (Eds.), 2013. Principles of Neural Science, Fifth. ed. McGraw Hill.

Kaufman, A.M., Geiller, T., Losonczy, A., 2020. A Role for the Locus Coeruleus in Hippocampal CA1 Place Cell Reorganization during Spatial Reward. Neuron 105, 1–9. https://doi.org/10.1016/j.neuron.2019.12.029

Kempadoo, K.A., Mosharov, E. V, Choi, S.J., Sulzer, D., Kandel, E.R., 2016. Dopamine release from the locus coeruleus to the dorsal hippocampus promotes spatial learning and memory. Proc. Natl. Acad. Sci. 113, 14835–14840. https://doi.org/10.1073/pnas.1616515114

Kentros, C.G., Agnihotri, N.T., Streater, S., Hawkins, R.D., Kandel, E.R., 2004. Increased

attention to spatial context increases both place field stability and spatial memory. Neuron 42, 283–295. https://doi.org/10.1016/S0896-6273(04)00192-8

Klausberger, T., Somogyi, P., 2008. Neuronal Diversity and of Hippocampal Circuit Operations Science 321, 53–57. https://doi.org/10.1126/science.1149381

Kobayashi, T., Nishijo, H., Fukuda, M., Bures, J.A.N., Ono, T., 1997. Task-Dependent Representations in Rat Hippocampal Place Neurons 597–613.

Kobayashi, T., Tran, A.H., Nishijo, H., Ono, T., Matsumoto, G., 2003. Contribution of hippocampal place cell activity to learning and formation of goal-directed navigation in rats. Neuroscience 117, 1025–1035. https://doi.org/10.1016/S0306-4522(02)00700-5

Kraus, B., Robinson, R., White, J., Eichenbaum, H., Hasselmo, M., 2013. Hippocampal "Time Cells": Time versus Path Integration. Neuron 78, 1090–1101. https://doi.org/10.1016/j.neuron.2013.04.015

Kucukdereli, H., Allen, N.J., Lee, A.T., Feng, A., Ozlu, M.I., Conatser, L.M., Chakraborty, C., Workman, G., Weaver, M., Sage, E.H., Barres, B.A., Eroglu, C., 2011. Control of excitatory CNS synaptogenesis by astrocyte-secreted proteins Hevin and SPARC. https://doi.org/10.1073/pnas.1104977108/-/DCSupplemental.www.pnas.org/cgi/doi/10.1073/pnas.1104977108

Leutgeb, S., Leutgeb, J.K., 2007. Pattern separation , pattern completion , and new neuronal codes within a continuous CA3 map. Learn. Mem. 14, 745–757. https://doi.org/10.1101/lm.703907.acteristics

Leutgeb, S., Leutgeb, J.K., Treves, A., Moser, M., Moser, E.I., 2004. Distinct Ensemble Codes in Hippocampal Areas CA3 and CA1. Science 305, 1295–1299.

Leutgeb, S., Moser, E.I., Mcnaughton, B.L., Moser, M., 2008. Independent Codes for Spatial and

Episodic Independent Codes for Spatial and Episodic Memory in Hippocampal Neuronal Ensembles. Science 619, 619–623. https://doi.org/10.1126/science.1114037

Li, Y., Liu, Z., Guo, Q., Luo, M., 2019. Long-term Fiber Photometry for Neuroscience Studies. Neurosci. Bull. 35, 425–433. https://doi.org/10.1007/s12264-019-00379-4

Lichtman, J.W., Denk, W., 2011. The Big and the Small: Challenges of Imaging the Brain's Circuits. Science 334, 618–623. https://doi.org/10.1126/science.1209168

Liddelow, S., Barres, B., 2015. SnapShot: Astrocytes in Health and Disease. Cell 162, 1170-1170.e1. https://doi.org/10.1016/j.cell.2015.08.029

Liddelow, S.A., Guttenplan, K.A., Clarke, L.E., Bennett, F.C., Bohlen, C.J., Schirmer, L., Bennett, M.L., Münch, A.E., Chung, W., Peterson, T.C., Wilton, D.K., Frouin, A., Napier, B.A., Panicker, N., Kumar, M., Buckwalter, M.S., Rowitch, D.H., Dawson, V.L., Dawson, T.M., Stevens, B., Barres, B.A., 2017. Neurotoxic reactive astrocytes are induced by activated microglia. Nat. Publ. Gr. 541, 481–487. https://doi.org/10.1038/nature21029

Lin, C.J., Yu, K., Hatcher, A., Huang, T., Lee, H.K., Carlson, J., Weston, M.C., Chen, F., Zhang, Y., Zhu, W., Mohila, C.A., Ahmed, N., Patel, A.J., Arenkiel, B.R., Creighton, C.J., Deneen, B., 2017. Identification of diverse astrocyte populations and their malignant analogs. Nat. Neurosci. 20, 396–405. https://doi.org/10.1038/nn.4493.Identification

Lisman, J., 2017. Glutamatergic synapses are structurally and biochemically complex because of multiple plasticity processes : long-term potentiation , long-term depression , short-term potentiation and scaling. Philos. Trans. R. Soc. B 372, 1–11.

Lisman, J., Buzsáki, G., Eichenbaum, H., Nadel, L., Ranganath, C., Redish, A.D., 2017. Viewpoints : how the hippocampus contributes to memory , navigation and cognition. Nat. Publ. Gr. 20, 1434–1447. https://doi.org/10.1038/nn.4661

Liu, X., Ramirez, S., Pang, P.T., Puryear, C.B., Govindarajan, A., Deisseroth, K., Tonegawa, S., 2012. Optogenetic stimulation of a hippocampal engram activates fear memory recall. Nature 484, 381–385. https://doi.org/10.1038/nature11028.Optogenetic

Lopez, L.L., Hauser, J., Feldon, J., Gargiulo, P.A., Yee, B.K., 2010. Evaluating spatial memory function in mice : A within-subjects comparison between the water maze test and its adaptation to dry land. Behav. Brain Res. 209, 85–92. https://doi.org/10.1016/j.bbr.2010.01.020

Louie, K., Wilson, M.A., 2001. Temporally Structured Replay of Awake Hippocampal Ensemble Activity during Rapid Eye Movement Sleep. Neuron 29, 145–156.

Lovett-Barron, M., Kaifosh, P., Kheirbek, M., Danielson, N., Zaremba, J., Reardon, T., Turi, G., Hen, R., Zemelman, B., Losonczy, A., 2014. Dendritic inhibition in the hippocampus supports fear learning. Science 343, 857–63. https://doi.org/10.1126/science.1247485

Ma, Z., Stork, T., Bergles, D.E., Freeman, M.R., 2016. Neuromodulators signal through astrocytes to alter neural circuit activity and behaviour. Nature 539, 428–432. https://doi.org/10.1038/nature20145

Magee, J.C., Grienberger, C., 2020. Synaptic Plasticity Forms and Functions. Annu. Rev. Neurosci. 43, 95–117.

Marder, E., 2012. Overview Neuromodulation of Neuronal Circuits : Back to the Future. Neuron 76, 1–11. https://doi.org/10.1016/j.neuron.2012.09.010

Martin, R., Bajo-Graneras, R., Mortalla, R., Perea, G., Araque, A., 2015. Circuit-specific signaling in astrocyte-neuron networks in basal ganglia pathways 349, 730–735.

Mather, M., Harley, C.W., 2016. The Locus Coeruleus: Essential for Maintaining Cognitive Function and the Aging Brain. Trends Cogn. Sci. 20, 214–226.

https://doi.org/10.1016/j.tics.2016.01.001.The

McNamara, C.G., Tejero-Cantero, Á., Trouche, S., Campo-Urriza, N., Dupret, D., 2014. Dopaminergic neurons promote hippocampal reactivation and spatial memory persistence. Nat. Neurosci. 17, 1658–1660. https://doi.org/10.1038/nn.3843

Milner, B., 2005. The Medial Temporal-Lobe Amnesic Syndrome. Psychiatr. Clin. North Am. 28, 599–611. https://doi.org/10.1016/j.psc.2005.06.002

Molofsky, A. V, Krenick, R., Ullian, E., Tsai, H.H., Deneen, B., Richardson, W.D., Barres, B.A., Rowitch, D.H., 2012. Astrocytes and disease: A neurodevelopmental perspective. Genes Dev. 26, 891–907. https://doi.org/10.1101 /gad.188326.112

Morel, L., Men, Y., Chiang, M.S.R., Tian, Y., Jin, S., Yelick, J., Higashimori, H., Yang, Y., 2019. Intracortical astrocyte subpopulations defined by astrocyte reporter Mice in the adult brain. Glia 67, 171–181. https://doi.org/10.1002/glia.23545

Morris, R.G.M., Garrud, P., Rawlins, J.N.P., O'Keefe, J., 1982. Place navigation impaired in rats with hippocampal lesions. Nature 297, 681–683.

Moser, M.B., Rowland, D.C., Moser, E.I., 2015. Place cells, grid cells, and memory. Cold Spring Harb. Perspect. Biol. 7, a021808. https://doi.org/10.1101/cshperspect.a021808

Mu, Y., Bennett, D. V, Rubinov, M., Narayan, S., Yang, C., Tanimoto, M., Mensh, B.D., Looger, L.L., Ahrens, M.B., 2019. Glia Accumulate Evidence that Actions Are Futile and Suppress Unsuccessful Behavior. Cell 178, 27–43. https://doi.org/10.1016/j.cell.2019.05.050

O'Dell, T.J., Connor, S.A., Guglietta, R., Nguyen, P. V, 2015. β-Adrenergic receptor signaling and modulation of long-term potentiation in the mammalian hippocampus. Learn. Mem. 22, 461–71. https://doi.org/10.1101/lm.031088.113

O'Keefe, J., Dostrovky, J., 1971. The hippocampus as a spatial map. Preliminary evidence from unit activity in the freely-moving rat. Brain Res. 34, 171–175.

O'Keefe, J., Nadel, L., 1978. The Hippocampus as a Cognitive Map. Oxford University Press, Oxford.

Oe, Y., Wang, X., Patriarchi, T., Konno, A., Ozawa, K., Yahagi, K., Hirai, H., Tian, L., McHugh, T.J., Hirase, H., 2020. Distinct temporal integration of noradrenaline signaling by astrocytic second messengers during vigilance. Nat. Commun. 11, 1–15. https://doi.org/10.1038/s41467-020-14378-x

Palacios-filardo, J., Mellor, J.R., 2019. Neuromodulation of hippocampal long-term synaptic plasticity. Curr. Opin. Neurobiol. 54, 37–43. https://doi.org/10.1016/j.conb.2018.08.009

Papouin, T., Dunphy, J.M., Tolman, M., Dineley, K.T., Haydon, P.G., 2017. Septal Cholinergic Neuromodulation Tunes the Astrocyte-Dependent Gating of Hippocampal NMDA Receptors to Wakefulness. Neuron 1–15. https://doi.org/10.1016/j.neuron.2017.04.021

Patriarchi, T., Cho, J.R., Merten, K., Howe, M.W., Marley, A., Xiong, W., Folk, R.W., Broussard, G.J., Liang, R., Jang, M.J., Zhong, H., Dombeck, D., von Zastrow, M., Nimmerjahn, A., Gradinaru, V., Williams, J.T., Tian, L., 2018. Ultrafast neuronal imaging of dopamine dynamics with designed genetically encoded sensors. Science (80-.). 360, 1–22. https://doi.org/10.1126/science.aat4422.Ultrafast

Paukert, M., Agarwal, A., Cha, J., Doze, V. a., Kang, J.U., Bergles, D.E., 2014. Norepinephrine controls astroglial responsiveness to local circuit activity. Neuron 82, 1263–1270. https://doi.org/10.1016/j.neuron.2014.04.038

Petravicz, J., Boyt, K.M., McCarthy, K.D., 2014. Astrocyte IP3R2-dependent Ca2+ signaling is not a major modulator of neuronal pathways governing behavior. Front. Behav. Neurosci. 8,

1–13. https://doi.org/10.3389/fnbeh.2014.00384

Petravicz, J., Fiacco, T. a, McCarthy, K.D., 2008. Loss of IP3 receptor-dependent Ca2+ increases in hippocampal astrocytes does not affect baseline CA1 pyramidal neuron synaptic activity. J. Neurosci. 28, 4967–4973. https://doi.org/10.1523/JNEUROSCI.5572-07.2008

Pinto, L., Dan, Y., 2015. Cell-Type-Specific Activity in Prefrontal Cortex during Goal-Directed Behavior. Neuron 87, 437–451. https://doi.org/10.1016/j.neuron.2015.06.021

Poo, M.-M., Pignatelli, M., Ryan, T.J., Tonegawa, S., Bonhoeffer, T., Martin, K.C., Rudenko, A., Tsai, L.-H., Tsien, R.W., Fishell, G., Mullins, C., Gonçalves, J.T., Shtrahman, M., Johnston, S.T., Gage, F.H., Dan, Y., Long, J., Buzsáki, G., Stevens, C., 2016. What is memory? The present state of the engram. BMC Biol. 14, 40. https://doi.org/10.1186/s12915-016-0261-6

Poskanzer, K.E., Yuste, R., 2016. Astrocytes regulate cortical state switching in vivo 2016. https://doi.org/10.1073/pnas.1520759113

Poskanzer, K.E., Yuste, R., 2011. Astrocytic regulation of cortical UP states. Proc. Natl. Acad. Sci. 108, 18453–18458. https://doi.org/10.1073/pnas.1112378108

Rajasethupathy, P., Sankaran, S., Marshel, J.H., Kim, C.K., Ferenczi, E., Lee, S.Y., Berndt, A., Ramakrishnan, C., Jaffe, A., Lo, M., Liston, C., Deisseroth, K., 2015. Projections from neocortex mediate top-down control of memory retrieval. Nature 526, 653–659. https://doi.org/10.1038/nature15389

Redondo, R.L., Morris, R.G.M., 2011. Making memories last : the synaptic tagging and capture hypothesis. Nat. Rev. Neurosci. 12, 17–30. https://doi.org/10.1038/nrn2963

Retailleau, A., Morris, G., 2018. Spatial Rule Learning and Corresponding CA1 Place Cell Reorientation Depend on Local Dopamine Article Spatial Rule Learning and Corresponding

CA1 Place Cell Reorientation Depend on Local Dopamine Release. Curr. Biol. 28, 836-846.e4. https://doi.org/10.1016/j.cub.2018.01.081

Rodriguez, P.C., Pereira, D.B., Borgkvist, A., Wong, M.Y., Barnard, C., Sonders, M.S., Zhang, H., Sames, D., Sulzer, D., 2013. Fluorescent dopamine tracer resolves individual dopaminergic synapses and their activity in the brain. Proc. Natl. Acad. Sci. U. S. A. 110, 870–5. https://doi.org/10.1073/pnas.1213569110

Rorabaugh, J.M., Chalermpalanupap, T., Botz-Zapp, C.A., Fu, V.M., Lembeck, N.A., Cohen, R.M., Weinshenker, D., 2017. Chemogenetic locus coeruleus activation restores reversal learning in a rat model of Alzheimer's disease. Brain 140, 3023–3038. https://doi.org/10.1093/brain/awx232

Royer, S., Zemelman, B. V, Losonczy, A., Kim, J., Chance, F., Magee, J.C., Ki, G. ouml rgy B. aacute, 2012. Control of timing, rate and bursts of hippocampal place cells by dendritic and somatic inhibition. Nat. Neurosci. 15, 1–10. https://doi.org/10.1038/nn.3077

Rueckemann, J.W., Buffalo, E.A., 2017. Spatial responses, immediate experience, and memory in the monkey hippocampus. Curr. Opin. Behav. Sci. 17, 155–160. https://doi.org/10.1016/j.cobeha.2017.08.008

Sara, S.J., Bouret, S., 2012. Review Orienting and Reorienting : The Locus Coeruleus Mediates Cognition through Arousal. Neuron 76, 130–141. https://doi.org/10.1016/j.neuron.2012.09.011

Sasaki, T., Leutgeb, S., Leutgeb, J.K., 2015. Spatial and memory circuits in the medial entorhinal cortex. Curr. Opin. Neurobiol. 32, 16–23. https://doi.org/10.1016/j.conb.2014.10.008

Schultz, W., 2016. Dopamine reward prediction-error signalling: a two-component response. Nat. Publ. Gr. 17, 183–195. https://doi.org/10.1038/nrn.2015.26

Schwarz, L.A., Miyamichi, K., Gao, X.J., Beier, K.T., Weissbourd, B., DeLoach, K.E., Ren, J., Ibanes, S., Malenka, R.C., Kremer, E.J., Luo, L., 2015. Viral-genetic tracing of the input–output organization of a central noradrenaline circuit. Nature 524, 88–92. https://doi.org/10.1038/nature14600

Scoville, W.B., Milner, B., 1957. Loss of recent memory after bilateral hippocampal lesions. Neurol Neurosurg Psychiat 20, 11–21.

Sheffield, M.E.J., Dombeck, D.A., 2014. Calcium transient prevalence across the dendritic arbour predicts place field properties. Nature 517, 200–204. https://doi.org/10.1038/nature13871

Shigetomi, E., Patel, S., Khakh, B.S., 2016. Probing the Complexities of Astrocyte Calcium Signaling. Trends Cell Biol. 26, 300–312. https://doi.org/10.1016/j.tcb.2016.01.003

Skaggs, W.E., McNaughton, B.L., Gothard, K.M., Markus, E., 1993. An Information-Theoretic Approach to Deciphering the Hippocampal Code. Adv. Neural Inf. Process. Syst. 5, 1030–1037. https://doi.org/10.1055/s-0028-1107772

Skaggs, W.E., Mcnaughton, B.L., Wilson, M.A., Barnes, C.A., 1996. Theta Phase Precession in Hippocampal Neuronal Populations and the Compression of Temporal Sequences. Hippocampus 172, 149–172.

Smith, C.C., Greene, R.W., 2012. CNS Dopamine Transmission Mediated by Noradrenergic Innervation. J. Neurosci. 32, 6072–6080. https://doi.org/10.1523/JNEUROSCI.6486-11.2012

Srinivasan, R., Huang, B.S., Venugopal, S., Johnston, A.D., Chai, H., Zeng, H., Golshani, P., Khakh, B.S., 2015. Ca(2+) signaling in astrocytes from Ip3r2(-/-) mice in brain slices and during startle responses in vivo. Nat. Neurosci. 18, 708–17. https://doi.org/10.1038/nn.4001

Srinivasan, R., Lu, T.-Y., Chai, H., Xu, J., Huang, B.S., Golshani, P., Coppola, G., Khakh, B.S., 2016. New Transgenic Mouse Lines for Selectively Targeting Astrocytes and Studying Calcium Signals in Astrocyte Processes In Situ and In Vivo. Neuron 1–15. https://doi.org/10.1016/j.neuron.2016.11.030

Stachenfeld, K.L., Botvinick, M.M., Gershman, S.J., 2017. The hippocampus as a predictive map. Nat. Neurosci. 20, 1643–1653. https://doi.org/10.1038/nn.4650

Stevens, B., Allen, N.J., Vazquez, L.E., Howell, G.R., Christopherson, K.S., Nouri, N., Micheva, K.D., Mehalow, A.K., Huberman, A.D., Stafford, B., Sher, A., Litke, A.M., Lambris, J.D., Smith, S.J., John, S.W.M., Barres, B.A., 2007. The Classical Complement Cascade Mediates CNS Synapse Elimination 1164–1178. https://doi.org/10.1016/j.cell.2007.10.036

Suzuki, A., Stern, S. a., Bozdagi, O., Huntley, G.W., Walker, R.H., Magistretti, P.J., Alberini, C.M., 2011. Astrocyte-neuron lactate transport is required for long-term memory formation. Cell 144, 810–823. https://doi.org/10.1016/j.cell.2011.02.018

Swift, K.M., Gross, B.A., Frazer, M.A., Bauer, D.S., Clark, K.J.D., Vazey, E.M., Aston-Jones, G., Li, Y., Pickering, A.E., Sara, S.J., Poe, G.R., 2018. Abnormal Locus Coeruleus Sleep Activity Alters Sleep Signatures of Memory Consolidation and Impairs Place Cell Stability and Spatial Memory. Curr. Biol. 1–11. https://doi.org/10.1016/J.CUB.2018.09.054

Takata, N., Mishima, T., Hisatsune, C., Nagai, T., Ebisui, E., Mikoshiba, K., Hirase, H., 2011. Astrocyte Calcium Signaling Transforms Cholinergic Modulation to Cortical Plasticity In Vivo. J. Neurosci. 31, 18155–18165. https://doi.org/10.1523/JNEUROSCI.5289-11.2011

Takeuchi, T., Duszkiewicz, A.J., Morris, R.G.M., 2013. The synaptic plasticity and memory hypothesis : encoding , storage and persistence.

Takeuchi, T., Duszkiewicz, A.J., Sonneborn, A., Spooner, P.A., Yamasaki, M., Morris, R.G.M.,

Watanabe, M., Smith, C.C., Fernández, G., Deisseroth, K., Robert, W., 2016. Locus coeruleus and dopaminergic consolidation of everyday memory. Nature 537, 357–362. https://doi.org/10.1038/nature19325

Tanaka, K.Z., He, H., Tomar, A., Niisato, K., Huang, A.J.Y., McHugh, T.J., 2018. The hippocampal engram maps experience but not place. Science 397, 392–397.

Teixeira, C.M., Rosen, Z.B., Suri, D., Sun, Q., Hersch, M., Sargin, D., Dincheva, I., Morgan, A.A., Spivack, S., Krok, A.C., Hirschfeld-Stoler, TessaLambe, E.K., Siegelbaum, S.A., Ansorge, M., 2018. Hippocampal 5-HT Input Regulates Memory Formation and Schaffer Collateral Excitation. Neuron 98, 992–1004. https://doi.org/10.1016/j.neuron.2018.04.030

Tolman, E.C., 1948. Cognitive maps in rats and men. Psychol. Rev. 55, 189–208.

Tonegawa, S., Liu, X., Ramirez, S., Redondo, R., 2015. Memory Engram Cells Have Come of Age. Neuron 87, 918–931. https://doi.org/10.1016/j.neuron.2015.08.002

Tonegawa, S., Morrissey, M.D., Kitamura, T., 2018. The role of engram cells in the systems consolidation of memory. Nat. Rev. Neurosci. 19. https://doi.org/10.1038/s41583-018-0031-2

Tsitsiklis, M., Miller, J., Qasim, S.E., Sharan, A., Stein, J.M., Jacobs, J., Tsitsiklis, M., Miller, J., Qasim, S.E., Inman, C.S., Gross, R.E., Willie, J.T., Smith, E.H., Sheth, S.A., Schevon, C.A., Sperling, M.R., Sharan, A., Stein, J.M., Jacobs, J., 2020. Single-Neuron Representations of Spatial Targets in Humans. Curr. Biol. 30, 245-253.e4. https://doi.org/10.1016/j.cub.2019.11.048

Tuncdemir, S.N., Lacefield, C.O., Hen, R., 2019. Contributions of adult neurogenesis to dentate gyrus network activity and computations. Behav. Brain Res. 374, 1–12. https://doi.org/10.1016/j.bbr.2019.112112

Turi, G., Li, W.-K., Chavlis, S., Pandi, I., O'Hare, J., Priestley, J.B., Grosmark, A.D., Liao, Z., Ladow, M., Zhang, J.F., Zemelman, B. V., Poirazi, P., Losonczy, A., 2019. Vasoactive intestinal polypeptide-expressing interneurons in the hippocampus support goal-oriented spatial learning. Neuron 101, 1–16. https://doi.org/10.1016/j.neuron.2019.01.009

Uematsu, A., Tan, B.Z., Ycu, E.A., Cuevas, J.S., Koivumaa, J., Junyent, F., Kremer, E.J., Witten, I.B., Deisseroth, K., Johansen, J.P., 2017. Modular organization of the brainstem noradrenaline system coordinates opposing learning states. https://doi.org/10.1038/nn.4642

Ulanovsky, N., Moss, C.F., 2007. Hippocampal cellular and network activity in freely moving echolocating bats. Nat. Neurosci. 10, 224–234. https://doi.org/10.1038/nn1829

Wagatsuma, A., Okuyama, T., Sun, C., Smith, L.M., Abe, K., Tonegawa, S., 2018. Locus coeruleus input to hippocampal CA3 drives single-trial learning of a novel context. Proc. Natl. Acad. Sci. 115, E310–E316. https://doi.org/10.1073/pnas.1714082115

Walling, S.G., Harley, C.W., 2004. Locus Ceruleus Activation Initiates Delayed Synaptic Potentiation of Perforant Path Input to the Dentate Gyrus in Awake Rats: A Novel β-Adrenergic- and Protein Synthesis-Dependent Mammalian Plasticity Mechanism. J. Neurosci. 24, 598–604. https://doi.org/10.1523/JNEUROSCI.4426-03.2004

Wang, F., Smith, N. a., Xu, Q., Fujita, T., Baba, a., Matsuda, T., Takano, T., Bekar, L., Nedergaard, M., 2012. Astrocytes Modulate Neural Network Activity by Ca2+-Dependent Uptake of Extracellular K+. Sci. Signal. 5, ra26–ra26. https://doi.org/10.1126/scisignal.2002334

Wang, S.-H., Redondo, R.L., Morris, R.G.M., 2010. Relevance of synaptic tagging and capture to the persistence of long-term potentiation and everyday spatial memory. Proc. Natl. Acad. Sci. 107, 19537–19542. https://doi.org/10.1073/pnas.1008638107

Weinshenker, D., 2018. Long Road to Ruin : Noradrenergic Dysfunction in Neurodegenerative Disease. Trends Neurosci. 41, 211–223. https://doi.org/10.1016/j.tins.2018.01.010

Wilson, M.A., Mcnaughton, B.L., 1994. Reactivation of Hippocampal Ensemble Memories During Sleep. Science 265, 676–679.

Xu, H., Baracskay, P., ONeill, J., Csicsvari, J., 2018. Assembly Responses of Hippocampal CA1 Place Cells Predict Learned Behavior in Goal-Directed Spatial Tasks on the Radial Eight-Arm Maze. Neuron 1–14. https://doi.org/10.1016/j.neuron.2018.11.015

Xu, J.-Y., Zhang, J., Chen, C., 2012. Long-lasting potentiation of hippocampal synaptic transmission by direct cortical input is mediated via endocannabinoids. J. Physiol. 590, 2305–2315. https://doi.org/10.1113/jphysiol.2011.223511

Yu, A.J., Dayan, P., 2005. Uncertainty, neuromodulation, and attention. Neuron 46, 681–692. https://doi.org/10.1016/j.neuron.2005.04.026

Zamanian, J., Xu, L., Foo, L., 2012. Genomic Analysis of Reactive Astrogliosis. J. … 32, 6391–6410. https://doi.org/10.1523/JNEUROSCI.6221-11.2012.Genomic

Zaremba, J.D., Diamantopoulou, A., Danielson, N.B., Grosmark, A.D., Kaifosh, P.W., Bowler, J.C., Liao, Z., Sparks, F.T., Gogos, J.A., Losonczy, A., 2017. Impaired hippocampal place cell dynamics in a mouse model of the 22q11.2 deletion. Nat. Neurosci. 20, 1612–1623. https://doi.org/10.1038/nn.4634

Zhang, Y., Barres, B.A., 2010. Astrocyte heterogeneity : an underappreciated topic in neurobiology. Curr. Opin. Neurobiol. 20, 588–594. https://doi.org/10.1016/j.conb.2010.06.005

Zhang, Y., Chen, K., Sloan, S.A., Bennett, M.L., Scholze, A.R., O'Keeffe, S., Phatnani, H.P., Guarnieri, P., Caneda, C., Ruderisch, N., Deng, S., Liddelow, S.A., Zhang, C., Daneman,

R., Maniatis, T., Barres, B.A., Wu, J.Q., 2014. An RNA-sequencing transcriptome and splicing database of glia, neurons, and vascular cells of the cerebral cortex. J. Neurosci. 34, 11929–11947. https://doi.org/10.1523/JNEUROSCI.1860-14.2014

Ziv, Y., Burns, L.D., Cocker, E.D., Hamel, E.O., Ghosh, K.K., Kitch, L.J., El Gamal, A., Schnitzer, M.J., 2013. Long-term dynamics of CA1 hippocampal place codes. Nat. Neurosci. 16, 264–6. https://doi.org/10.1038/nn.3329